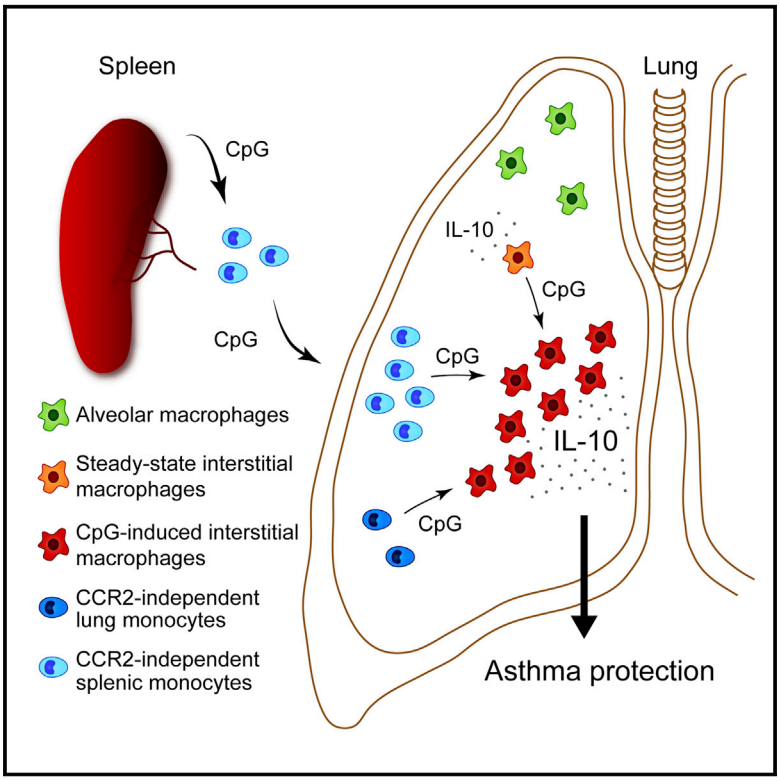
Article

Immunity

Exposure to Bacterial CpG DNA Protects from Airway Allergic Inflammation by Expanding Regulatory Lung Interstitial Macrophages

Graphical Abstract



Authors

Catherine Sabatel, Coraline Radermecker, Laurence Fievez, ..., Florent Ginhoux, Thomas Marichal, Fabrice Bureau

Correspondence

t.marichal@ulg.ac.be (T.M.), fabrice.bureau@ulg.ac.be (F.B.)

In Brief

Exposure to unmethylated CpG DNA (CpG) from bacteria is associated with a reduced risk of developing asthma. Sabatel et al. find that CpG exposure leads to higher numbers of lung interstitial macrophages that prevent allergic inflammation through the production of the regulatory cytokine interleukin-10.

Highlights

- Exposure to bacterial CpG DNA (CpG) expands regulatory lung interstitial macrophages (IMs)
- Transfer of WT but not *Il10*$^{-/-}$ IMs protects from allergen-induced airway inflammation
- CpG-induced IMs arise from local and splenic reservoir monocytes
- Migration of regulatory IM precursors to the lung does not require CCR2

Accession Numbers

E-MTAB-5012

Sabatel et al., 2017, Immunity *46*, 457–473
March 21, 2017 © 2017 Elsevier Inc.
http://dx.doi.org/10.1016/j.immuni.2017.02.016

CellPress

Immunity
Article

Exposure to Bacterial CpG DNA Protects from Airway Allergic Inflammation by Expanding Regulatory Lung Interstitial Macrophages

Catherine Sabatel,[1,2,11] Coraline Radermecker,[1,2,11] Laurence Fievez,[1,11] Genevieve Paulissen,[1] Svetoslav Chakarov,[3] Claudia Fernandes,[1] Sabine Olivier,[1] Marie Toussaint,[4] Dimitri Pirottin,[1,2] Xue Xiao,[2,5] Pascale Quatresooz,[6] Jean-Claude Sirard,[7] Didier Cataldo,[8] Laurent Gillet,[2,5] Hicham Bouabe,[9] Christophe J. Desmet,[1] Florent Ginhoux,[3] Thomas Marichal,[1,2,*] and Fabrice Bureau[1,2,10,12,*]

[1]Laboratory of Cellular and Molecular Immunology, GIGA Research, University of Liège, 4000 Liège, Belgium
[2]Faculty of Veterinary Medicine, University of Liège, 4000 Liège, Belgium
[3]Singapore Immunology Network, Agency for Science, Technology, and Research, Singapore 138648, Singapore
[4]Airway Disease Infection Section, National Heart and Lung Institute, Imperial College London, London W2 1PG, UK
[5]Laboratory of Immunology-Vaccinology, Fundamental and Applied Research for Animals & Health, University of Liège, 4000 Liège, Belgium
[6]Centre de Recherche sur les Protéines Prion, Department of Human Histology, University of Liège, 4000 Liège, Belgium
[7]INSERM U1019, CNRS UMR 8204, Center for Infection and Immunity of Lille, University of Lille, CHU Lille, Institut Pasteur de Lille, 59000 Lille, France
[8]Laboratory of Tumor and Developmental Biology, GIGA Research, University of Liège, 4000 Liège, Belgium
[9]Laboratory of Lymphocyte Signalling and Development, Babraham Institute, Cambridge CB22 3AT, UK
[10]Walloon Excellence in Life Sciences and Biotechnology, Wallonia, Belgium
[11]Co-first author
[12]Lead Contact
*Correspondence: t.marichal@ulg.ac.be (T.M.), fabrice.bureau@ulg.ac.be (F.B.)
http://dx.doi.org/10.1016/j.immuni.2017.02.016

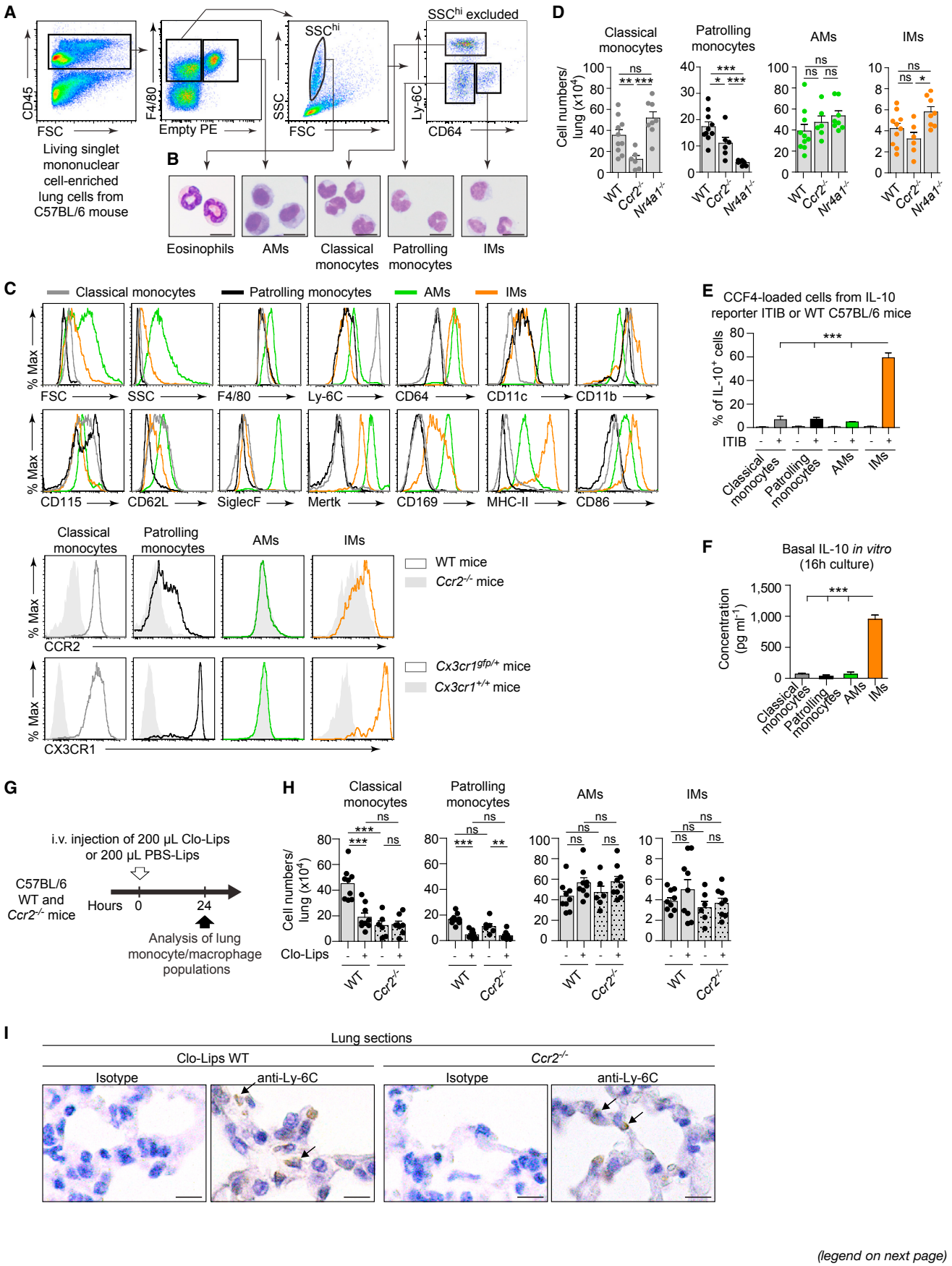
SUMMARY

Living in a microbe-rich environment reduces the risk of developing asthma. Exposure of humans or mice to unmethylated CpG DNA (CpG) from bacteria reproduces these protective effects, suggesting a major contribution of CpG to microbe-induced asthma resistance. However, how CpG confers protection remains elusive. We found that exposure to CpG expanded regulatory lung interstitial macrophages (IMs) from monocytes infiltrating the lung or mobilized from the spleen. Trafficking of IM precursors to the lung was independent of CCR2, a chemokine receptor required for monocyte mobilization from the bone marrow. Using a mouse model of allergic airway inflammation, we found that adoptive transfer of IMs isolated from CpG-treated mice recapitulated the protective effects of CpG when administered before allergen sensitization or challenge. IM-mediated protection was dependent on IL-10, given that *Il10*$^{-/-}$ CpG-induced IMs lacked regulatory effects. Thus, the expansion of regulatory lung IMs upon exposure to CpG might underlie the reduced risk of asthma development associated with a microbe-rich environment.

INTRODUCTION

The increased prevalence of allergic asthma over the past few decades points to alterations in the environment (Eder et al., 2006). The hygiene hypothesis postulates that decreased exposure to environmental and commensal microbes or their products, partly because of changes associated with urban lifestyles, is responsible for this rise (Strachan, 1989; von Mutius, 2016). In line with this hypothesis, epidemiological studies associate growing up on a farm, where exposure to bacterial endotoxin (lipopolysaccharide [LPS]) is high, with reduced risk of allergic sensitization (Braun-Fahrländer et al., 2002; von Mutius, 2016). However, whether LPS mediates the aforementioned protective effects is uncertain. Indeed, concurrent studies in non-rural environments have suggested that exposure to LPS is instead a risk factor for increased asthma prevalence and severity (Thorne et al., 2005). Moreover, although LPS has demonstrated protective effects in some animal models (Schuijs et al., 2015), it has also been shown to promote experimental asthma (Eisenbarth et al., 2002; Hammad et al., 2009).

Another candidate for mediating the protective effects of microbe-rich environments is bacterial DNA, which contains unmethylated CpG motifs with immunomodulatory properties (Krieg, 2006). Bacterial DNA, like LPS, is present in high amounts in dust from rural homes (Roy et al., 2003), and treatment with synthetic CpG DNA (CpG) consistently prevents allergic sensitization in animal models (Kline et al., 1998; Sur et al., 1999). Moreover, CpG is able to reverse established asthma in animals (Broide et al., 1998; Kline et al., 2002) and has shown efficacy in attenuating allergic disorders in human clinical trials (Beeh et al., 2013; Creticos et al., 2006; Krieg, 2006). How CpG exerts these immunomodulatory effects remains unclear. It was initially proposed that CpG, which is often co-administered with allergens, redirects allergen-specific T helper 2 (Th2) cell responses toward Th1 or regulatory T cell responses (Broide et al., 1998; Kline et al., 2002; Kline et al., 1998; Krieg, 2012). However,



(legend on next page)

CpG is capable of conferring protection in the absence of allergens (Beeh et al., 2013; Broide et al., 1998; Krieg, 2012), suggesting that it acts independently of the adaptive immune system.

In 2009, we identified a small population of regulatory macrophages in the lung interstitium of mice (Bedoret et al., 2009). These lung interstitial macrophages (IMs), also found in humans (Hoppstädter et al., 2010), spontaneously produce the immunosuppressive cytokine interleukin-10 (IL-10), a hallmark of regulatory macrophages (Mosser and Edwards, 2008). Moreover, when exposed to low doses of LPS, IMs, which are located in the vicinity of lung dendritic cells (DCs), can counteract the capacity of LPS-activated DCs to induce Th2 responses against harmless antigens (Bedoret et al., 2009). In agreement with this, mice lacking functional IMs, but not wild-type (WT) mice, develop overt asthmatic reactions when exposed to low doses of a mixture of allergen and LPS (Bedoret et al., 2009). However, the immunosuppressive effects of IMs are overwhelmed when the airways are exposed to high levels of allergens and LPS, given that 100% of WT mice develop asthma upon exposure to high doses of house dust mite (HDM) extracts, a phenomenon that requires Toll-like receptor 4 (TLR4) activation by HDM-borne LPS (Hammad et al., 2009). We therefore reasoned that pathogen-associated molecular patterns (PAMPs) other than LPS could improve the immunosuppressive effects of IMs and thereby explain how a microbe-rich environment reduces the risk of asthma development.

Here, we found that CpG is able to robustly expand the IM population. CpG-induced IMs (CpG IMs) developed from local and splenic reservoir monocytes and were able, by producing IL-10, to confer protection against allergic inflammation even when mice were sensitized and challenged with high doses of HDM. Our findings reveal a role for regulatory IMs shed in the protective effect of CpG exposure in allergic airway inflammation and suggest that similar mechanisms might underlie the reduced risk of human asthma development that is associated with exposure to a microbe-rich environment.

RESULTS

A Simplified Flow Cytometry Strategy Discriminates Lung Monocyte and Macrophage Subsets in Mice

In order to identify the monocyte and macrophage populations associated with the lung at steady state, we set up a simplified six-step, five-color flow cytometry staining procedure on mononuclear-cell-enriched lung cells isolated from whole, non-lavaged, perfused lungs of naive C57BL/6 WT mice. To encompass all monocyte and macrophage populations, we gated sequentially on living singlet cells (step 1), $CD45^+$ immune cells (step 2), and cells positive for the pan-monocyte and -macrophage marker F4/80 (step 3) (Figure 1A). Alveolar macrophages (AMs), the most abundant lung phagocytic cells present in the airways (Figure S1A), were identified as large (FSC^{hi}) autofluorescent $CD11c^{hi}SiglecF^{hi}CD64^+Mertk^+CD169^+$ cells (step 4) (Figures 1A–1C). F4/80-expressing lung-resident eosinophils (Mesnil et al., 2016) were excluded on the basis of their high granularity (SSC^{hi}) (step 5). The remaining $CD45^+F4/80^+$ cells were further separated into three populations according to their expression of the monocyte and macrophage markers Ly-6C (Geissmann et al., 2003) and CD64 (Gautier et al., 2012) (step 6) (Figures 1A and 1B).

Ly-$6C^{hi}CD64^{lo}$ cells were classical monocytes, given that they exhibited a monocytic morphology, expressed the typical markers of classical monocytes (Ly-$6C^{hi}CCR2^+CX3CR1^{int}$ $CD62L^+$), and were less abundant in *Ccr2*$^{-/-}$ mice (Figure 1B–1D), in which classical monocyte emigration from the bone marrow (BM) is compromised (Serbina and Pamer, 2006). Ly-$6C^{lo}CD64^{lo}$ cells also displayed a monocytic morphology, expressed the characteristic markers of patrolling monocytes (Ly-$6C^{lo}CCR2^{lo}CX3CR1^{hi}CD62L^-$), and were significantly reduced in mice lacking NR4A1 (Figure 1B–1D), a transcription factor controlling differentiation and survival of patrolling monocytes (Hanna et al., 2011), demonstrating that these cells were patrolling monocytes.

Finally, Ly-$6C^{lo}CD64^{hi}$ cells were identified as IMs. Indeed, these cells were absent in the broncho-alveolar lavage fluid (BALF) (Figure S1A) and were positive for MHC-II and the macrophage markers Mertk and CD169 (Figure 1C). IMs were already present after birth (Figure S1B), expressed low levels of CCR2, and were found in similar numbers in 6- to 10-week-old *Ccr2*$^{-/-}$, *Nr4a1*$^{-/-}$, and WT mice (Figure 1D). However, their numbers were significantly lower in 1-year-old *Ccr2*$^{-/-}$ mice than in age-matched controls (Figure S1C), suggesting that IMs represent a heterogeneous population and are partially maintained by classical monocytes in adults, as reported by others (Tan and Krasnow, 2016). To test this, we sutured $CD45.1^+$ WT and $CD45.2^+$ *Ccr2*$^{-/-}$ mice together for 6 months and analyzed the enrichment in WT partner cells within the *Ccr2*$^{-/-}$ host (Figure S1D). Parabiotic mice efficiently exchanged their circulation, as attested by the percentage of enrichment in blood B cells that

Figure 1. Identification of Monocyte and Macrophage Populations in the Mouse Lung

(A) Gating strategy.

(B) Photographs of FACS-sorted populations gated in (A).

(C and D) Surface phenotype (C) and absolute numbers (D) of the indicated populations in the lungs of WT (C and D), *Ccr2*$^{-/-}$ (D), and *Nr4a1*$^{-/-}$ (D) mice.

(E) Percentage of IL-10^+ cells within the cell populations as assessed by detection of 450 nm florescence (blue product) in CCF4-substrate-loaded cells isolated from IL-10-β-lactamase reporter ITIB or WT mice.

(F) Basal IL-10 concentration in culture supernatants of primary cell culture.

(G) Experimental outline for data in (H).

(H) Absolute numbers of the indicated populations in the lungs of WT and *Ccr2*$^{-/-}$ mice treated with i.v. PBS-Lips or Clo-Lips.

(I) Representative anti-Ly-6C immunostainings of lung sections from Clo-Lip-treated WT mice and *Ccr2*$^{-/-}$ mice.

Data in (A)–(C) and (I) represent one of at least six mice from at least three independent experiments. Data in (D) and (H) show the mean + SEM pooled from three independent experiments (n = 6–10 per group). Data in (E) and (F) show the mean + SEM from one of three independent experiments (n = 3–4 per group). p values were calculated with a one-way (D–F) or two-way (H) ANOVA followed by Tukey's post hoc tests (*$p < 0.05$; **$p < 0.01$; ***$p < 0.001$; ns, not significant). Scale bars, 10 μm. See also Figure S1 for additional information regarding the phenotype, localization, and IL-10 production by lung monocytes and macrophages.

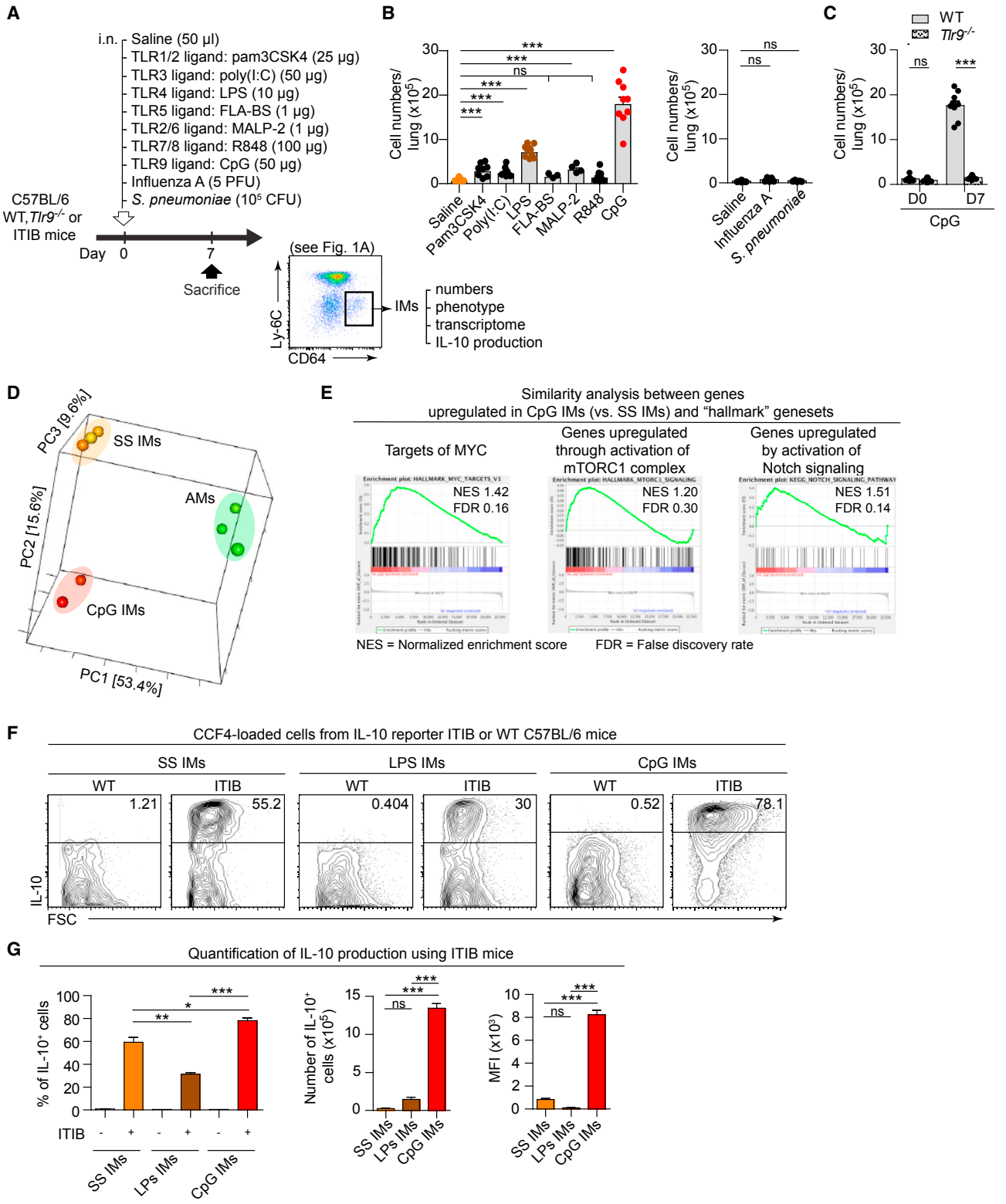


Figure 2. TLR9-Dependent Expansion of IL-10-Producing IMs upon Intranasal CpG Treatment

(A) Experimental outline.

(B and C) Absolute numbers of IMs in the lungs of WT mice 7 days after i.n. stimulation with the indicated TLR ligands or i.n. infection with influenza A or *S. pneumoniae* (B) and *Tlr9*$^{-/-}$ and control mice before and 7 days after i.n. injection of CpG (C). Data show mean + SEM and are pooled from three independent experiments (n = 6–12 per group).

(legend continued on next page)

reached 50%. Conversely, because CCR2 is required for the egress of classical monocytes from the BM, WT monocytes constituted more than 90% of the monocytes present in the blood of *Ccr2*$^{-/-}$ mice. Lung AMs were not enriched in WT cells, confirming that AMs can self-renew by local proliferation at steady state (Hashimoto et al., 2013). However, 35% of the IM pool was constituted by WT partner cells after 6 months of parabiosis, strongly supporting that IMs are, at least in part, replenished by circulating blood monocytes in adults, a feature shared with gut macrophages (Bain et al., 2014).

IMs constitutively expressed IL-10, as quantified in vivo by the use of IL-10-β-lactamase reporter ITIB mice (Bouabe et al., 2011) and ex vivo by ELISA (Figures 1E and 1F; Figure S1E). Notably, a spontaneous IM-derived IL-10 production was dependent on the adaptor molecule MYD88 but independent of TLR9 (Figure S1F), concordant with the fact that LPS, which mediates signaling through MYD88, sustains IM-derived IL-10 at steady state (Bedoret et al., 2009). Upon CpG or LPS stimulation, the increased ability of IMs to produce IL-10 relied on TLR9 and MyD88 or only MyD88, respectively (Figure S1F).

When applied to the lungs during HDM-induced airway allergy, the flow cytometry strategy identified similar cell populations (Figure S1G).

To determine which cells were truly located in the lung tissue, we depleted blood-vessel-associated monocytes and macrophages by injecting clodronate-containing liposomes (Clo-Lips) intravenously 24 hr before analysis (Figure 1G). This regimen had no effect on AMs or IMs but efficiently depleted patrolling monocytes and a substantial part (≈60%) of Ly-6C^{hi} monocytes (Figure 1H), showing that most monocytes, except some Ly-6C^{hi} monocytes, were associated with the lung vasculature. Concordant with this, combined in vivo and ex vivo anti-CD45 stainings confirmed that AMs, IMs, and only a fraction of Ly-6C^{hi} monocytes were truly located in the lungs of WT mice (Figures S1H and S1I). Anti-Ly-6C immunostaining of lung sections from Clo-Lip-treated WT and *Ccr2*$^{-/-}$ mice confirmed that the Ly-6C^{+} cells were located in the lung parenchyma (Figure 1I). Notably, in *Ccr2*$^{-/-}$ mice, Clo-Lip injection did not affect the amount of Ly-6C^{hi} monocytes, whose numbers and localization were similar to those from Clo-Lip-treated WT mice (Figures 1H and 1I), indicating that these monocytes established in the lung independently of CCR2. In the following sections, we refer to these CCR2-independent, lung-infiltrating monocytes, which were already present at the age of 3 days (Figure S1J), as lung monocytes. To assess whether lung monocytes represented a monocyte population distinct from classical CCR2-dependent blood monocytes, we performed a transcriptomic comparison of Ly-6C^{hi} monocytes recovered from perfused lung of WT mice (≈60% of CCR2-dependent classical blood monocytes and ≈40% of lung monocytes) and *Ccr2*$^{-/-}$ mice (more than 95% of lung monocytes). This analysis revealed only one differentially expressed gene, namely *Ccr2* (Figures S1K and S1L), showing that lung monocytes fully corresponded to classical Ly-6C^{hi} monocytes.

CpG Induces TLR9-Dependent IM Expansion

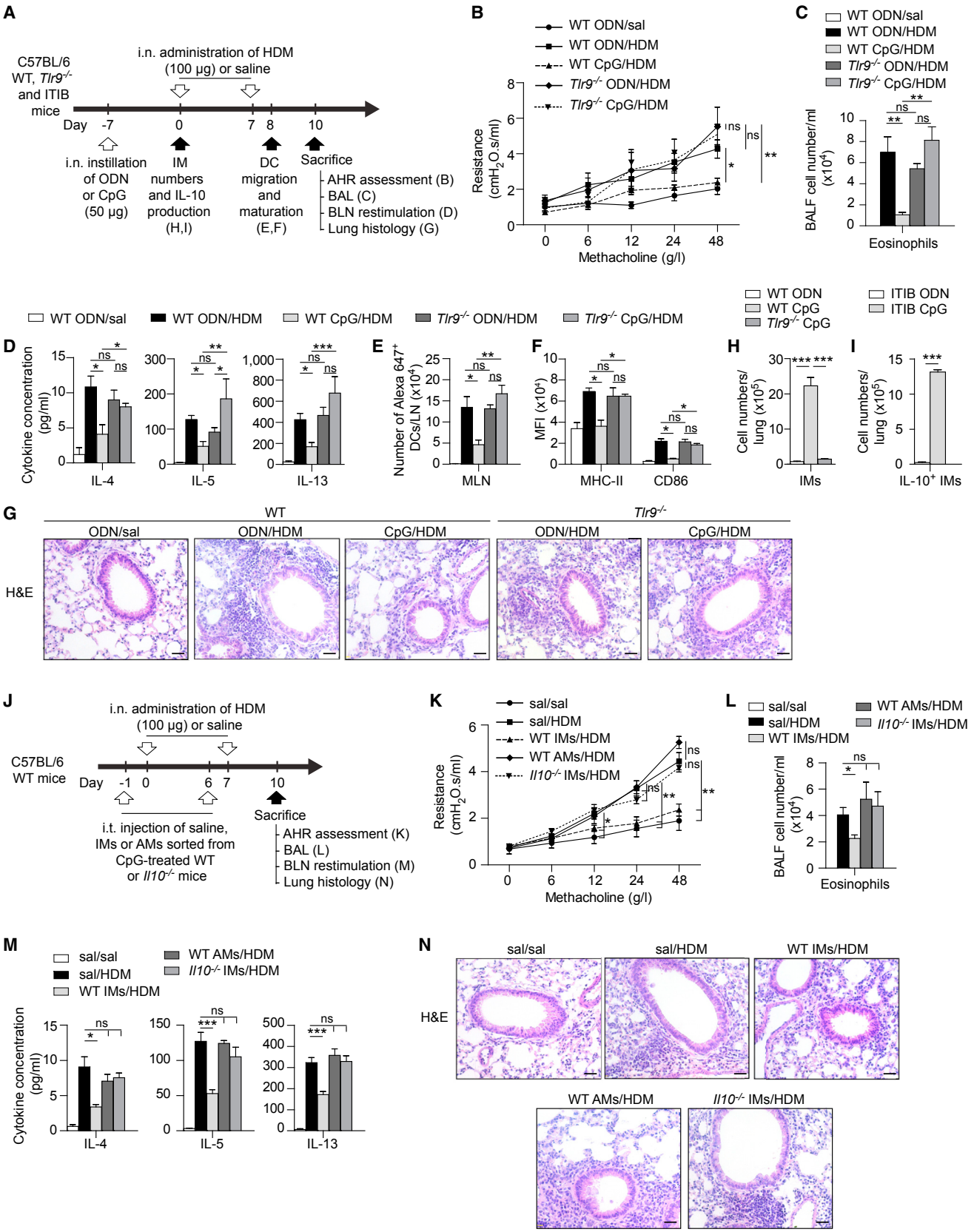
We hypothesized that exposure to certain PAMPs, such as LPS or CpG, might protect against asthma by enhancing the immunosuppressive potential of IMs. First, we confirmed expression of most TLRs on IMs (Figure S2A) and assessed how local exposure to PAMPs, especially TLR ligands, or a local infection would quantitatively affect IMs (Figure 2A; Figure S2B). Although several PAMPs, including LPS, were able to significantly expand IMs, CpG was by far the most potent in increasing IM numbers 1 week after a single intranasal (i.n.) exposure (42.5-fold with an average of 1.7×10^6 cells) (Figure 2B; Figure S2C), a phenomenon that was dependent on signaling through TLR9 (Figure 2C). Such expansion persisted up to 8 weeks after treatment, was also observed to a lesser extent when CpG was administered by a systemic route, and was associated with the presence of a small fraction of CpG IMs into the BALF (Figures S2D–S2G). Conversely, pulmonary infection with *Influenza A virus* (PR8) or *Streptococcus pneumoniae* did not have any significant effect on IM numbers 7 days after infection (Figure 2B). Of note, AM counts remained unchanged after CpG treatment and were moderately increased after LPS treatment (Figures S2H and S2I).

We compared gene expression profiles between CpG IMs and steady-state IMs (SS IMs). Principal-component analysis (PCA) revealed that CpG IMs clustered more closely with SS IMs than with AMs (Figure 2D), but 285 genes were differentially regulated between CpG IMs and SS IMs (fold change > 2, $p < 0.01$). Among genes upregulated in CpG IMs, gene-set enrichment analysis (GSEA) revealed a significant enrichment of genes implicated in macrophage activation and differentiation, such as targets of c-MYC (Aziz et al., 2009) or genes upregulated by activation of mTORC1 or NOTCH signaling (Covarrubias et al., 2016; Monsalve et al., 2009) (Figure 2E).

Protein expression of several surface markers was comparable between CpG IMs and SS IMs, except for CD11b and CD115, which were upregulated in CpG IMs, and for CD62L, SiglecF, and CD169, which were downregulated (Figure S2J).

Functionally, in comparison with SS IMs, CpG IMs exhibited a hypersuppressive profile. Indeed, the percentage of IL-10^{+} cells within CpG IMs was increased, leading to a 55-fold increase in the numbers of IL-10-producing IMs upon CpG treatment (Figures 2F and 2G). Furthermore, the level of IL-10 expression within CpG IMs was substantially greater than that in SS IMs (Figures 2F and 2G), leading to a global 550-fold increase in

(D) PCA comparing SS IMs, CpG IMs, and AMs. Percentages indicate the variability explained by each component.
(E) GSEA between CpG IMs and defined gene sets.
(F) Density plots showing IL-10 expression of IMs as assessed by detection of 450 nm fluorescence (blue product) in CCF4-substrate-loaded cells isolated from IL-10-β-lactamase reporter ITIB or WT mice. Numbers indicate the percentage of IL-10^{+} cells within the population, quantified in (G).
(G) Percentages (left), numbers (middle), and geometric mean fluorescence intensity (MFI, right) of IL-10^{+} cells within the cell populations. Data show the mean + SEM and represent one of two independent experiments (n = 3–4 per group).
p values were calculated with a one-way (B and G) or two-way (C) ANOVA followed by Tukey's post hoc tests (*$p < 0.05$; **$p < 0.01$; ***$p < 0.001$; ns, not significant). Abbreviations: D, day; PFU, plaque-forming units; and CFU, colony-forming units. See also Figure S2 for additional information regarding IM numbers, localization, phenotype, and AM numbers.



(legend on next page)

the amount of IM-derived IL-10 expressed in the lungs after CpG treatment. LPS stimulation did not promote such an enhanced suppressive profile (Figures 2F and 2G).

All together, our data show that IMs specifically expanded in response to CpG exposure and that CpG IMs acquired distinct transcriptomic, phenotypic, and functional features.

CpG-Induced IMs Prevent Allergic Sensitization to Inhaled Allergens

We wondered whether the hypersuppressive profile of CpG IMs might contribute to the protective effects of CpG on asthmatic sensitization. First, we developed a mouse model of asthma prevention by CpG, during which WT mice were intranasally exposed to CpG 7 days before two weekly i.n. instillations of 100 μg HDM (Figure 3A). This regimen of HDM exposure bypassed the regulatory functions of SS IMs, given that 100% of HDM-exposed WT mice developed airway hyperreactivity (AHR), BALF eosinophilia, HDM-specific lymph node (LN) Th2 responses, peribronchial inflammation, and increased mucus production, as well as increased activation of lung DCs and enhanced DC migration to the LNs (Figures 3B–3G; Figures S3A and S3B). In this model, CpG pre-exposure promoted robust expansion of IL-10-producing CpG IMs (Figures 3H and 3I) and protected WT mice, but not *Tlr9*$^{-/-}$ mice, from HDM-induced asthmatic features and DC activation (Figures 3B–3G; Figures S3A and S3B).

Second, to test whether CpG IMs were sufficient to confer such protection, we performed adoptive-transfer experiments (Figure 3J). AHR, eosinophilia, HDM-specific Th2 responses, lung inflammation, and mucus production were significantly reduced when CpG IMs sorted from lungs of CpG-treated WT mice were transferred before HDM exposures (Figures 3K–3N; Figures S3C and S3D). Such protection was specific to CpG IMs and relied on CpG-IM-derived IL-10, given that transfer of WT AMs or *Il10*$^{-/-}$ CpG IMs failed to improve the characteristic features of asthma (Figures 3J–3N; Figures S3C and S3D).

These results demonstrate that IL-10-producing IMs were essential for the protective effects of CpG against sensitization to inhaled allergens.

CpG-Induced IMs Mediate the Immunotherapeutic Effects of CpG on Established Asthma

CpG has already proven its efficacy in attenuating established asthma in animal models and in human clinical trials. Here, we developed a model of immunotherapy based on CpG treatment of HDM-sensitized WT mice before HDM challenge (Figure 4A).

CpG was more potent in expanding IL-10-producing CpG IMs and in decreasing AHR, eosinophilic inflammation, HDM-specific Th2 responses, mucus production, and DC activation than in sham-treated asthmatic counterparts, features that were not observed in *Tlr9*$^{-/-}$ mice (Figures 4B–4I; Figures S4A and S4B). Moreover, CpG IMs were sufficient to confer protection, given that adoptive transfer of CpG IMs before HDM challenge markedly decreased airway allergy in HDM-sensitized mice, an effect that was not observed when WT AMs or *Il10*$^{-/-}$ CpG IMs were transferred (Figures 4J–4N; Figures S4C and S4D). Importantly, the expansion of IL-10-producing IMs and the immunotherapeutic effects of CpG persisted up to 8 weeks after CpG treatment (Figures S4E–S4L). Moreover, similar CpG-induced IM-mediated protection was observed in an asthma model based on systemic sensitization with ovalbumin and alum (Figures S4M–S4Q).

CpG Expands IMs Mainly from CCR2-Independent Monocytes

Given the crucial contribution of CpG IMs to asthma prevention and treatment in our models, we sought to determine the origin of these macrophages. In adult tissues, macrophages are maintained or expanded by local proliferation or differentiation from CCR2-dependent BM-derived classical monocytes (Ginhoux and Guilliams, 2016).

First, to assess the proliferative ability of IMs, we analyzed the incorporation of EdU by IMs after CpG treatment. CpG exposure did not increase the percentage of EdU^{+} IMs at the time points analyzed, providing no support for local proliferation of IMs after CpG treatment (Figure 5A).

Second, we quantified the numbers of CpG IMs in *Ccr2*$^{-/-}$ mice. Surprisingly, CpG IM numbers were only slightly decreased in *Ccr2*$^{-/-}$ mice (Figure 5B), whereas LPS IM numbers were robustly reduced (Figure S5A), supporting the idea that CpG IMs, unlike LPS IMs, developed mostly from monocytes that were recruited independently of the BM. To test this, we used mixed BM competitive CD45.1/2 chimeras engrafted with CD45.1^{+} WT and CD45.2^{+} *Ccr2*$^{-/-}$ BM cells (Figure 5C). 8 weeks after reconstitution, >85% of blood Ly-6C^{hi} monocytes were of CD45.1^{+} WT origin, whereas B lymphocytes and neutrophils had a 1:1 ratio of CD45.1^{+} WT to CD45.2^{+} *Ccr2*$^{-/-}$ cells (Figures 5D and 5E). 8 and 12 weeks after reconstitution, the numbers of lung AMs and IMs were comparable with those before irradiation (Figures S5B and S5C) and originated mainly from CD45.1^{+} WT donor cells, showing that the depleted niches were repopulated by CCR2-dependent classical monocytes after irradiation (Figures 5D–5F). 7 days after CpG treatment, BM-competitive chimeras exhibited increased IM numbers (Figures S5B and S5C), and this expansion was associated with a drastic enrichment of CD45.2^{+} *Ccr2*$^{-/-}$ donor

Figure 3. Contribution of CpG IMs to the Prevention of Experimental Asthma

(A–I) Experimental outline (A), dynamic airway resistance upon methacholine inhalation (B), BALF eosinophil counts (C), cytokine concentrations in culture supernatants of bronchial LN (BLN) cells restimulated with HDM (D), quantification of lung DC migration to the BLN (E) and expression of MHC-II and CD86 at day 8 (F), H&E staining of lung sections (G), and numbers of CpG IMs (H) and IL-10^{+} CpG IMs (I) at day 0.

(J–N) Experimental outline (J), dynamic airway resistance upon methacholine inhalation (K), BALF eosinophil counts (L), cytokine concentrations in culture supernatants of BLN cells restimulated with HDM (M), and H&E staining of lung sections (N).

Data show the mean + SEM (B and K) or mean + SEM and are pooled from at least three independent experiments (n = 6–16 per group) (C–F, H, I, L, and M) or represent one of two independent experiments (n = 4 per group) (H and I). p values were calculated with one-way ANOVA followed by Tukey's post hoc tests (B–F, H, and K–M) or a two-tailed Student's t test (I) (*$p < 0.05$; **$p < 0.01$; ***$p < 0.001$; ns, not significant). Data in (G) and (N) represent one of at least six mice from at least two independent experiments. Scale bars, 32 μm. See also Figure S3 for periodic-acid-Schiff (PAS) stainings.

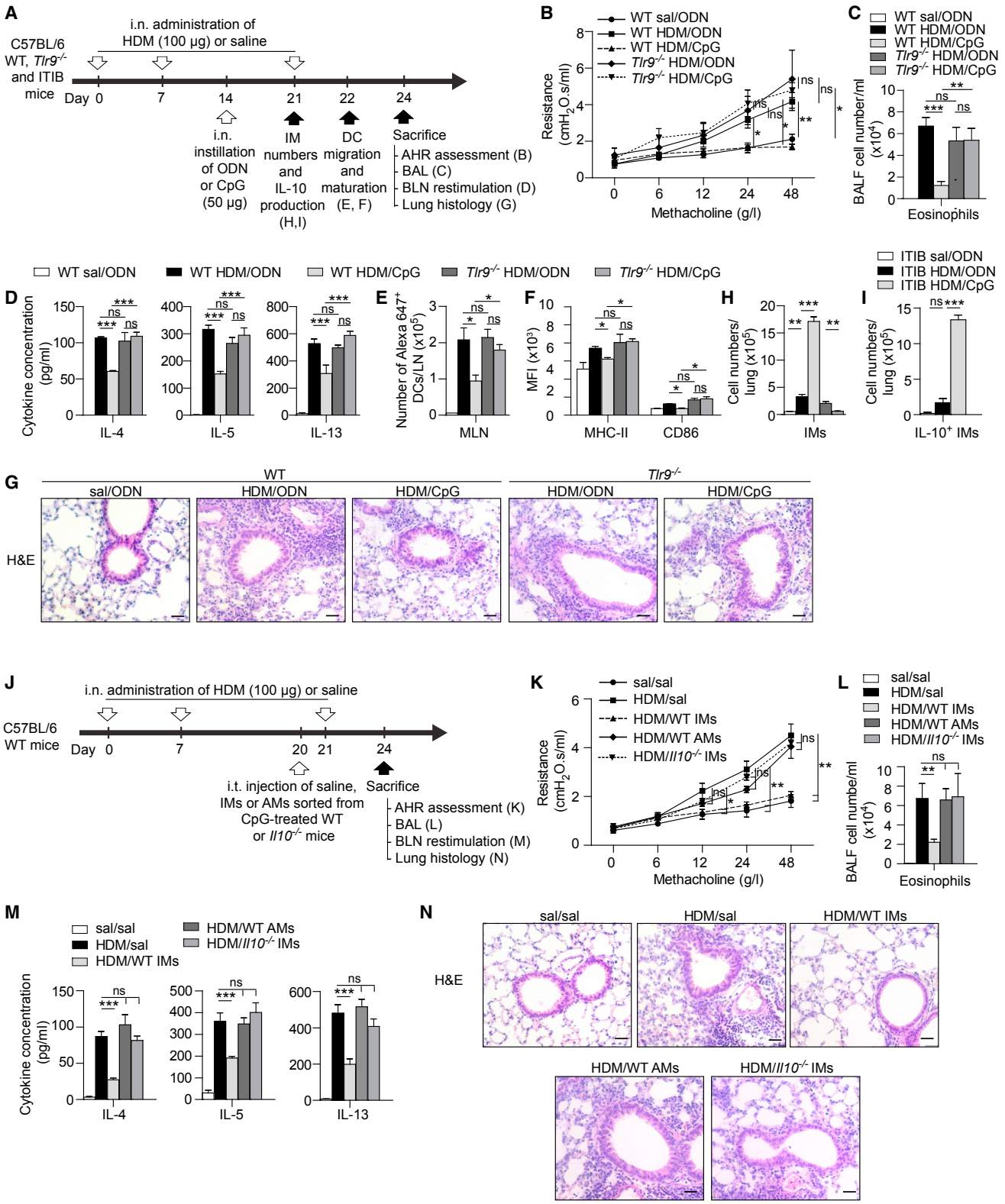


Figure 4. Contribution of CpG IMs to the Treatment of Experimental Asthma

(A–I) Experimental outline (A), dynamic airway resistance upon methacholine inhalation (B), BALF eosinophil counts (C), cytokine concentrations in culture supernatants of BLN cells restimulated with HDM (D), quantification of lung DC migration to the BLN (E) and expression of MHC-II and CD86 at day 22 (F), H&E staining of lung sections (G), and numbers of CpG IMs (H) and IL-10$^+$ CpG IMs (I) at day 21.

(legend continued on next page)

cells to the level of that observed in blood B lymphocytes, namely 100% of CCR2 independence when mice were analyzed at 12 weeks of age (Figures 5D–5F). These results demonstrate that CpG IMs mainly arose from CCR2-independent precursors. Notably, when chimeric mice were exposed to LPS, IM chimerism was not substantially affected and was similar to that of blood Ly-6C^{hi} monocytes, demonstrating that LPS IMs arose from BM-derived classical monocytes (Figures S5D and S5E).

All together, these results support that CpG IMs neither expanded through local proliferation nor substantially differentiated from CCR2-dependent BM-derived classical monocytes but instead mainly originated from CCR2-independent cells.

Lung and Splenic Monocytes Are the Precursors of CpG IMs

Earlier in this article, we defined lung monocytes as CCR2-independent classical monocytes infiltrating the lung parenchyma (Figure 6A). Given that IM expansion upon CpG sensing was mainly independent of CCR2, we hypothesized that lung monocytes could act as a local reservoir for CpG IMs.

First, we validated the CCR2 independence of lung monocytes by conducting parabiosis and mixed-BM-chimera experiments. CD45.1^{+} WT and CD45.2^{+} *Ccr2*$^{-/-}$ mice exchanged their circulation for 6 months, and the enrichment of WT and *Ccr2*$^{-/-}$ partner cells within the *Ccr2*$^{-/-}$ and WT hosts, respectively, was analyzed 24 hr after intravenous (i.v.) Clo-Lip treatment (Figure 6B). Notably, for lung monocytes, a comparable enrichment of partner cells was observed in WT and *Ccr2*$^{-/-}$ hosts (Figure 6B), indicating that these cells were continually replenished by circulating cells independently of CCR2. In BM-reconstituted competitive chimeras, lung monocytes were also repopulated with CCR2-independent engrafted cells, consistent with our findings in parabiotic mice (Figures 6C–6E; Figures S6A and S6B).

Our data so far are consistent with the idea that a precursor-product relationship could exist between lung monocytes and CpG IMs. When we analyzed the kinetics of the appearance of CpG IMs in vivo, we observed a differentiation pattern from Ly-6C^{hi}CD64^{lo} to Ly-6C^{lo}CD64^{hi} cells in both WT and *Ccr2*$^{-/-}$ mice (Figure 6F). With the progressive acquisition of CD64 and the subsequent loss of Ly-6C, the Ly-6C/CD64 plot looked like a waterfall (arrows in Figure 6F), suggesting that lung monocytes might give rise to CpG IMs.

Next, we tested whether lung monocytes could respond to CpG and differentiate into IM-like cells ex vivo. Lung monocytes sorted via fluorescence-activated cell sorting (FACS) expressed higher levels of *Tlr9* than did AMs or IMs (Figure 6G) and were able to respond to CpG, as shown by increased phosphorylation of Erk kinase (Häcker et al., 1999) (Figure 6H). Ex vivo CpG treatment of lung monocytes promoted their survival and triggered the same waterfall over time as in vivo treatment did (Figures 6I and 6J), a phenomenon that was dependent on TLR9 (Figure S6C). Of note, this waterfall was not observed in LPS-stimulated lung monocytes (Figure S6D). Our data thus support that lung monocytes can differentiate into CpG IMs. Nevertheless, the quantity of lung Ly-6C^{hi} cells and CpG IMs 1 and 7 days after CpG treatment, respectively (Figures 6K and 5B), largely exceeded the number of lung monocytes present at steady state (Figure 1H). We thus tested whether such lung monocytes were able to proliferate in situ, but no increase in EdU incorporation was detected 1 day after CpG treatment (Figure 6L; Figure S6E), when their numbers were >10-fold higher than on day 0 in both WT and *Ccr2*$^{-/-}$ mice (Figure 6K). Of note, after LPS treatment, this increased number of Ly-6C^{hi} cells was seen only in WT mice and not in *Ccr2*$^{-/-}$ mice, adding further support to the BM origin of LPS IMs (Figure S6F). These results suggest that, specifically upon CpG stimulation, additional CCR2-independent monocytes were recruited from a distal reservoir and differentiated into CpG IMs.

Interestingly, the spleen has been shown to constitute a reservoir of CCR2-independent monocytes, which were already present in 3-day-old mice (Figure S7A) and which can migrate to inflammatory tissues in an angiotensin II type 1 (AT-1)-receptor-dependent manner (Swirski et al., 2009). Splenic monocytes expressed higher levels of *Tlr9* than did AMs (Figure 7A), and, like for lung monocytes, ex vivo CpG stimulation promoted their survival and differentiation into CpG-IM-like cells (Figure 7B), showing that they can respond to CpG. Notably, 1 day after i.n. CpG treatment, splenic monocyte numbers were significantly decreased, which was associated with an increase in Ly-6C^{hi} monocytes in the lungs of both WT mice and mice lacking AT-1 receptor (*Agtr1a*$^{-/-}$) (Figures 7C and 7D). To assess the exact contribution of splenic monocytes to the pool of lung monocytes and CpG IMs, we quantified their numbers 1 and 7 days after CpG treatment, respectively, in splenectomized *Ccr2*$^{-/-}$ mice. As shown in Figures 7E and 7F, the pools of lung monocytes and CpG IMs were significantly reduced when the spleen was absent. SS IM numbers were unaffected by splenectomy (Figure 7F). Thus, the spleen constitutes a reservoir of monocytes that can seed the lung independently of angiotensin signaling and differentiate into CpG IMs.

Of note, when injected subcutaneously in *Ccr2*$^{-/-}$ mice, CpG induced recruitment of monocytes not only in the lung but also in other organs such as the heart and liver. However, except in the lung, this was not associated with an increase in macrophage numbers 7 days later. Conversely, i.n. CpG injection in *Ccr2*$^{-/-}$ mice promoted the recruitment of monocytes in the lung, but not in the heart or liver (Figures 7G and 7H). All together, these data suggest that CpG could mobilize CCR2-independent monocytes but that additional lung-specific signals directed their seeding into the lung and their differentiation into regulatory IMs.

(J–N) Experimental outline (J), dynamic airway resistance upon methacholine inhalation (K), BALF eosinophil counts (L), cytokine concentrations in culture supernatants of BLN cells restimulated with HDM (M), and H&E staining of lung sections (N).

Data show the mean + SEM (B and K) or mean + SEM and are pooled from at least three independent experiments (n = 6–16 per group) (C–F, H, I, L, and M) or represent one of two independent experiments (n = 4 per group) (H and I). p values were calculated with one-way ANOVA followed by Tukey's post hoc tests (*$p < 0.05$; **$p < 0.01$; ***$p < 0.001$; ns, not significant). Data in (G) and (N) represent one of at least six mice from at least two independent experiments. Scale bars, 32 μm. See also Figure S4 for PAS stainings, the long-term therapeutic model, and the assessment of the protective effects of CpG IMs in an ovalbumin and alum model.

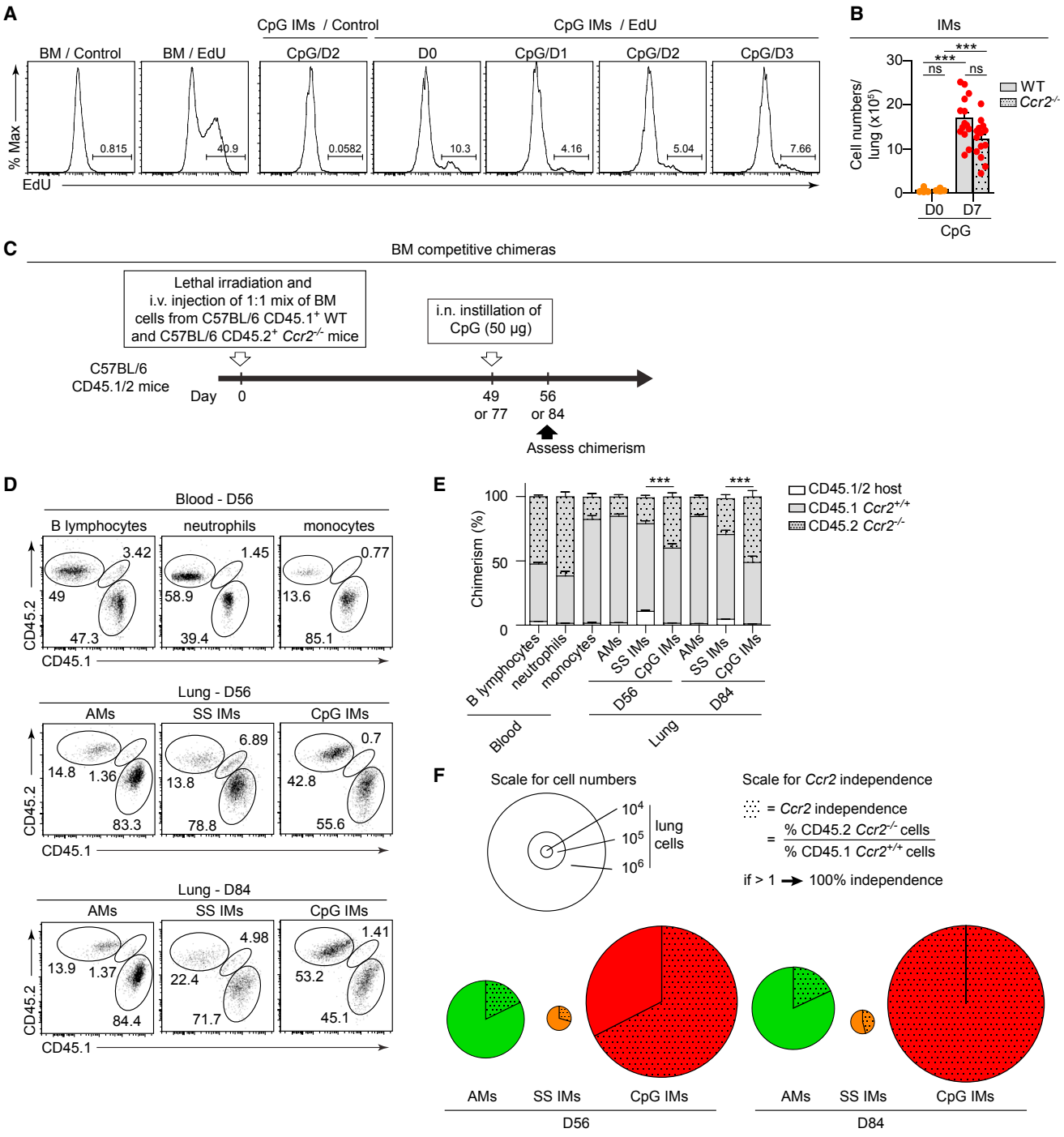


Figure 5. Level of Dependence of CpG IMs on CCR2

(A) IM incorporation of i.p. EdU injection 24 hr before each time point was assessed at day 0 and 1, 2, or 3 days after i.n. CpG treatment of WT mice. BM cells were used as controls. Numbers indicate the percentage of EdU^+ cells. Results represent one of at least five mice from two independent experiments.

(B) Absolute numbers of IMs in the lungs of WT and $Ccr2^{-/-}$ mice before and 7 days after i.n. CpG treatment (50 µg).

(C) Experimental outline for experiments using mixed BM competitive chimeras shown in (D)–(F).

(D) Dot plots showing the percentage of WT and $Ccr2^{-/-}$ BM-derived cells and host radio-resistant cells within the indicated populations.

(E) Percentage of BM chimerism and radio-resistance of the indicated populations.

(F) Pie charts depicting the average absolute cell number (surface area) and the CCR2 independence (dotted area) in the indicated cell populations.

(legend continued on next page)

In an attempt to identify the chemokines involved in splenic monocyte recruitment, we performed a chemokine array on lung extracts and found that CpG instillation induced increased levels of several chemokines, an effect that was, however, also observed with LPS (Figures 7I and 7J). Among those chemokines, CCL2 (MCP-1), CCL5 (RANTES), and CCL9 (MIP-1γ) were not only the most prominent ones but also the ones whose receptors (i.e., CCR2, CCR5, and CCR1, respectively) were the most expressed in Ly-6C^{hi} monocytes (Figures 7I–7K). To assess the potential role of these chemokines, we used neutralizing antibodies in vivo. Individual or combined inhibition of CCL2, CCL5, and CCL9, however, did not influence the numbers of lung monocytes in *Ccr2*$^{-/-}$ mice 1 day after CpG treatment (Figures S7B–S7D), suggesting that splenic monocytes were attracted to the lung independently of those signals.

DISCUSSION

We have shown that IMs substantially expanded in response to CpG, which, unlike LPS, has demonstrated consistent anti-allergic effects in humans and animals (Beeh et al., 2013; Broide et al., 1998; Creticos et al., 2006; Krieg, 2006; Sur et al., 1999). Not only were CpG IMs 42 times more numerous than SS IMs, but their overall IL-10 production was also increased 550-fold. This increased regulatory capacity of CpG IMs was associated with protection against asthma sensitization and exacerbation in experimental models in which the suppressive activity of SS IMs was overcome. Using WT mice adoptively transferred with WT or *Il10*$^{-/-}$ CpG IMs and *Tlr9*$^{-/-}$ mice, in which CpG-mediated IM expansion was abolished, we further demonstrated that CpG IMs were not only necessary but also sufficient for mediating the protective effects of CpG through the production of IL-10. Finally, we showed that the number of CpG IMs remained elevated for at least 8 weeks after CpG administration, which, in addition to the fact that CpG has been reported to induce sustained epigenetic modifications in macrophages (Ostuni et al., 2013), could account for the long-lasting innate effects of CpG. Given that SS IMs exert their suppressive activity by inhibiting maturation and migration of lung DCs (Bedoret et al., 2009), which are essential for both development and restimulation of Th2 cells (Lambrecht et al., 2000; van Rijt et al., 2005), and that DC activation was dampened in CpG-treated HDM-challenged mice, we speculate that CpG durably reinforces the ability of IMs to control DC function and, therefore, to break the link between innate and adaptive immunity. This study thus provides a possible mechanism, i.e., induction of hypersuppressive IMs, by which CpG exerts its immunotherapeutic effects in animals and humans and by which exposure to the environmental microbiome, especially to farm dust, which is known to be rich in bacterial DNA (Roy et al., 2003), protects from asthma (Braun-Fahrländer et al., 2002; von Mutius, 2016).

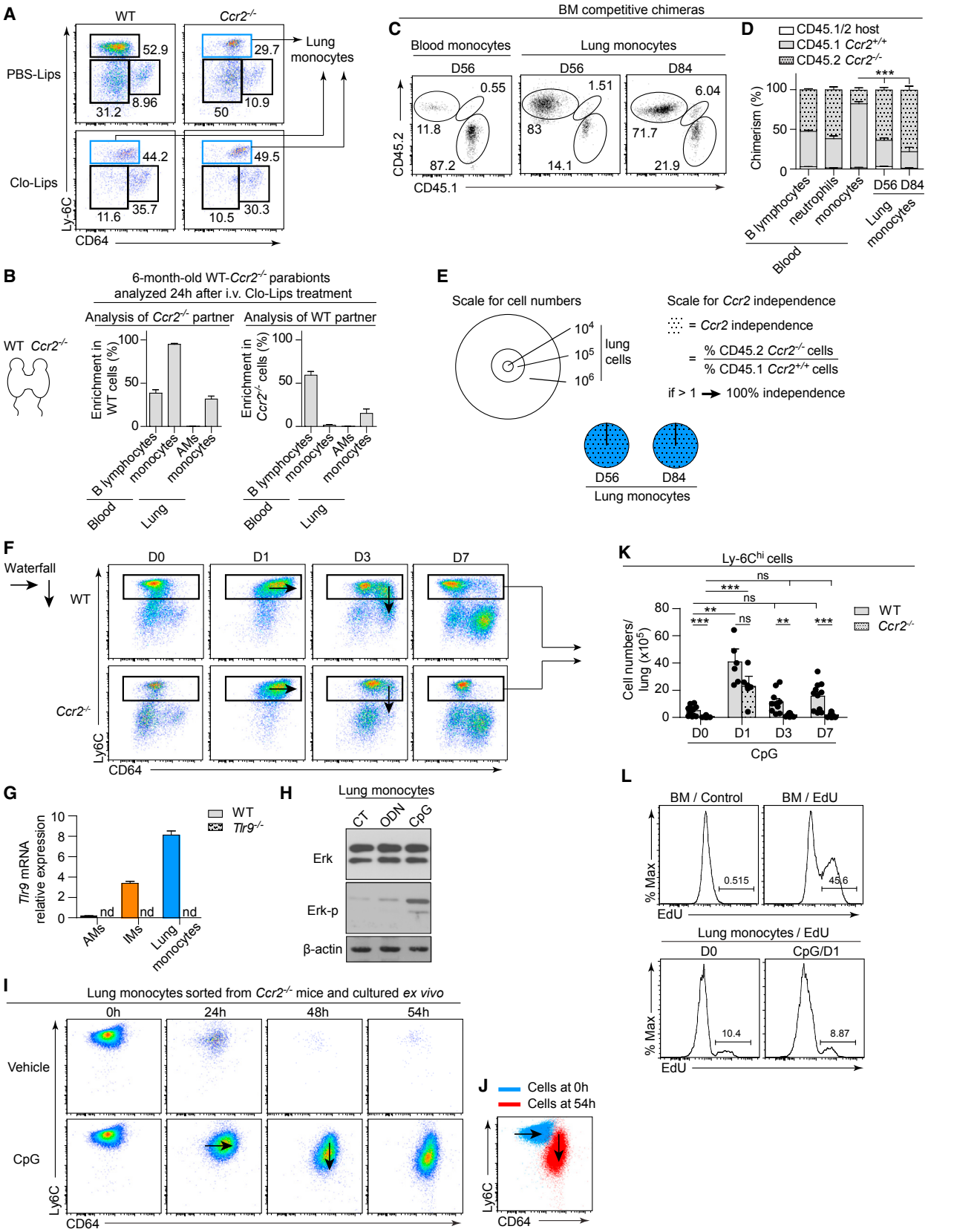
The "mononuclear phagocyte system" model, proposed in 1968 by van Furth and collaborators (van Furth and Cohn, 1968), postulates that tissue-resident macrophages are maintained from a constant supply of blood monocytes that extravasate into tissues. However, this model has been challenged by recent studies demonstrating that, under normal conditions, most macrophages arise from embryonic progenitors and self-renew in tissues throughout adulthood (Ginhoux and Guilliams, 2016; Gomez Perdiguero et al., 2015). The only exceptions are gut, dermis, and heart macrophages that, in accordance with the model of van Furth, rely on the constant recruitment of CCR2-dependent classical monocytes to maintain their population (Bain et al., 2014; Epelman et al., 2014; Tamoutounour et al., 2013). Our data from parabiotic mice support that IMs are also, at least in part, maintained by circulating monocytes in adults, as reported recently (Tan and Krasnow, 2016). During inflammation, macrophages expand through the same mechanisms, namely local proliferation and differentiation from recruited CCR2-dependent BM-derived classical monocytes (Davies et al., 2013). Our results from experiments in *Ccr2*$^{-/-}$, clodronate-treated, chimeric, parabiotic, and splenectomized mice are consistent with an unexpected model in which most CpG IMs can expand from CCR2-independent lung and splenic reservoir monocytes after CpG stimulation. In this model, CpG exerts multiple functions. First, it promotes the mobilization of splenic reservoir monocytes to the lung independently of MCP-1, RANTES, and MIP-1γ. Second, it triggers differentiation of not only these recruited monocytes but also the herein identified CCR2-independent, lung-infiltrating monocytes into IMs with a hypersuppressive profile.

Noteworthy, CpG and LPS appeared to have distinct effects on the recruitment of monocytes to the lung and their differentiation into suppressive IMs. First, CpG induced a substantial mobilization of monocytes from the spleen (i.e., a CCR2-independent reservoir), whereas LPS mainly triggered mobilization from the BM (i.e., a CCR2-dependent reservoir). Second, CpG acted directly on monocytes in vitro to promote their differentiation into macrophages, whereas LPS did not. Third, CpG exposure was able to strikingly increase IM ability to produce IL-10, which was not the case for LPS. Because CpG and LPS are known to act via distinct TLRs, which are expressed at different levels on different structural and immune cells, CpG and LPS most likely induce distinct biological responses in the spleen, BM, lungs, and monocytes themselves, creating a specific microenvironment tailoring IM origin, differentiation, and function.

Given that the numbers of lung reservoir monocytes were identical in WT and *Ccr2*$^{-/-}$ mice, it was tempting to speculate that these cells were different from classical monocytes. However, both cell types had indistinguishable transcriptomes, attesting that lung reservoir monocytes are actually classical monocytes. Although classical monocytes are thought to depend on CCR2 to leave the BM, our results indicate that a fraction of classical monocytes might exit the BM in a CCR2-independent manner to seed the pulmonary and splenic monocyte

(E and F) The percentages of chimerism and of CCR2 independence of blood B lymphocytes, neutrophils (i.e., 50% chimerism and 100% CCR2 independence), and monocytes (i.e., ≈10% chimerism and ≈20% CCR2 independence) were used as controls.

Data in (B) and (E) show the mean + SEM and are pooled from three independent experiments (n = 12–15 per group). p values were calculated with a two-way (B) or one-way (E) ANOVA followed by Tukey's post hoc tests (*p < 0.05; **p < 0.01; ***p < 0.001; ns, not significant). D, day. See also Figure S5 for the CCR2 dependence of LPS IMs and numbers of AMs, SS IMs, LPS IMs, and CpG IMs before irradiation and after BM reconstitution.



(legend on next page)

reservoirs. Identifying the network of chemokine(s) and chemokine receptor(s) orchestrating the traffic of these cells will require additional work.

It has been suggested that the anti-allergic properties of CpG were mediated by plasmacytoid DCs (pDCs), which are known to not only express TLR9 but also play a key role in preventing experimental asthma (de Heer et al., 2004; Krieg, 2006). However, lung pDCs, unlike the other pDC subsets, lack TLR9 expression and therefore cannot account for the role of CpG in regulating lung immune responses (Chen et al., 2006). We have shown here that lung and splenic reservoir monocytes expressed TLR9, which was required for differentiation of CCR2-independent monocytes into IMs after CpG stimulation. Our study thus identifies those reservoir monocytes as the TLR9-expressing cells mediating the immunomodulatory effects of CpG in the lung. Of note, it has been demonstrated that human IMs express TLR9 and are able to increase their production of IL-10 upon bacterial DNA stimulation (Hoppstädter et al., 2010), suggesting that our findings in mice are relevant to humans. Moreover, polymorphisms in the TLR9 promoter region have been associated with an increased risk of asthma development (Lazarus et al., 2003; Smit et al., 2009), supporting the idea that environmental CpG exerts a protective role in humans and that loss of functional TLR9 in human IMs might contribute to asthma development.

In conclusion, our study shows that lung and splenic reservoir monocytes use TLR9 to specifically sense bacterial CpG and massively differentiate into IMs endowed with enhanced anti-allergic properties. These findings are of pathophysiological importance because they provide a possible mechanistic explanation for the hygiene hypothesis and for the protective effects of synthetic CpG in experimental models and human clinical trials. Moreover, they reinforce the idea that therapeutic strategies aimed at ameliorating the inhibitory properties of IMs could help control asthma.

EXPERIMENTAL PROCEDURES

A full description of the experimental procedures can be found in the Supplemental Information.

Mice

WT, *Cx3cr1*$^{GFP/+}$, *Ccr2*$^{-/-}$, *Nr4a1*$^{-/-}$, *Myd88*$^{-/-}$, *Il10*$^{-/-}$, and *Agtr1a*$^{-/-}$ C57BL/6 mice were from the Jackson Laboratory. *Tlr9*$^{-/-}$ and IL-10-β-lactamase reporter (ITIB) mice were generated by others (see Supplemental Information). All mice were used at 6–10 weeks of age unless otherwise indicated. All experimental procedures and protocols were approved by the local ethics committee. Additional information can be found in the Supplemental Information.

Reagents and Antibodies

Mouse non-CpG DNA (ODN, 5′-GCTTGATGACTCAGCCGGAA-3′; reference no. HC4034) and CpG DNA (5′-TCCATGACGTTCCTGATGCT-3′; reference no. HC4033) were from Sanbio. HDM extracts (HDM from *Dermatophagoides farinae*) were from Greer Laboratories. Additional reagents and antibodies are described in the Supplemental Information.

Cell Isolation, Staining, and Flow Cytometry

To obtain single-lung-cell suspensions, we perfused lungs with 10 mL of PBS through the right ventricle, cut them into small pieces, and digested them for 1 hr at 37°C in HBSS containing 1 mg/mL collagenase A (Roche) and 0.05 mg/mL DNase I (Roche). We then enriched single-cell suspensions in mononuclear cells by harvesting cells from the 1.080:1.038 g/mL interface with a density gradient (Easycoll from VWR).

Cell phenotyping and sorting were performed on a FACSCANTO II and a FACSARIA III (BD Biosciences), respectively. Additional information can be found in the Supplemental Information.

Vascular Monocyte and Macrophage Depletion

WT or *Ccr2*$^{-/-}$ mice were injected intravenously with 200 μL of Clo-Lips or empty liposomes (PBS-Lips), and lung cells were harvested 24 hr later.

HDM-Induced Model of Asthma and CpG Treatments

Lightly isoflurane-anesthetized WT, *Tlr9*$^{-/-}$, or ITIB mice were sensitized by two weekly i.n. instillations of vehicle (LPS-free saline) or HDM extracts (100 μg in 50 μL) on days 0 and 7. In experiments shown in Figure 3, mice received i.n. installation of 50 μL saline containing 50 μg ODN or 50 μg CpG 7 days before the first HDM treatment (day −7) and were sacrificed at day 10. In experiments shown in Figure 4, mice received i.n. installation of 50 μL saline containing 50 μg ODN or 50 μg CpG 7 days after the second HDM treatment (day 14). Mice were then challenged by an i.n. instillation of vehicle or HDM (100 μg in 50 μL) and were sacrificed at day 24. For adoptive-transfer experiments, WT mice were transferred intratracheally with 1.5 × 10^6 AMs or CpG IMs sorted from CpG-treated WT or *Il10*$^{-/-}$ mice or with vehicle (50 μL saline) 24 hr before HDM administrations.

Figure 6. CpG-Induced Differentiation of IMs from TLR9-Responsive CCR2-Independent Lung Monocytes

(A) Dot plots of lung-associated classical monocytes (Ly-6C^{hi}), patrolling monocytes (Ly-6C^{lo}CD64^{lo}), and IMs (Ly-6C^{lo}CD64^{hi}) in the indicated groups (same strategy as in Figure 1A). The gate in blue represents lung monocytes. Numbers indicate the percentages of gated cells in the subpopulation.

(B) Analysis of 6-month-old WT *Ccr2*$^{-/-}$ parabionts 24 hr after i.v. Clo-Lip treatment. The percentage of enrichment in partner cells within each host is shown. Bar graphs (mean + SEM) show summary data pooled from two pairs of parabionts.

(C–E) Mixed BM competitive chimeras were analyzed at day 56 or 84, 24 hr after i.v. injection of Clo-Lip. (C) Dot plots showing the percentage of WT and *Ccr2*$^{-/-}$ BM-derived cells and host radio-resistant cells within the indicated populations. (D) Percentage of BM chimerism and radio-resistance of the indicated populations. (E) Pie charts depicting the average absolute cell number and the CCR2 independence (dotted area) in the indicated cell populations.

(F) Waterfall (i.e., differentiation pattern from Ly-6C^{hi}CD64^{lo} to Ly-6C^{lo}CD64^{hi} cells) after i.n. CpG treatment in vivo.

(G) *Tlr9* mRNA expression in AMs, IMs, and lung monocytes sorted from WT or *Tlr9*$^{-/-}$ mice.

(H) Western blot of Erk and phospho-Erk (Erk-p) in lung monocytes sorted from *Ccr2*$^{-/-}$ mice and stimulated ex vivo with saline (CT), ODN, or CpG.

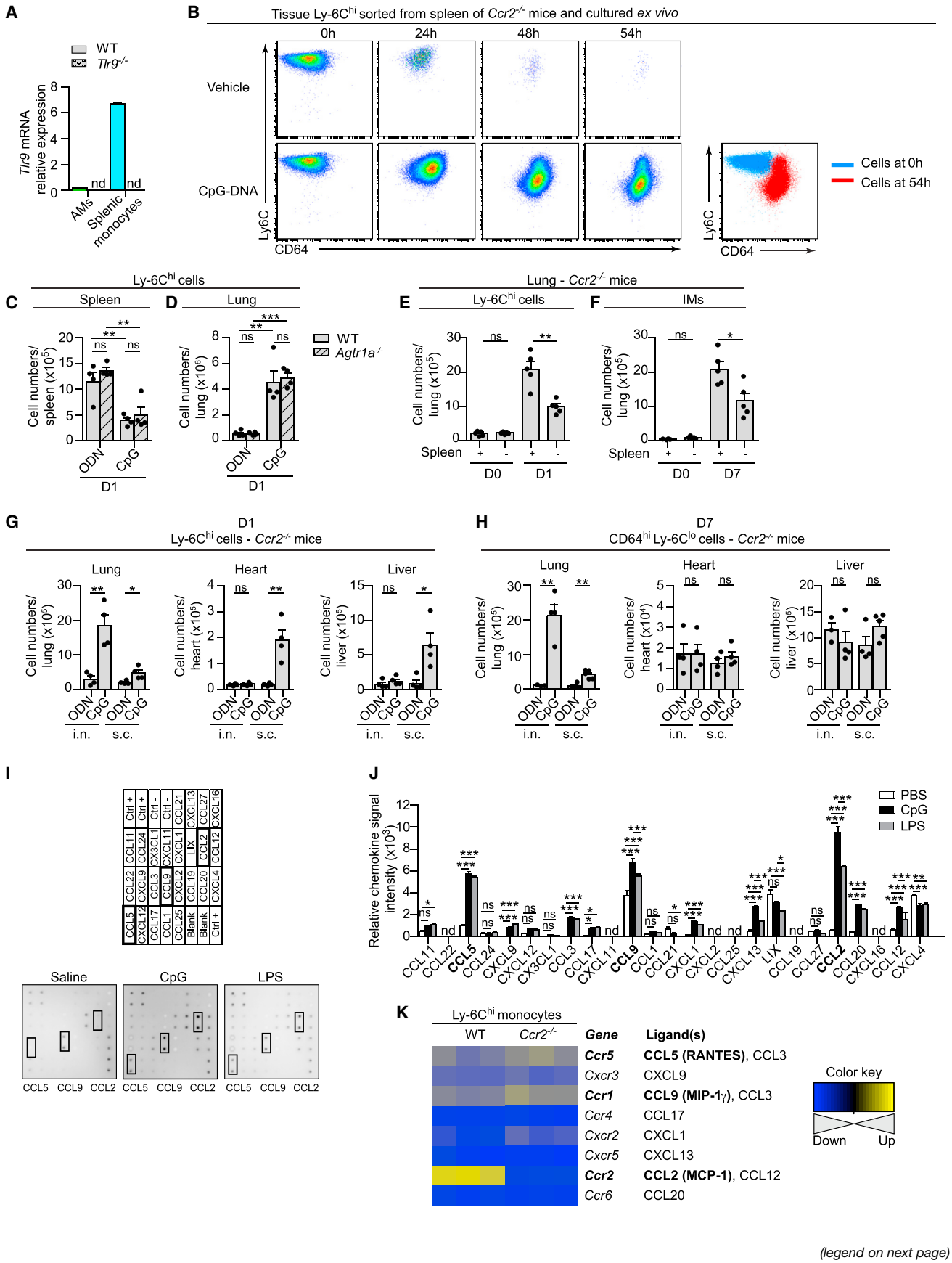
(I) Waterfall of lung monocytes sorted from *Ccr2*$^{-/-}$ mice and stimulated ex vivo with vehicle or CpG.

(J) Superposition of dot plots of living lung monocytes before and 54 hr after stimulation with CpG.

(K) Absolute numbers of lung monocytes in WT and *Ccr2*$^{-/-}$ mice before and 1, 3, and 7 days after i.n. CpG instillation.

(L) Incorporation of i.p. EdU injection 24 hr before was assessed at day 0 and 1 day after i.n. CpG instillation in *Ccr2*$^{-/-}$ mice. WT BM cells were used as controls. Numbers indicate the percentage of EdU$^+$ cells.

Data in (A), (F), (H), (I), and (L) represent one of at least six samples from three independent experiments. Data in (D), (G), and (K) show the mean + SEM and are pooled from three independent experiments (n = 6–15 per group) (D and K) or two independent sorting experiments (n = 4 samples per group) (G). p values were calculated with a one-way (D) or two-way (K) ANOVA followed by Tukey's post hoc tests (*$p < 0.05$; **$p < 0.01$; ***$p < 0.001$; ns, not significant). D, day. See also Figure S6 for numbers of lung monocytes before irradiation and after BM reconstitution, as well as after LPS treatment, and ex vivo differentiation of LPS- or CpG-stimulated lung monocytes from WT or *Tlr9*$^{-/-}$ mice, respectively.



(legend on next page)

We estimated AHR by assessing dynamic airway resistance in anesthetized animals with a FlexiVent small animal ventilator (SCIREQ). Mice were sacrificed, and BALF, lung, and LN cells were harvested and analyzed as described previously (Marichal et al., 2010).

Additional details can be found in the Supplemental Information.

Additional Methods

Methodological details regarding cytologic examination, immunohistochemistry, microarrays, GSEAs, IL-10 detection, generation of mixed BM chimeras and parabiotic mice, EdU incorporation, ex vivo stimulation of tissue monocytes with CpG and LPS, western blot, real-time PCR, splenectomy, chemokine detection, and inhibition are described in the Supplemental Information.

Statistical Analyses

Statistical analyses were performed with R (version 3.2.4). Data from independent experiments were pooled for analysis in each data panel unless otherwise indicated. Raw data were transformed when needed and were back-transformed for graphical presentation. Assumptions of the normal distribution of residuals and homoscedasticity were verified with diagnostic plots. We considered a p value lower than 0.05 to be significant (*$p < 0.05$; **$p < 0.01$; ***$p < 0.001$; ns, not significant).

ACCESSION NUMBERS

The accession number for the microarray data reported in this paper is Array Express: E-MTAB-5012.

SUPPLEMENTAL INFORMATION

Supplemental Information include Supplemental Experimental Procedures and seven figures and can be found with this article online at http://dx.doi.org/10.1016/j.immuni.2017.02.016.

AUTHOR CONTRIBUTIONS

F.B. conceived the project; C.S., C.R., L.F., C.J.D., T.M., and F.B. designed the experiments with help from F.G.; T.M. and F.B. supervised the project; C.S., C.R., and L.F. did most of the experiments and compiled the data; C.F., S.O., and M.T. participated in several experiments; S.C. performed the experiments with parabiotic mice; J.-C.S. provided the *S. pneumonia* clinical isolate; G.P. performed the immunohistochemistry and helped with histological examinations; X.X., D.P., and L.G. performed the microarray analyses; T.M. and L.F. performed splenectomies; H.B. provided the ITIB mice and helped with experiments involving such mice; D.C. and P.Q. made their equipment and facilities available for AHR measurement and microbial infection, respectively; C.S. and L.F. prepared the figures; T.M. and F.B. wrote the manuscript; and all authors provided feedback on the manuscript.

ACKNOWLEDGMENTS

We thank Dr. François Trottein (Institut Pasteur de Lille) for providing *Influenza A virus*; Prof. Hans Nauwynck (Ghent University) for advice; Dr. Natalia Kosovilka from the Stanford PAN facility; Dr. Sandra Ormenese and Raafat Stephan from the Cell Imaging and Flow Cytometry GIGA Platform; Dr. Pierre Drion and other staff members from the Mouse Facility and Transgenics GIGA Platform; Dr. Chantal Humblet from the GIGA Immunohistology Platform; and Raja Fares, Cédric François, and Ilham Sbai for excellent technical and secretarial assistance. The Laboratory of Cellular and Molecular Immunology is supported by the F.R.S.-FNRS for the FRFS-WELBIO under grant CR-2012S-01R, by the Belgian Program on Interuniversity Attraction Poles (IUAP; T-TIME; P7/39), and by an "Action de Recherche Concertée de la Fédération Wallonie-Bruxelles de Belgique" (12/07-03-ITPKC). C.S. and C.R. are research fellows of the F.R.S.-FNRS, L.F. is supported by the FRFS-WELBIO (CR-2012S-01R), T.M. is supported by the Acteria Foundation, and C.D. and T.M. are research associates of the F.R.S.-FNRS.

Received: August 9, 2016
Revised: December 21, 2016
Accepted: January 24, 2017
Published: March 21, 2017

REFERENCES

Aziz, A., Soucie, E., Sarrazin, S., and Sieweke, M.H. (2009). MafB/c-Maf deficiency enables self-renewal of differentiated functional macrophages. Science *326*, 867–871.

Bain, C.C., Bravo-Blas, A., Scott, C.L., Gomez Perdiguero, E., Geissmann, F., Henri, S., Malissen, B., Osborne, L.C., Artis, D., and Mowat, A.M. (2014). Constant replenishment from circulating monocytes maintains the macrophage pool in the intestine of adult mice. Nat. Immunol. *15*, 929–937.

Bedoret, D., Wallemacq, H., Marichal, T., Desmet, C., Quesada Calvo, F., Henry, E., Closset, R., Dewals, B., Thielen, C., Gustin, P., et al. (2009). Lung interstitial macrophages alter dendritic cell functions to prevent airway allergy in mice. J. Clin. Invest. *119*, 3723–3738.

Beeh, K.M., Kanniess, F., Wagner, F., Schilder, C., Naudts, I., Hammann-Haenni, A., Willers, J., Stocker, H., Mueller, P., Bachmann, M.F., and Renner, W.A. (2013). The novel TLR-9 agonist QbG10 shows clinical efficacy in persistent allergic asthma. J. Allergy Clin. Immunol. *131*, 866–874.

Bouabe, H., Liu, Y., Moser, M., Bösl, M.R., and Heesemann, J. (2011). Novel highly sensitive IL-10-beta-lactamase reporter mouse reveals cells of the innate immune system as a substantial source of IL-10 in vivo. J. Immunol. *187*, 3165–3176.

Braun-Fahrländer, C., Riedler, J., Herz, U., Eder, W., Waser, M., Grize, L., Maisch, S., Carr, D., Gerlach, F., Bufe, A., et al.; Allergy and Endotoxin

Figure 7. Mobilization of CCR2-Independent Spleen Reservoir Monocytes to the Lung and Differentiation into CpG IMs

(A) *Tlr9* mRNA expression in splenic monocytes and AMs sorted from WT or $Tlr9^{-/-}$ mice.

(B) Waterfall of splenic monocytes sorted from $Ccr2^{-/-}$ mice and stimulated ex vivo with vehicle or CpG. The right panel shows the superposition of dot plots of living lung monocytes before and 54 hr after stimulation with CpG. Data represent one of at least four samples from two independent experiments.

(C and D) Absolute numbers of Ly-$6C^{hi}$ monocytes in the spleen (C) and lung (D) of WT and $Agtr1a^{-/-}$ mice 1 day after i.n. CpG treatment. Data show the mean + SEM and represent one of two independent experiments (n = 4 per group).

(E and F) Absolute numbers of Ly-$6C^{hi}$ monocytes (E) or IMs (F) in splenectomized and sham-operated mice before (day 0) and 1 day (E) or 7 days (F) after i.n. CpG treatment.

(G and H) Absolute numbers of Ly-$6C^{hi}$ monocytes (G) and Ly-$6C^{lo}CD64^{hi}$ macrophages (H) 1 day (G) and 7 days (H) after i.n. or subcutaneous ODN or CpG treatment of $Ccr2^{-/-}$ mice.

(I and J) Chemokine array was performed on whole lung proteins extracted 8 hr after i.n. PBS, LPS, or CpG treatment of WT mice. (I) Representative blots depicting the detected signals; the boxes show the most induced chemokines. (J) Quantification of chemokine signal intensity.

(K) Heatmap showing gene expression of the receptors for chemokines that were significantly induced by CpG in (J).

Data in (A), (E)–(H), and (J) show the mean + SEM and are pooled from two (A, F–H, and J) or three (E) independent experiments (n = 3–6 per group). p values were calculated with a two-way ANOVA followed by Tukey's post hoc tests (*$p < 0.05$; **$p < 0.01$; ***$p < 0.001$; ns, not significant). Ctrl, control; D, day. See also Figure S7 for the numbers of spleen monocytes in $Ccr2^{-/-}$ mice and in vivo chemokine neutralization experiments.

Study Team (2002). Environmental exposure to endotoxin and its relation to asthma in school-age children. N. Engl. J. Med. *347*, 869–877.

Broide, D., Schwarze, J., Tighe, H., Gifford, T., Nguyen, M.D., Malek, S., Van Uden, J., Martin-Orozco, E., Gelfand, E.W., and Raz, E. (1998). Immunostimulatory DNA sequences inhibit IL-5, eosinophilic inflammation, and airway hyperresponsiveness in mice. J. Immunol. *161*, 7054–7062.

Chen, L., Arora, M., Yarlagadda, M., Oriss, T.B., Krishnamoorthy, N., Ray, A., and Ray, P. (2006). Distinct responses of lung and spleen dendritic cells to the TLR9 agonist CpG oligodeoxynucleotide. J. Immunol. *177*, 2373–2383.

Covarrubias, A.J., Aksoylar, H.I., Yu, J., Snyder, N.W., Worth, A.J., Iyer, S.S., Wang, J., Ben-Sahra, I., Byles, V., Polynne-Stapornkul, T., et al. (2016). Akt-mTORC1 signaling regulates Acly to integrate metabolic input to control of macrophage activation. eLife *5*, e11612.

Creticos, P.S., Schroeder, J.T., Hamilton, R.G., Balcer-Whaley, S.L., Khattignavong, A.P., Lindblad, R., Li, H., Coffman, R., Seyfert, V., Eiden, J.J., and Broide, D.; Immune Tolerance Network Group (2006). Immunotherapy with a ragweed-toll-like receptor 9 agonist vaccine for allergic rhinitis. N. Engl. J. Med. *355*, 1445–1455.

Davies, L.C., Rosas, M., Jenkins, S.J., Liao, C.T., Scurr, M.J., Brombacher, F., Fraser, D.J., Allen, J.E., Jones, S.A., and Taylor, P.R. (2013). Distinct bone marrow-derived and tissue-resident macrophage lineages proliferate at key stages during inflammation. Nat. Commun. *4*, 1886.

de Heer, H.J., Hammad, H., Soullié, T., Hijdra, D., Vos, N., Willart, M.A., Hoogsteden, H.C., and Lambrecht, B.N. (2004). Essential role of lung plasmacytoid dendritic cells in preventing asthmatic reactions to harmless inhaled antigen. J. Exp. Med. *200*, 89–98.

Eder, W., Ege, M.J., and von Mutius, E. (2006). The asthma epidemic. N. Engl. J. Med. *355*, 2226–2235.

Eisenbarth, S.C., Piggott, D.A., Huleatt, J.W., Visintin, I., Herrick, C.A., and Bottomly, K. (2002). Lipopolysaccharide-enhanced, toll-like receptor 4-dependent T helper cell type 2 responses to inhaled antigen. J. Exp. Med. *196*, 1645–1651.

Epelman, S., Lavine, K.J., Beaudin, A.E., Sojka, D.K., Carrero, J.A., Calderon, B., Brija, T., Gautier, E.L., Ivanov, S., Satpathy, A.T., et al. (2014). Embryonic and adult-derived resident cardiac macrophages are maintained through distinct mechanisms at steady state and during inflammation. Immunity *40*, 91–104.

Gautier, E.L., Shay, T., Miller, J., Greter, M., Jakubzick, C., Ivanov, S., Helft, J., Chow, A., Elpek, K.G., Gordonov, S., et al.; Immunological Genome Consortium (2012). Gene-expression profiles and transcriptional regulatory pathways that underlie the identity and diversity of mouse tissue macrophages. Nat. Immunol. *13*, 1118–1128.

Geissmann, F., Jung, S., and Littman, D.R. (2003). Blood monocytes consist of two principal subsets with distinct migratory properties. Immunity *19*, 71–82.

Ginhoux, F., and Guilliams, M. (2016). Tissue-Resident Macrophage Ontogeny and Homeostasis. Immunity *44*, 439–449.

Gomez Perdiguero, E., Klapproth, K., Schulz, C., Busch, K., Azzoni, E., Crozet, L., Garner, H., Trouillet, C., de Bruijn, M.F., Geissmann, F., and Rodewald, H.R. (2015). Tissue-resident macrophages originate from yolk-sac-derived erythro-myeloid progenitors. Nature *518*, 547–551.

Häcker, H., Mischak, H., Häcker, G., Eser, S., Prenzel, N., Ullrich, A., and Wagner, H. (1999). Cell type-specific activation of mitogen-activated protein kinases by CpG-DNA controls interleukin-12 release from antigen-presenting cells. EMBO J. *18*, 6973–6982.

Hammad, H., Chieppa, M., Perros, F., Willart, M.A., Germain, R.N., and Lambrecht, B.N. (2009). House dust mite allergen induces asthma via Toll-like receptor 4 triggering of airway structural cells. Nat. Med. *15*, 410–416.

Hanna, R.N., Carlin, L.M., Hubbeling, H.G., Nackiewicz, D., Green, A.M., Punt, J.A., Geissmann, F., and Hedrick, C.C. (2011). The transcription factor NR4A1 (Nur77) controls bone marrow differentiation and the survival of Ly6C- monocytes. Nat. Immunol. *12*, 778–785.

Hashimoto, D., Chow, A., Noizat, C., Teo, P., Beasley, M.B., Leboeuf, M., Becker, C.D., See, P., Price, J., Lucas, D., et al. (2013). Tissue-resident macrophages self-maintain locally throughout adult life with minimal contribution from circulating monocytes. Immunity *38*, 792–804.

Hoppstädter, J., Diesel, B., Zarbock, R., Breinig, T., Monz, D., Koch, M., Meyerhans, A., Gortner, L., Lehr, C.M., Huwer, H., and Kiemer, A.K. (2010). Differential cell reaction upon Toll-like receptor 4 and 9 activation in human alveolar and lung interstitial macrophages. Respir. Res. *11*, 124.

Kline, J.N., Waldschmidt, T.J., Businga, T.R., Lemish, J.E., Weinstock, J.V., Thorne, P.S., and Krieg, A.M. (1998). Modulation of airway inflammation by CpG oligodeoxynucleotides in a murine model of asthma. J. Immunol. *160*, 2555–2559.

Kline, J.N., Kitagaki, K., Businga, T.R., and Jain, V.V. (2002). Treatment of established asthma in a murine model using CpG oligodeoxynucleotides. Am. J. Physiol. Lung Cell. Mol. Physiol. *283*, L170–L179.

Krieg, A.M. (2006). Therapeutic potential of Toll-like receptor 9 activation. Nat. Rev. Drug Discov. *5*, 471–484.

Krieg, A.M. (2012). CpG still rocks! Update on an accidental drug. Nucleic Acid Ther. *22*, 77–89.

Lambrecht, B.N., De Veerman, M., Coyle, A.J., Gutierrez-Ramos, J.C., Thielemans, K., and Pauwels, R.A. (2000). Myeloid dendritic cells induce Th2 responses to inhaled antigen, leading to eosinophilic airway inflammation. J. Clin. Invest. *106*, 551–559.

Lazarus, R., Klimecki, W.T., Raby, B.A., Vercelli, D., Palmer, L.J., Kwiatkowski, D.J., Silverman, E.K., Martinez, F., and Weiss, S.T. (2003). Single-nucleotide polymorphisms in the Toll-like receptor 9 gene (TLR9): frequencies, pairwise linkage disequilibrium, and haplotypes in three U.S. ethnic groups and exploratory case-control disease association studies. Genomics *81*, 85–91.

Marichal, T., Bedoret, D., Mesnil, C., Pichavant, M., Goriely, S., Trottein, F., Cataldo, D., Goldman, M., Lekeux, P., Bureau, F., and Desmet, C.J. (2010). Interferon response factor 3 is essential for house dust mite-induced airway allergy. J. Allergy Clin. Immunol. *126*, 836–844.e13.

Mesnil, C., Raulier, S., Paulissen, G., Xiao, X., Birrell, M.A., Pirottin, D., Janss, T., Starkl, P., Ramery, E., Henket, M., et al. (2016). Lung-resident eosinophils represent a distinct regulatory eosinophil subset. J. Clin. Invest. *126*, 3279–3295.

Monsalve, E., Ruiz-García, A., Baladrón, V., Ruiz-Hidalgo, M.J., Sánchez-Solana, B., Rivero, S., García-Ramírez, J.J., Rubio, A., Laborda, J., and Díaz-Guerra, M.J. (2009). Notch1 upregulates LPS-induced macrophage activation by increasing NF-kappaB activity. Eur. J. Immunol. *39*, 2556–2570.

Mosser, D.M., and Edwards, J.P. (2008). Exploring the full spectrum of macrophage activation. Nat. Rev. Immunol. *8*, 958–969.

Ostuni, R., Piccolo, V., Barozzi, I., Polletti, S., Termanini, A., Bonifacio, S., Curina, A., Prosperini, E., Ghisletti, S., and Natoli, G. (2013). Latent enhancers activated by stimulation in differentiated cells. Cell *152*, 157–171.

Roy, S.R., Schiltz, A.M., Marotta, A., Shen, Y., and Liu, A.H. (2003). Bacterial DNA in house and farm barn dust. J. Allergy Clin. Immunol. *112*, 571–578.

Schuijs, M.J., Willart, M.A., Vergote, K., Gras, D., Deswarte, K., Ege, M.J., Madeira, F.B., Beyaert, R., van Loo, G., Bracher, F., et al. (2015). Farm dust and endotoxin protect against allergy through A20 induction in lung epithelial cells. Science *349*, 1106–1110.

Serbina, N.V., and Pamer, E.G. (2006). Monocyte emigration from bone marrow during bacterial infection requires signals mediated by chemokine receptor CCR2. Nat. Immunol. *7*, 311–317.

Smit, L.A., Siroux, V., Bouzigon, E., Oryszczyn, M.P., Lathrop, M., Demenais, F., and Kauffmann, F.; Epidemiological Study on the Genetics and Environment of Asthma, Bronchial Hyperresponsiveness, and Atopy (EGEA) Cooperative Group (2009). CD14 and toll-like receptor gene polymorphisms, country living, and asthma in adults. Am. J. Respir. Crit. Care Med. *179*, 363–368.

Strachan, D.P. (1989). Hay fever, hygiene, and household size. BMJ *299*, 1259–1260.

Sur, S., Wild, J.S., Choudhury, B.K., Sur, N., Alam, R., and Klinman, D.M. (1999). Long term prevention of allergic lung inflammation in a mouse model of asthma by CpG oligodeoxynucleotides. J. Immunol. *162*, 6284–6293.

Swirski, F.K., Nahrendorf, M., Etzrodt, M., Wildgruber, M., Cortez-Retamozo, V., Panizzi, P., Figueiredo, J.L., Kohler, R.H., Chudnovskiy, A., Waterman, P., et al. (2009). Identification of splenic reservoir monocytes and their deployment to inflammatory sites. Science *325*, 612–616.

Tamoutounour, S., Guilliams, M., Montanana Sanchis, F., Liu, H., Terhorst, D., Malosse, C., Pollet, E., Ardouin, L., Luche, H., Sanchez, C., et al. (2013). Origins and functional specialization of macrophages and of conventional and monocyte-derived dendritic cells in mouse skin. Immunity *39*, 925–938.

Tan, S.Y., and Krasnow, M.A. (2016). Developmental origin of lung macrophage diversity. Development *143*, 1318–1327.

Thorne, P.S., Kulhánková, K., Yin, M., Cohn, R., Arbes, S.J., Jr., and Zeldin, D.C. (2005). Endotoxin exposure is a risk factor for asthma: the national survey of endotoxin in United States housing. Am. J. Respir. Crit. Care Med. *172*, 1371–1377.

van Furth, R., and Cohn, Z.A. (1968). The origin and kinetics of mononuclear phagocytes. J. Exp. Med. *128*, 415–435.

van Rijt, L.S., Jung, S., Kleinjan, A., Vos, N., Willart, M., Duez, C., Hoogsteden, H.C., and Lambrecht, B.N. (2005). In vivo depletion of lung CD11c+ dendritic cells during allergen challenge abrogates the characteristic features of asthma. J. Exp. Med. *201*, 981–991.

von Mutius, E. (2016). The microbial environment and its influence on asthma prevention in early life. J. Allergy Clin. Immunol. *137*, 680–689.

Immunity, Volume *46*

Supplemental Information

Exposure to Bacterial CpG DNA Protects from Airway Allergic Inflammation by Expanding Regulatory Lung Interstitial Macrophages

Catherine Sabatel, Coraline Radermecker, Laurence Fievez, Genevieve Paulissen, Svetoslav Chakarov, Claudia Fernandes, Sabine Olivier, Marie Toussaint, Dimitri Pirottin, Xue Xiao, Pascale Quatresooz, Jean-Claude Sirard, Didier Cataldo, Laurent Gillet, Hicham Bouabe, Christophe J. Desmet, Florent Ginhoux, Thomas Marichal, and Fabrice Bureau

Supplemental Figures and Legends

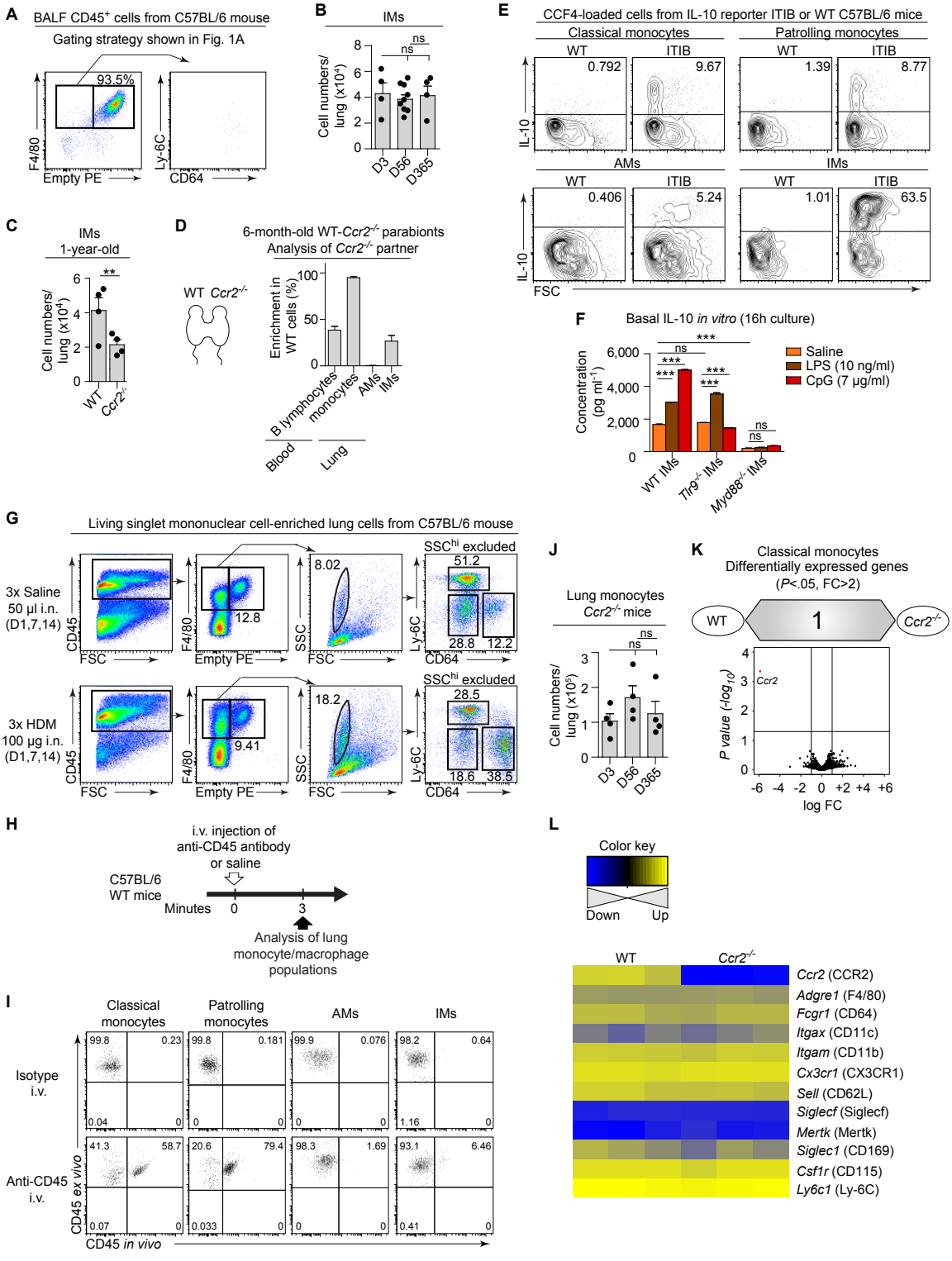


Figure S1, related to Figure 1. Identification of monocyte and macrophage populations in the mouse lung: additional analyses. (A) Analysis of steady-state BALF $CD45^+$ cells using the gating strategy shown in Figure 1A. >90% of cells are identified as AMs at steady-state. (B-C) Absolute numbers of IMs (B) at different time points after birth in WT mice and (C) in 1-year-old WT and *Ccr2*$^{-/-}$ mice. (D) WT and *Ccr2*$^{-/-}$ mice were sutured together for 6 months. The % of enrichment in WT partner cells within the *Ccr2*$^{-/-}$ host is shown. (E) Density plots showing steady-state IL-10 expression as assessed by detection of 450 nm fluorescence (blue fluorescent product of the CCF4 substrate) in CCF4 substrate-loaded cells isolated from IL-10-β-lactamase reporter ITIB or WT control mice. Numbers indicate % of $IL\text{-}10^+$ cells within the cell populations. (F) IL-10 concentration in culture supernatants of FACS-sorted IMs from WT, *Tlr9*$^{-/-}$ or *Myd88*$^{-/-}$ mice stimulated with LPS (10 ng ml^{-1}) or CpG (7 µg ml^{-1}) for 16 hours. (G) Gating strategy identifying monocytes and macrophages in the mouse lung (developed in Figure 1A) applied at day 17 to WT mice having received 3 weekly i.n. instillations of saline (50µL) or HDM (100 µg in 50 µL). (H) Experimental outline for data shown in I. Briefly, APC-conjugated anti-CD45 antibodies were given i.v. 3 minutes before euthanasia, and the indicated cell populations were analyzed by flow cytometry. (I) Representative dot plots showing binding of anti-CD45 *in vivo vs.* anti-CD45 *ex vivo* staining on the indicated populations. (J) Absolute numbers of lung monocytes at different time points after birth in *Ccr2*$^{-/-}$ mice. (K) Summary of differentially expressed genes (DE) ($P<0.05$, FC >2) showing DE genes in red in volcano plot and the total number of DE genes in the middle of the bidirectional arrows. (L) Heatmap showing relative expression of DE genes of cell surface markers displayed in Figure 1C. (A,E,G,I) Results are representative of 1 of ≥5 mice coming from ≥2 independent experiments, each of them giving similar results. (D) Bar graphs (mean + SEM) showing summary data pooled from two pairs of parabionts. (B,C,J) Data shown mean + SEM and are pooled from 2 independent experiments (n=4-9/group). (F) Data show mean + SEM and are representative of 1 of 2 independent sorting experiments. *P* values were calculated using (B,J) a one-way or (F) a two-way ANOVA followed by Tukey's post hoc tests, or (C) a two-tailed Student's *t* test. D, day.

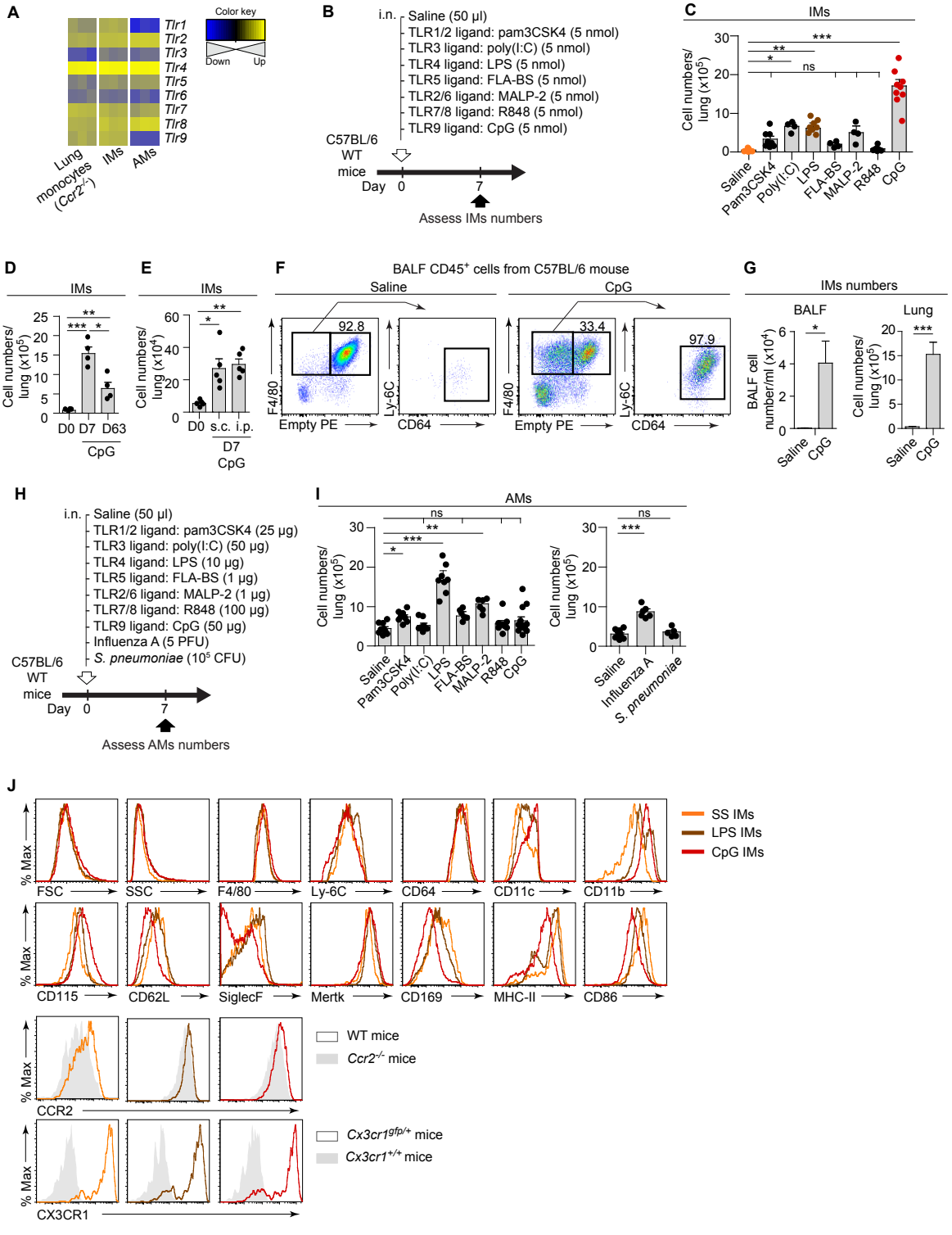

A
Color key
Down
Up
Tlr1
Tlr2
Tlr3
Tlr4
Tlr5
Tlr6
Tlr7
Tlr8
Tlr9
Lung monocytes (Ccr2-/-)
IMs
AMs
B
i.n.
Saline (50 µl)
TLR1/2 ligand: pam3CSK4 (5 nmol)
TLR3 ligand: poly(I:C) (5 nmol)
TLR4 ligand: LPS (5 nmol)
TLR5 ligand: FLA-BS (5 nmol)
TLR2/6 ligand: MALP-2 (5 nmol)
TLR7/8 ligand: R848 (5 nmol)
TLR9 ligand: CpG (5 nmol)
C57BL/6 WT mice
Day 0
7
Assess IMs numbers
C
IMs
Cell numbers/ lung (x10^5)
***
**
*
ns
Saline
Pam3CSK4
Poly(I:C)
LPS
FLA-BS
MALP-2
R848
CpG
D
IMs
Cell numbers/ lung (x10^5)
D0 D7 D63
CpG
E
IMs
Cell numbers/ lung (x10^4)
D0 s.c. i.p.
D7
CpG
F
BALF CD45+ cells from C57BL/6 mouse
Saline
CpG
92.8
33.4
97.9
F4/80
Empty PE
Ly-6C
CD64
G
IMs numbers
BALF
Lung
BALF cell number/ml (x10^4)
Cell numbers/ lung (x10^5)
Saline
CpG
H
i.n.
Saline (50 µl)
TLR1/2 ligand: pam3CSK4 (25 µg)
TLR3 ligand: poly(I:C) (50 µg)
TLR4 ligand: LPS (10 µg)
TLR5 ligand: FLA-BS (1 µg)
TLR2/6 ligand: MALP-2 (1 µg)
TLR7/8 ligand: R848 (100 µg)
TLR9 ligand: CpG (50 µg)
Influenza A (5 PFU)
S. pneumoniae (10^5 CFU)
C57BL/6 WT mice
Day 0
7
Assess AMs numbers
I
AMs
Cell numbers/ lung (x10^5)
ns
**
***
*
Saline
Pam3CSK4
Poly(I:C)
LPS
FLA-BS
MALP-2
R848
CpG
Influenza A
S. pneumoniae
J
% Max
FSC
SSC
F4/80
Ly-6C
CD64
CD11c
CD11b
CD115
CD62L
SiglecF
Mertk
CD169
MHC-II
CD86
SS IMs
LPS IMs
CpG IMs
CCR2
WT mice
Ccr2-/- mice
CX3CR1
Cx3cr1gfp/+ mice
Cx3cr1+/+ mice

Figure S2, related to Figure 2. Quantification of IM and AM numbers, and localization and surface phenotype of IMs upon exposure to TLR ligands. (A) Heatmap showing relative expression of *Tlr* on lung monocytes sorted from *Ccr2*$^{-/-}$ mice, and AMs and IMs sorted from WT mice. (B) Experimental outline for data shown in C. (C) Absolute numbers of IMs in the lungs of WT mice 7 days following i.n. stimulation with the indicated doses of TLR ligands (i.e. 5 nmol) (D) Absolute numbers of CpG IMs before and 7 or 63 days after i.n. CpG instillation. (E) C57BL/6 WT mice were injected s.c. or i.p. with 50 µg CpG (in 100 µl and 200 µl, respectively). Seven days later (D7), numbers of IMs were determined in the lung and compared with mice analyzed at D0. (F-G) Quantification of IMs in the BALF of mice i.n. instilled with saline or CpG 7 days earlier. (F) Representative dot plot of BALF CD45^{+} cells using the gating strategy shown in Figure 1A. Numbers indicate the % within the CD45^{+} BALF cells. (G) Absolute BALF and lung IM numbers. (H) Experimental outline for data shown in I. Briefly, WT C57BL/6 mice were instilled i.n. with 50 µl saline, or 50 µl saline containing the indicated stimulants or pathogens (doses used are shown in brackets). (I) Absolute numbers of AMs in the lungs of C57BL/6 WT mice 7 days after i.n. stimulation with the indicated TLR ligands and i.n. infection with influenza A virus (PR8 strain) or *S. pneumoniae* (serotype 1). (J) Surface phenotype of lung IMs at steady-state (SS IMs) or 7 days after i.n. LPS (LPS IMs) or CpG-DNA (CpG IMs) instillations. (C,E,I) Data show mean + SEM and are pooled from 2-3 independent experiments (n=3-12/group). *P* values were calculated using a one-way ANOVA followed by Tukey's post hoc tests. (D,G) Data show mean + SEM and are representative of 1 of 2 independent experiments (n=4/group). *P* values were calculated using (D) a one-way ANOVA followed by Tukey's post hoc tests and (G) a two-tailed unpaired Student's *t* test. (F,J) Data are representative of 1 of ≥6 mice coming from (F) 2 or (J) ≥3 independent experiments, each of them giving comparable results. D, day.

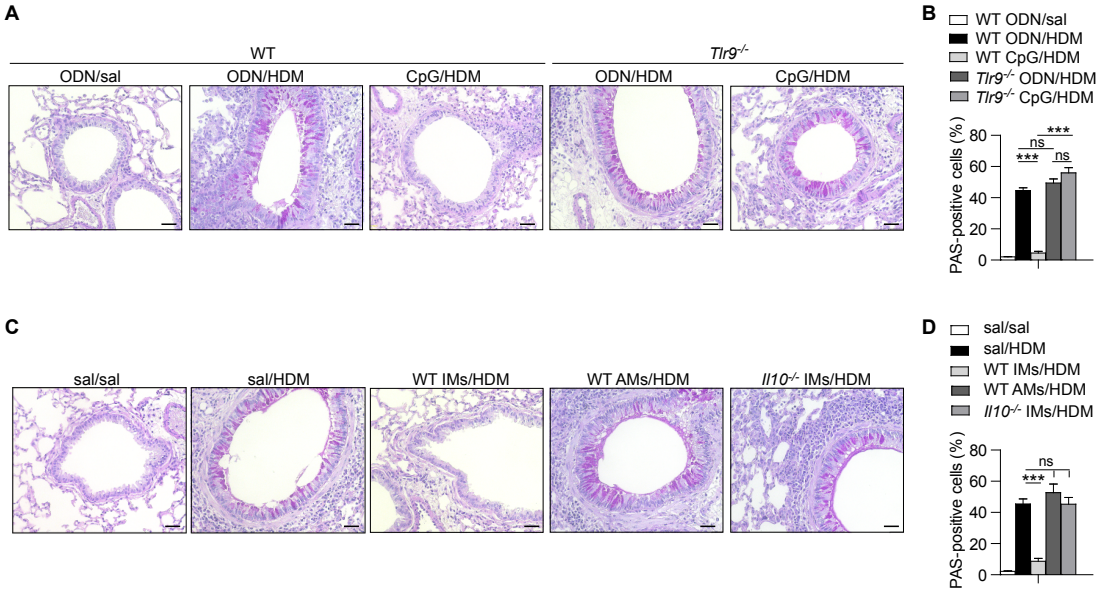

A
WT
Tlr9-/-
ODN/sal
ODN/HDM
CpG/HDM
ODN/HDM
CpG/HDM
B
WT ODN/sal
WT ODN/HDM
WT CpG/HDM
Tlr9-/- ODN/HDM
Tlr9-/- CpG/HDM
PAS-positive cells (%)
0
20
40
60
80
ns
***
***
ns
C
sal/sal
sal/HDM
WT IMs/HDM
WT AMs/HDM
Il10-/- IMs/HDM
D
sal/sal
sal/HDM
WT IMs/HDM
WT AMs/HDM
Il10-/- IMs/HDM
PAS-positive cells (%)
0
20
40
60
80
ns
***

Figure S3, related to Figure 3. Contribution of CpG IMs to the prevention of experimental asthma: mucus production. (A-B) Experimental outline is shown in Figure 3A. Briefly, WT C57BL/6 and *Tlr9*$^{-/-}$ mice were instilled i.n. with 50 µg ODN or 50 µg CpG, were sensitized 7 and 14 days later with 100 µg HDM or saline and were sacrificed 3 days later. (A) Representative Periodic Acid-Schiff (PAS) staining of lung sections of the indicated groups of mice. (B) Quantification of mucus production as the % positivity of PAS-stained goblet cells per total epithelial cells. (C-D) Experimental outline is shown in Figure 3J. Briefly, WT C57BL/6 were transferred i.t. on day -1 and 6 with saline or $1.5.10^6$ AMs or CpG IMs sorted from WT or *Il10*$^{-/-}$ mice, sensitized 1 day later with 100 µg HDM or saline and sacrificed 3 days after the second sensitization. (C) PAS staining of lung sections of the indicated groups of mice. (D) Quantification of mucus production as the % positivity of PAS-stained goblet cells per total epithelial cells. (A and C) Data are representative of one of ≥6 mice analyzed, each of them giving comparable results. (B and D) Data show mean + SEM and are pooled from 2 independent experiments (n=4-6 mice/group). *P* values were calculated using a one-way ANOVA followed by Tukey's post hoc tests. Scale bar: 32 µm.

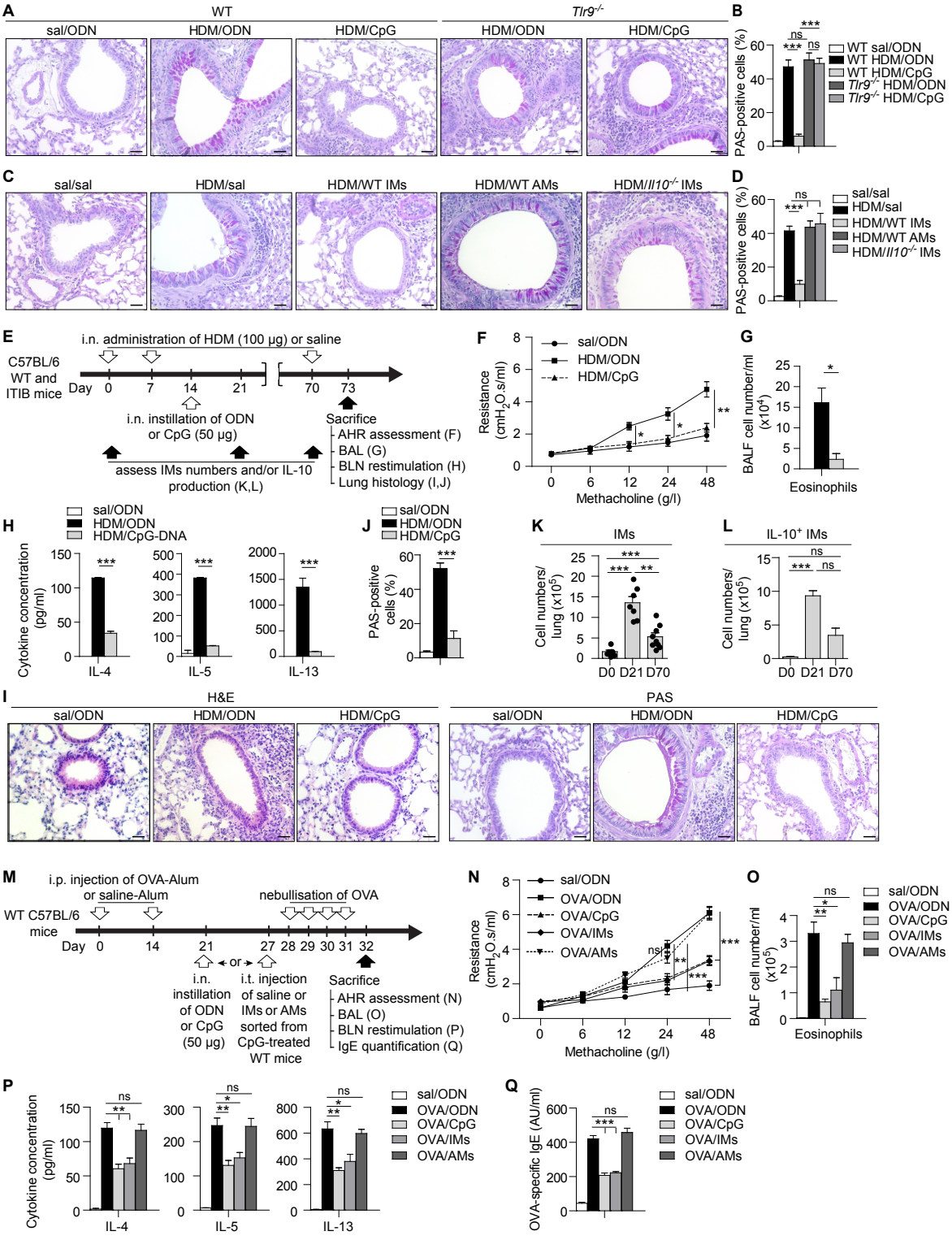

A
WT
Tlr9-/-
sal/ODN
HDM/ODN
HDM/CpG
HDM/ODN
HDM/CpG
B
PAS-positive cells (%)
WT sal/ODN
WT HDM/ODN
WT HDM/CpG
Tlr9-/- HDM/ODN
Tlr9-/- HDM/CpG
C
sal/sal
HDM/sal
HDM/WT IMs
HDM/WT AMs
HDM/Il10-/- IMs
D
sal/sal
HDM/sal
HDM/WT IMs
HDM/WT AMs
HDM/Il10-/- IMs
E
i.n. administration of HDM (100 µg) or saline
C57BL/6 WT and ITIB mice
Day 0 7 14 21 70 73
i.n. instillation of ODN or CpG (50 µg)
Sacrifice
AHR assessment (F)
BAL (G)
BLN restimulation (H)
Lung histology (I,J)
assess IMs numbers and/or IL-10 production (K,L)
F
sal/ODN
HDM/ODN
HDM/CpG
Resistance (cmH2O.s/ml)
Methacholine (g/l)
G
BALF cell number/ml (x10^4)
Eosinophils
H
sal/ODN
HDM/ODN
HDM/CpG-DNA
Cytokine concentration (pg/ml)
IL-4
IL-5
IL-13
J
sal/ODN
HDM/ODN
HDM/CpG
PAS-positive cells (%)
K
IMs
Cell numbers/ lung (x10^5)
D0 D21 D70
L
IL-10+ IMs
Cell numbers/ lung (x10^5)
D0 D21 D70
I
H&E
PAS
sal/ODN
HDM/ODN
HDM/CpG
M
i.p. injection of OVA-Alum or saline-Alum
nebullisation of OVA
WT C57BL/6 mice
Day 0 14 21 27 28 29 30 31 32
or
i.n. instillation of ODN or CpG (50 µg)
i.t. injection of saline or IMs or AMs sorted from CpG-treated WT mice
Sacrifice
AHR assessment (N)
BAL (O)
BLN restimulation (P)
IgE quantification (Q)
N
sal/ODN
OVA/ODN
OVA/CpG
OVA/IMs
OVA/AMs
Resistance (cmH2O.s/ml)
Methacholine (g/l)
O
BALF cell number/ml (x10^5)
Eosinophils
P
Cytokine concentration (pg/ml)
IL-4
IL-5
IL-13
Q
OVA-specific IgE (AU/ml)

Figure S4, related to Figure 4. Contribution of CpG IMs to the treatment of experimental asthma: mucus production, long-lasting effects of CpG on IM numbers and HDM-induced experimental asthma, and contribution of CpG and CpG IMs in the protection against OVA-induced experimental asthma. (A-B) Experimental outline is shown in Figure 4A. Briefly, WT C57BL/6 and *Tlr9*$^{-/-}$ mice were instilled i.n. with 100 µg HDM or saline at days 0 and 7, were exposed to CpG or ODN at day 14 and challenged with HDM at day 21. Mice were sacrificed 3 days after the HDM challenge. (A) Representative Periodic Acid-Schiff (PAS) staining of lung sections of the indicated groups of mice. (B) Quantification of mucus production as the % positivity of PAS-stained goblet cells per total epithelial cells. (C-D) Experimental outline is shown in Figure 4J. Briefly, WT mice previously sensitized with 2 i.n. administrations of HDM were transferred i.t. with saline or $1.5.10^6$ AMs or CpG IMs sorted from WT or *Il10*$^{-/-}$ mice, challenged 1 day later with 100 µg HDM and sacrificed 3 days later. (C) PAS staining of lung sections of the indicated groups of mice. (D) Quantification of mucus production as the % positivity of PAS-stained goblet cells per total epithelial cells. (A and C) Data are representative of one of ≥6 mice analyzed, each of them giving comparable results. (B and D) Data show mean + SEM and are pooled from 2 independent experiments (n=4-6 mice/group). *P* values were calculated using a one-way ANOVA followed by Tukey's post hoc tests. Scale bar: 32 µm. (E) Experimental outline for data shown in F-L. Briefly, C57BL/6 WT or ITIB mice (panel J) mice were sensitized with 2 weekly i.n. administrations of HDM (100 µg) or saline and instilled 7 days later (D14) i.n. with CpG or ODN. On D56, mice were challenged with 100 µg HDM and were sacrificed on D73. IM numbers were assessed at the indicated time points. (F) Dynamic airway resistance upon methacholine inhalation. (G) BALF eosinophil counts. (H) Cytokine concentrations in culture supernatants of BLN cells restimulated with HDM. (I) Hematoxylin and eosin (H&E) and Periodic Acid Schiff (PAS) stainings of lung sections. (J) Quantification of mucus production as the % positivity of PAS-stained goblet cells per total epithelial cells. (K,L) Numbers of (K) CpG IMs and (L) IL-10$^+$ CpG IMs at D0, 21 and 70. (F) Data show mean + SEM and are representative of 1 of 3 independent experiments (n=4/group), each of them giving similar results. (G,H,K) Data show mean + SEM and are pooled from 3 independent experiments (n=6-12/group), each of them giving comparable results. (L) Data show mean + SEM and are pooled from 2 independent experiments (n=4/group). (I) Data are representative of one of ≥6 mice analyzed, each of them giving comparable results. (J) Data show mean + SEM and are pooled from 2 independent experiments (n=4-6 mice/group). (F-H;K,L,J) *P* values were calculated using a one-way ANOVA followed by Tukey's post hoc tests. Scale bars: 32 µm. (M) Experimental outline for data shown in N-Q. Briefly, C57BL/6 WT mice were sensitized i.p. with OVA admixed with alum at D0 and 14 and instilled 7 days later (D21) i.n. with CpG or ODN. Alternatively, mice were transferred on D27 with $1.5.10^6$ AMs or CpG IMs sorted from WT mice. From D28 to D31, mice were challenged with inhalations of OVA 1% (1 hour/day). Mice were sacrificed on D32. (N) Dynamic airway resistance upon methacholine inhalation. (O) BALF eosinophil counts. (P) Cytokine concentrations in culture supernatants of BLN cells restimulated with OVA. (Q) Quantification of serum OVA-specific IgE. (N-Q) Data shown mean + SEM and are representative of 1 of 2 independent experiments (n=4-6/group), each of them giving similar results. *P* values were calculated using a one-way ANOVA followed by Tukey's post hoc tests.

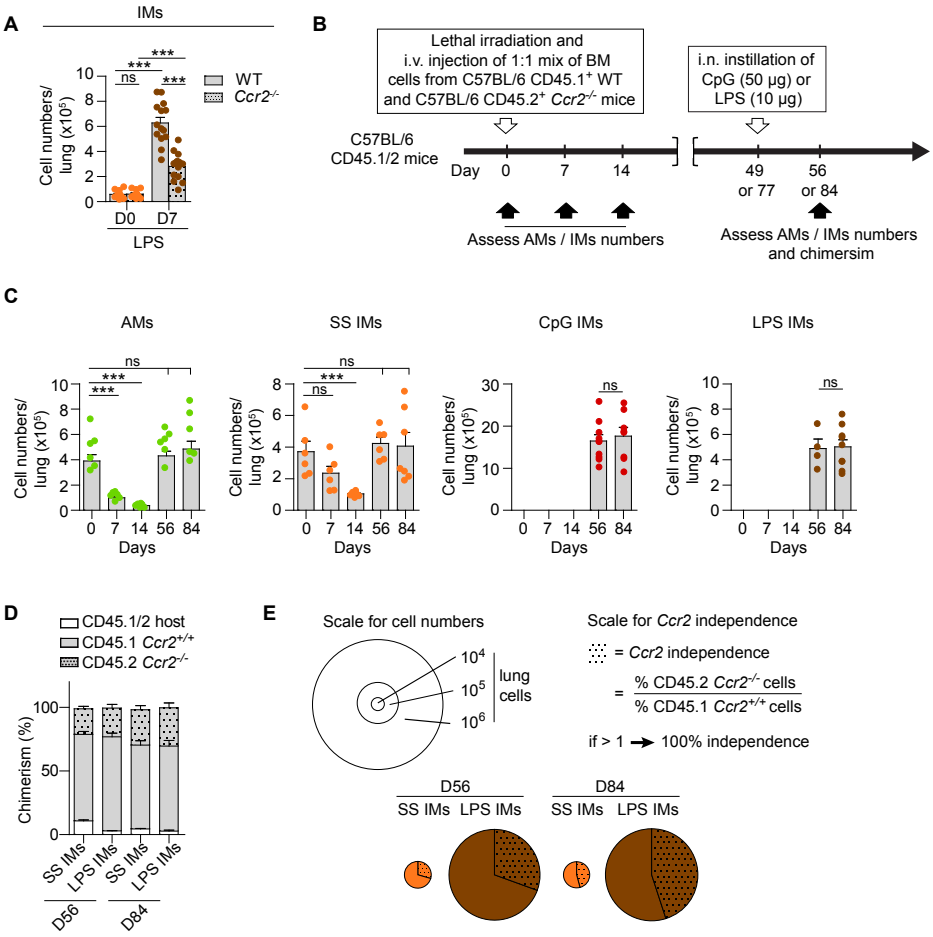

A
IMs
Cell numbers/ lung (x10⁵)
WT
Ccr2-/-
D0
D7
LPS
B
Lethal irradiation and i.v. injection of 1:1 mix of BM cells from C57BL/6 CD45.1+ WT and C57BL/6 CD45.2+ Ccr2-/- mice
i.n. instillation of CpG (50 µg) or LPS (10 µg)
C57BL/6 CD45.1/2 mice
Day 0 7 14
49 or 77
56 or 84
Assess AMs / IMs numbers
Assess AMs / IMs numbers and chimersim
C
AMs
SS IMs
CpG IMs
LPS IMs
Days
D
CD45.1/2 host
CD45.1 Ccr2+/+
CD45.2 Ccr2-/-
Chimerism (%)
SS IMs
LPS IMs
D56
D84
E
Scale for cell numbers
lung cells
Scale for Ccr2 independence
= Ccr2 independence
% CD45.2 Ccr2-/- cells / % CD45.1 Ccr2+/+ cells
if > 1 → 100% independence

Figure S5, related to Figure 5. Dependence of LPS IMs on CCR2, and numbers of AMs and IMs before irradiation and following BM reconstitution. (A) Absolute numbers of IMs in the lungs of WT and *Ccr2*$^{-/-}$ mice before and 7 days after i.n. LPS treatment (10 µg). (B) Experimental outline for data shown in C-E. Briefly, CD45.1/2^{+} mice were lethally irradiated and reconstituted with equal amounts of CD45.1^{+} WT and CD45.2^{+}*Ccr2*$^{-/-}$ BM cells. Some mice were instilled with CpG or LPS at day 49 or 77 and analyzed 7 days later. (C) Macrophage numbers were assessed over time, as indicated. Absolute numbers of the indicated populations before (D0, day 0) irradiation, and 7, 14, 56 and 84 days after BM reconstitution. (D) The chimerism of SS IMs and LPS IMs was assessed at day 56 or 84. % of BM chimerism and radio-resistance of the indicated populations. (E) Pie charts depicting the average absolute cell number (surface area) and the CCR2 independence (dotted area) in the indicated cell populations. (D and E) The % of chimerism and the % of CCR2 independence of blood B lymphocytes, neutrophils (i.e., 50% chimerism, 100% CCR2 independence) and monocytes (i.e. ≈10% chimerism, ≈20% CCR2 independence) were used as controls and are shown in Figure 5, D-F. (A,C,D) Data show mean ± SEM and are pooled from (A,D) 3 independent experiments (n=10-15/group), or (C) 2 independent experiments (n=6-7/group), each of them giving similar results. *P* values were calculated using (A) a two-way ANOVA or (C,D) a one-way ANOVA followed by Tukey's test for multiple comparisons. D, day.

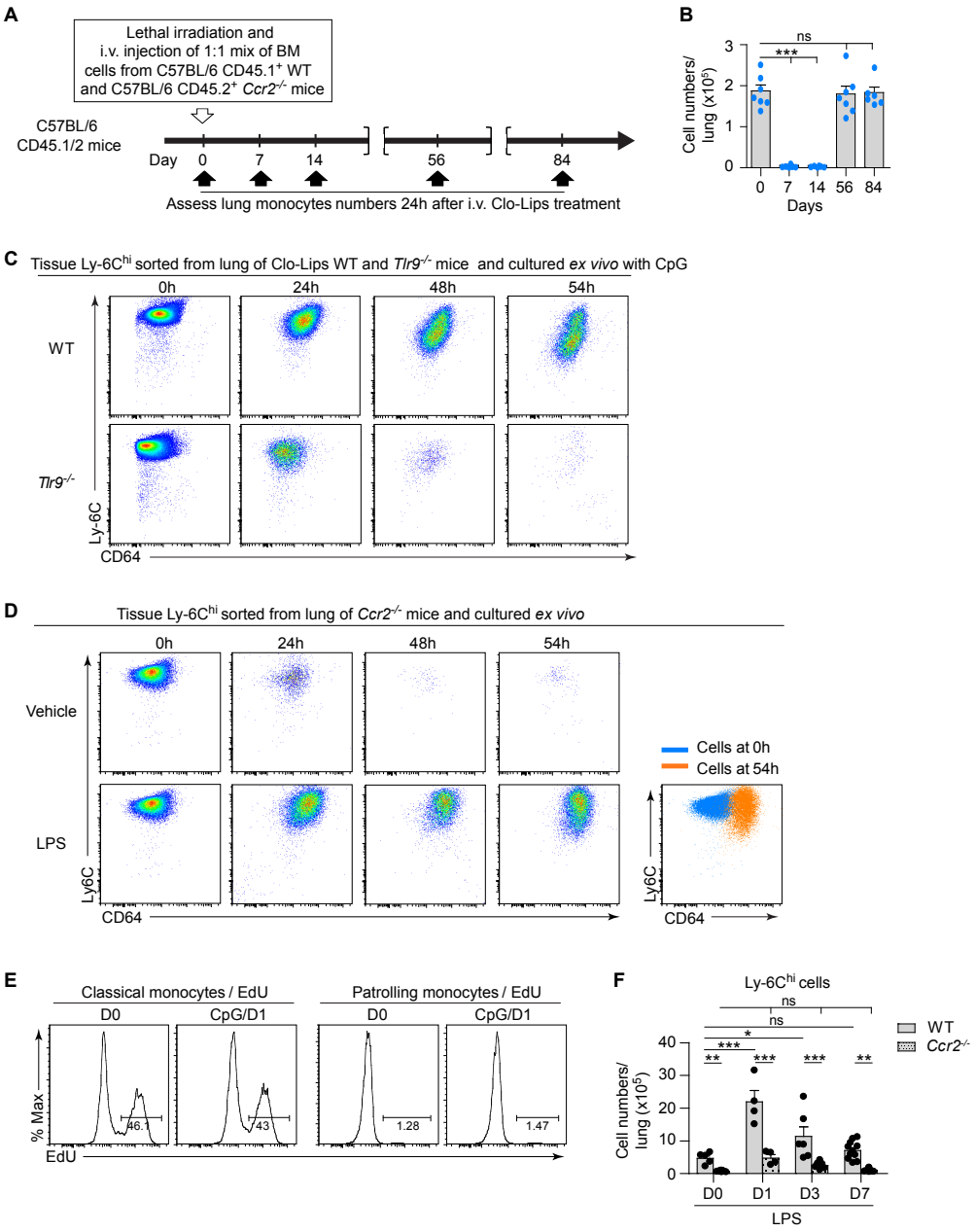

A
Lethal irradiation and
i.v. injection of 1:1 mix of BM
cells from C57BL/6 CD45.1+ WT
and C57BL/6 CD45.2+ Ccr2-/- mice
C57BL/6
CD45.1/2 mice
Day 0 7 14 56 84
Assess lung monocytes numbers 24h after i.v. Clo-Lips treatment
B
Cell numbers/ lung (x10^5)
ns
***
0 7 14 56 84
Days
C
Tissue Ly-6C^hi sorted from lung of Clo-Lips WT and Tlr9-/- mice and cultured ex vivo with CpG
0h 24h 48h 54h
WT
Tlr9-/-
Ly-6C
CD64
D
Tissue Ly-6C^hi sorted from lung of Ccr2-/- mice and cultured ex vivo
0h 24h 48h 54h
Vehicle
LPS
Ly6C
CD64
Cells at 0h
Cells at 54h
E
Classical monocytes / EdU
Patrolling monocytes / EdU
D0 CpG/D1 D0 CpG/D1
% Max
EdU
46.1
43
1.28
1.47
F
Ly-6C^hi cells
Cell numbers/ lung (x10^5)
D0 D1 D3 D7
LPS
WT
Ccr2-/-

Figure S6, related to Figure 6. Numbers of lung monocytes before irradiation and following BM reconstitution, differentiation of lung monocytes upon CpG or LPS stimulation *ex vivo*, monocyte EdU incorporation upon CpG treatment and numbers of lung monocytes in WT and *Ccr2*$^{-/-}$ mice before and 1, 3 and 7 days after i.n. LPS instillation. (A) Experimental outline for data shown in B. Briefly, CD45.1/2^{+} mice were lethally irradiated and reconstituted with equal amounts of CD45.1^{+} WT and CD45.2^{+} *Ccr2*$^{-/-}$ BM cells. Numbers of lung monocytes were assessed over time, as indicated. (B) Absolute numbers of lung monocytes before (D0, day 0) irradiation, and 7, 14, 56 and 84 days after BM reconstitution. Data show mean + SEM and are pooled from 2 independent experiments (n=6-7/group), each of them giving similar results. (C) Dot plots of living lung monocytes sorted from Clo-Lip-treated C57BL/6 WT and *Tlr9*$^{-/-}$ mice and cultured *ex vivo* before and 24, 48 or 54 hours after stimulation with vehicle or CpG. (D) Dot plots of living lung monocytes sorted from *Ccr2*$^{-/-}$ mice and cultured *ex vivo* before and 24, 48 or 54 hours after stimulation with vehicle or LPS. On the right panel, superposition of dot plots of living lung monocytes cultured *ex vivo* before (0h) and 54 hours (54h) after stimulation with LPS. (C-D) Data are representative of one of ≥5 samples coming from 3 independent experiments. (E) Incorporation of EdU (injected i.p. 24 hours before) in classical Ly-6C^{hi} and patrolling Ly-6C^{lo} lung associated monocytes was assessed at day 0 and 1 day after i.n. CpG instillation in WT mice. WT BM cells were used as controls (shown in Figure 6L). Numbers indicate % of EdU^{+} cells. Results are representative of one of ≥4 mice coming from 2 independent experiments. (F) Absolute numbers of lung monocytes in WT and *Ccr2*$^{-/-}$ mice before and 1, 3 and 7 days after i.n. LPS instillation. Data show mean + SEM and are pooled from 2 independent experiments (n=4-10/group). *P* values were calculated using (B) a one-way ANOVA or (F) a two-way ANOVA followed by Tukey's post hoc tests.

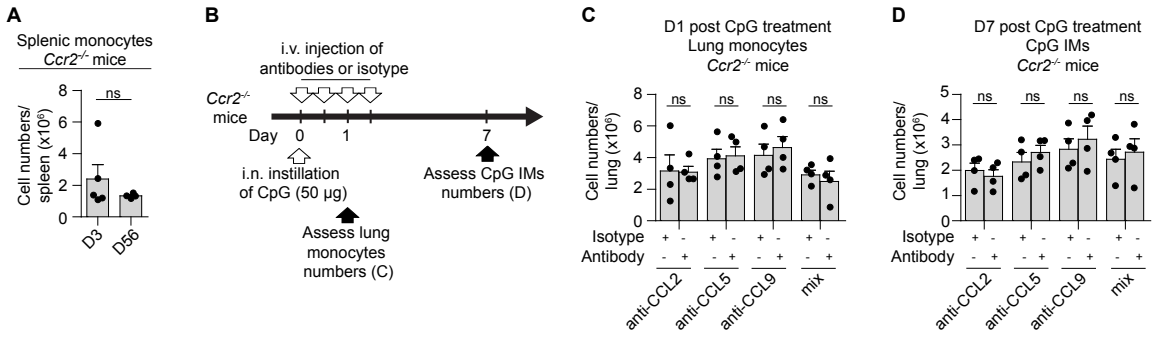

A
Splenic monocytes
Ccr2-/- mice
Cell numbers/ spleen (x10⁶)
ns
D3
D56
B
i.v. injection of antibodies or isotype
Ccr2-/- mice
Day 0 1 7
i.n. instillation of CpG (50 µg)
Assess CpG IMs numbers (D)
Assess lung monocytes numbers (C)
C
D1 post CpG treatment
Lung monocytes
Ccr2-/- mice
Cell numbers/ lung (x10⁶)
Isotype
Antibody
anti-CCL2
anti-CCL5
anti-CCL9
mix
D
D7 post CpG treatment
CpG IMs
Ccr2-/- mice

Figure S7, related to Figure 7. Analyses of *Ccr2*$^{-/-}$ mice: numbers of spleen monocytes, and numbers of monocytes and macrophages in the lung following chemokine neutralization and i.n. CpG treatment. (A) Absolute numbers of spleen monocytes at different time points after birth in *Ccr2*$^{-/-}$ mice. (B) Experimental outline for *in vivo* chemokine neutralization experiments shown in C-D. Absolute numbers of (C) lung monocytes 1 day or (D) CpG IMs 7 days after i.n. CpG instillation in *Ccr2*$^{-/-}$ mice which received i.p. injection of the indicated antibodies. Data show mean + SEM and are pooled from 2 independent experiments (n=4-5/group). *P* values were calculated using (A) a one-way or (C,D) a two-way ANOVA followed by Tukey's post hoc tests.

Supplemental Experimental Procedures

Mice

WT CD45.2$^+$ C57BL/6 and WT CD45.1$^+$ C57BL/6 mice were from the Jackson Laboratory. CD45.1/2$^+$ WT C57BL/6 mice were obtained by crossing CD45.1$^+$ with CD45.2$^+$ mice. *Agtr1a*$^{-/-}$, *Ccr2*$^{-/-}$, *Cx3cr1*$^{gfp/+}$, *Il-10*$^{-/-}$, *Myd88*$^{-/-}$ and *Nr4a1*$^{-/-}$ mice on the C57BL/6 background were from the Jackson Laboratory. *Tlr9*$^{-/-}$ (Hemmi et al., 2000) and IL-10-β-lactamase reporter (ITIB) (Bouabe et al., 2011) mice were described elsewhere. All mice, except parabiotic mice that were generated at the Singapore Immunology Network (SIgN, Singapore), were housed and bred in institutional specific pathogen-free facilities at the GIGA-Research center of the University of Liege (Belgium) and were used at 6-10 weeks of age, unless otherwise indicated. All experimental procedures and protocols were reviewed and approved by the Institutional Animal Care and Use Ethics Committee of the University of Liege (Belgium), except for experiments involving parabiotic mice that were approved by the local ethical committee at the Singapore Immunology Network (SIgN, Singapore).

The "Guide for the Care and Use of Laboratory Animals", prepared by the Institute of Laboratory Animal Resources, National Research Council, and published by the National Academy Press, as well as European and local legislations, were followed carefully.

Reagents and Antibodies

2.4G2 Fc receptor blocking antibodies were produced in house. Fluorogenic coumarin-cephalosporin-fluorescein (4)-acetoxymethyl (CCF4-AM) was from Invitrogen. Pam3CSK4, Poly(I:C), FLA-BS and R848 were from InvivoGen. MALP-2 was from Enzo Life Sciences. LPS from E. *coli* O55:B5 was from Sigma. Mouse non-CpG DNA (ODN, 5'-gcttgatgactcagccggaa-3'; Ref. HC4034) and CpG-DNA (5'-tccatgacgttcctgatgct-3'; Ref. HC4033) were from Sanbio. Clodronate-containing liposomes or control liposomes were from Foundation Clodronate Liposomes. 5-ethynyl-2'-deoxy-uridine (EdU) was from Jena Bioscience. HDM extracts (HDM from *Dermatophagoides farinae*) were from Greer Laboratories. OVA grade III and grade V were purchased from Sigma Aldrich. Fluorescent HDM was produced by labelling with the Alexa fluor 647 Protein Labelling kit (Molecular Probes).

PE-conjugated anti-B220 (clone RA3-6B2), APC-, FITC-, PerCP-Cy5.5- and V500-conjugated anti-CD45.2 (clone 104), PE-conjugated anti-CD64 (clone X54-5:7.1), PE-Cy7-conjugated anti-CD11b (clone M1/70), APC- and APC-Cy7-conjugated anti-CD11c (clone HL3), PerCP-Cy5.5-, BV421-conjugated anti-CD49b (clone DX5), FITC-conjugated anti-Ly6C (clone AL-21), PE- and PE-Cy7-conjugated anti-Ly6g (clone 1A8), APC-conjugated anti-MHCII (clone AF6-120.1), PE-conjugated anti-NK1.1 (clone PK136), PE-conjugated anti-SiglecF (clone E50-2440) were purchased from BD Pharmingen. APC-conjugated anti-CD45.1 (clone A20), FITC-conjugated anti-CD11b (clone M1/70), efluor660-conjugated anti-CD169 (clone SER-4), PerCP-Cy5.5-conjugated anti-CD19 (clone 1D3), PE-conjugated anti-CD115 (clone AFS98), efluor 450-conjugated anti-CD3 (clone 17A2), PerCP-Cy5.5-conjugated anti-CD62L (clone MEL-14), biotin-conjugated anti-CD86 (clone GL-1), efluor 660-, PerCP-efluor710-conjugated anti-CD90.2 (clone 30H12), PE-conjugated anti-F4/80 (clone BM8) were from eBioscience. BV421-conjugated anti-CD64 (clone X54-5:7.1) and

PerCP-Cy5.5-conjugated anti-MHCII (clone M5/M4.15.2) were from Biolegend. PE-conjugated anti-CCR2 (clone 475301), and APC-conjugated anti-merTK (clone 108928) were from R&D systems. Anti-CD11b MicroBeads were from Miltenyi Biotec. Appropriate isotype control antibodies were purchased from the same respective manufacturers.

Rabbit anti-phospho-p44/42 MAPK (Erk1/2) and anti-β-Actin (clone D6A8) antibodies were from Cell Signaling Technology. Horseradish peroxidase (HRP)-conjugated goat anti-rabbit IgG antibody was from Kirkegaard & Perry Laboratories.

Goat anti-CCL2, rat anti-CCL5 (clone 53405) and rat anti-CCL9 (clone 62105) neutralizing antibodies were from R&D Systems. Appropriate isotype control antibodies were purchased from the same manufacturer.

Cell isolation, staining and flow cytometry

To obtain single-lung-cell suspensions, lungs were perfused with 10 ml of PBS through the right ventricle, cut into small pieces, and digested for 1 h at 37°C in HBSS containing 1 mg ml^{-1} collagenase A (Roche) and 0.05 mg ml^{-1} DNase I (Roche). Single-cell suspensions were then enriched in mononuclear cells by harvesting cells from the 1.080:1.038 g ml^{-1} interface using a density gradient (Easycoll from VWR). Blood was collected and mixed with EDTA (100 mM), and red blood cells were lysed with RBC lysis buffer (eBioscience). To obtain single-heart and liver-cell suspensions, these organs were cut into small pieces and digested for 1 h at 37°C in HBSS containing 1 mg ml^{-1} collagenase A (Roche) and 0.05 mg ml^{-1} DNase I (Roche).

Cell phenotyping and sorting were performed on a FACSCANTO II and a FACSARIA III (BD Biosciences), respectively. Staining reactions were performed at 4°C after incubation with 2.4G2 Fc receptor blocking antibodies to reduce non-specific binding.

Regarding cell phenotyping and sorting, FSC-W and FSC-A discrimination was used to exclude doublet cells, and ViaProbe (7-AAD) cell viability solution (BD Biosciences) was used to discriminate between dead and living cells. In experiments aimed at isolating lung Ly-$6C^{hi}CD64^{lo}$ classical monocytes, Ly-$6C^{lo}CD64^{lo}$ patrolling monocytes, AMs, SS IMs, CpG IMs, or splenic monocytes, lung mononuclear cells and splenic cells were first enriched in CD11b-expressing cells by MACS using CD11b microbeads. Results were analyzed with FlowJo software (Tree Star).

Cytologic examination

Cytologic examination of FACS-sorted populations was performed on cytospin preparations stained with Hemacolor® (Merck KgaA). Sections were examined with a FSX100 microscope (Olympus).

Vascular monocytes/macrophage depletion

WT or *Ccr2*$^{-/-}$ mice were injected i.v. with 200 µl of clodronate-containing liposomes (Clo-Lips) or empty liposomes (PBS-Lips), and lung cells were harvested 24 hours later.

Assessment of IL-10 expression in ITIB mice and IL-10 production *ex vivo*

To assess IL-10 expression using IL-10-β-lactamase reporter ITIB mice (Bouabe et al., 2011), lung cells from IL-10-β-lactamase reporter ITIB and control WT mice were resuspended in a

CCF4-AM-containing solution supplemented with probenecid (Invitrogen), prepared according to the manufacturer's instructions, and incubated 90 min at 29°C. Briefly, CCF4-AM is a lipophilic ester derivative that consists of a cephalosporin core bridging a 7-hydroxycoumarin to a fluorescein. Once inside the cell, the ester groups are readily hydrolysed by cytoplasmic esterases, releasing the negatively charged form, CCF4, which is thus trapped in the cytosol (using inhibitor for anion transporters, such as probenecid, further increase trapping substrate/product within the cells). Exciting intact CCF4 at 405 nm induces fluorescence resonance energy transfer (FRET) from the coumarin to the fluorescein that subsequently emits green light. After cleavage of the ß-lactam ring of CCF4 by ß-lactamase, which is expressed under the control of the *Il10* gene promoter, the two fluorophores are separated, resulting in the disruption of FRET. Excitation at 409 nm now results in blue fluorescence detectable at 450 nm. CCF4-loaded cells were then classically stained and analyzed by flow cytometry. CCF4-loaded WT cells were used as negative controls.

For IL-10 production *ex vivo*, classical monocytes, patrolling monocytes, AMs and IMs were FACS-sorted from naive WT mice and $2x10^5$ cells were cultured in 200 µl of RPMI medium supplemented with 10% foetal bovine serum (FBS) and additives (L-glutamine 8mM, MEAA 0.1 mM, Pyruvate Na 1mM, Penicillin/streptomycin 50 UI ml^{-1}, β-mercaptoethanol 0.5mM) in a 96 well plate during 16 h. In some experiments, IMs isolated from WT, *Tlr9*$^{-/-}$ or *Myd88*$^{-/-}$ mice were cultured and stimulated during 16h with LPS (10 ng ml^{-1}) or CpG (7 µg ml^{-1}). Concentrations of IL-10 were measured by ELISA (eBioscience) in culture supernatants.

Quantification of monocytes/macrophages numbers

Lung cell numbers were counted following whole lung digestion and mononuclear cell enrichment by the use of a hemocytometer. The numbers of monocytes/macrophages were determined according to the gating strategy shown in Figure 1A.

Total BALF cell numbers were counted by the use of a hemacytometer. The numbers of SS IMs and CpG IMs were determined according to the gating strategy shown in Figure 1A.

Total splenic, cardiac, liver and bone marrow cell numbers were counted following tissue dissociation by the use of a hemacytometer. The numbers of splenic, cardiac, liver and bone marrow monocytes or macrophages were determined according to the gating strategy described by Swirski and collaborators (Swirski et al., 2009) or shown in Figure 1A, respectively.

Immunohistochemistry

Lungs were fixed in 4% formalin, paraffin-embedded and cut in 5 µm thick sections. Deparaffinized tissues were dewaxed and endogenous peroxides were blocked with hydrogen peroxide 3% (Merck). Tissue sections were then immersed in protein block serum free (Dako) for 10 min at room temperature. Mouse lung sections were stained with a rat anti-mouse Ly-6C (dilution 1/50) for 2 h at room temperature (Abcam) followed by a HRP-coupled rabbit anti-rat staining (dilution 1/400) for 40 min at room temperature (Abcam). Peroxidase activity was revealed using the 3,3'-diaminobenzidine hydrochloride kit (Dako), and tissues were then counter-colored with Carazzi's hematoxylin. Slides were mounted on Eukitt medium (Fluka Analytical).

In vivo labeling of vascular leukocytes

WT mice were injected i.v. with 0.5 µg of anti-CD45.2 antibodies. The antibody was allowed to circulate for 3 minutes prior to euthanasia in order to label all leukocytes in the vascular space. Lungs were then harvested without being perfused and the monocyte/macrophage populations were analyzed by flow cytometry.

Airway exposure to TLR ligands and pathogens

Lightly isoflurane anesthetized mice were instilled i.n. with 50 µl saline or 50 µl saline containing various TLR ligands (i.e. Pam3CSK4 25 µg; Poly(I:C) 50 µg; LPS 10 µg; FLA-BS 1 µg; MALP-2 1 µg; CpG-DNA 50 µg) or respiratory pathogens (i.e. influenza A 5 PFU; *S. pneumoniae* serotype 1, clinical isolate E1586, 10^5 CFU). The doses of TLR ligands used were chosen according to the ones found in the literature: Pam3CSK4 (Andrade et al., 2013; Chen et al., 2016); Poly(I :C) (Errea et al., 2015; LeMessurier et al., 2013); LPS (Chen et al., 2014; Hiroshima et al., 2014); FLA-BS (Errea et al., 2015; Munoz et al., 2010); MALP-2 (Reppe et al., 2015); R848 (Marino et al., 2011; Van et al., 2011); CpG (Hickey et al., 2013; Vogel and Brown, 2015). Influenza type A virus strain A/PR/8/34 (PR8) was provided by Dr François Trottein (Institut Pasteur de Lille, France). In experiments shown in Figure S2B and S2C, the concentration of the TLR ligands used was corresponding to 5 nmoles for each stimulant.

House dust mite-induced model of asthma and CpG treatments.

Lightly isoflurane anesthetized WT, ITIB or *Tlr9*$^{-/-}$ mice were sensitized by two weekly i.n. instillations of vehicle (LPS-free saline) or HDM extracts (100 µg in 50 µl) on day 0 and on day 7. In experiments shown in Figure 3E and 3F, mice were sensitized by HDM on day 0 and AlexaFluor-labeled HDM on day 7.

For assessing the effects of CpG in preventing asthma development (Figure 3), mice were instilled i.n. with 50 µl saline containing 50 µg ODN or 50 µg CpG 7 days before the first HDM treatment. Mice were sacrificed 3 days after the second HDM treatment (day 10). In adoptive transfer experiments, WT mice were transferred i.t. with $1.5x10^6$ AMs or CpG IMs sorted from CpG-treated WT or *Il-10*$^{-/-}$ mice (mortality rate varying between 40 and 60% in CpG-injected *Il-10*$^{-/-}$ mice, but not WT mice, unpublished observation), or vehicle (50 µl saline), 24 hours before each HDM treatment (days -1 and 6).

For assessing the curative effects of CpG on established asthma (Figure 4), mice were instilled i.n. with 50 µl saline containing 50 µg ODN or 50 µg CpG 7 days after the second HDM treatment (day 14). Seven days later (day 21), mice were challenged by an i.n. instillation of vehicle (LPS-free saline) or HDM (100 µg in 50 µl). In experiments shown in Figure 4E and 4F, mice were challenged by AlexaFluor-labeled HDM on day 21. Mice were sacrificed at day 24. In adoptive transfer experiments, WT mice were transferred i.t. with $1.5x10^6$ AMs or CpG IMs sorted from CpG-treated WT or *Il-10*$^{-/-}$ mice (mortality rate varying between 40 and 60% in CpG-injected *Il-10*$^{-/-}$ mice, but not WT mice, unpublished observation), or vehicle (50 µl saline), 24 hours before the last HDM challenge (day 20). In

experiments assessing the long-lasting effects of CpG on established asthma, mice were challenged with HDM 8 weeks after a single CpG instillation and were sacrificed 3 days later.

Assessment of the asthmatic response in HDM-exposed mice

AHR was estimated by assessing dynamic airway resistance in anesthetized animals subjected to increasing doses of methacholine using a FlexiVent small animal ventilator (SCIREQ), as previously described (Gueders et al., 2009). Mice were sacrificed and BALF, lungs and lymph node cells were harvested and analyzed as described previously (Marichal et al., 2010). Briefly, BALF eosinophilia was evaluated by total and differential cell counts, lung inflammation and mucus production were evaluated on H&E- and PAS-stained lung sections, respectively. Mucus production was also quantified as the percentage of PAS-stained goblet cells per total epithelial cells in randomly selected bronchi. Seven randomly selected sections were analyzed per murine lung. Bronchial lymph node cells were cultured *in vitro* in supplemented Click's medium (10% FBS, L-glutamine 8mM, modified essential amino acids 0.1 mM, sodium pyruvate 1mM, Penicillin/Streptomycin 50 UI ml^{-1} and β-mercaptoethanol 0.5mM) with or without HDM restimulation (30 μg ml^{-1}). Culture supernatants were assayed for cytokine production (IL-4, IL-5, IL-13) by ELISA (eBioscience) after 3 days of culture.

To assess DC maturation and migration, mice were injected i.n. with 100 μg of HDM labeled with Alexa fluor-647 or saline at day 7 (Figure 3E and 3F) or at day 21 (Figure 4E and 4F). Mice were sacrificed 24 hours later. BLN were minced, and total cell numbers were counted by the use of a hemacytometer. The number of antigen-positive DCs (i.e. $HDM^{+}CD11c^{hi}MHC\text{-}II^{hi}$ cells) was determined in the BLN by flow cytometry. The extent of lung DC maturation was determined by quantifying surface expression of the maturation markers CD86 and MHC-II on lung total DCs (i.e. non-autofluorescent $CD11c^{hi}MHC\text{-}II^{int/hi}$ cells) by flow cytometry.

OVA/Alum-induced model of asthma and CpG treatments

WT mice were sensitized on days 0 and 14 by i.p. injection of 100 μl saline containing 10 μg OVA (grade V) admixed with 100 μl Imject Alum (Pierce). Sham-immunized mice received 100 μl saline mixed with 100 μl Imject Alum. On days 28–31, mice were challenged by exposure to an aerosol of 1% OVA (w/v; grade III) in saline for 1 hour. For assessing the curative effects of CpG on established asthma, mice were instilled i.n. with 50 μl saline containing 50 μg ODN or 50 μg CpG 7 days before the aerosol challenge (day 21). Mice were sacrificed 24 hours after the last challenge (day 32). In adoptive transfer experiments, WT mice were transferred i.t. with $1.5x10^{6}$ of AMs or CpG IMs sorted from CpG-treated WT mice or vehicle (50 μl saline) 24 hours before the OVA challenge (day 27).

Read-outs used for assessment of the asthmatic response was performed similarly as for the HDM-induced asthma models, except that BLN were restimulated with OVA (50 μg ml^{-1}, grade V) and that a quantification of OVA-specific IgE was also performed, as described (Marichal et al., 2011).

Generation of bone marrow mixed chimeras and parabiotic mice

Twelve week-old $CD45.1/2^{+}$ WT C57BL/6 mice were lethally irradiated with two doses of 6 Gy 3 hours apart. Two hours after the second irradiation, these mice were injected i.v. with

$2x10^6$ BM cells consisting of a 1:1 mix of BM cells obtained from $CD45.1^+$ C57BL/6 and $CD45.2^+$ *Ccr2*$^{-/-}$ C57BL/6 mice. Mice were treated with antibiotics (Baytril, Bayer, 0.05 $mg.ml^{-1}$ in drinking water) from the day before irradiation until the time of sacrifice. Cell numbers were evaluated 7, 14, 56 and 84 days later and chimerism was assessed 56 and 84 days later. In some experiments, such BM mixed chimeras were instilled with CpG or LPS 7 days before the analysis.

Parabiotic mice were generated by suturing age- and weight-matched WT $CD45.1^+$ and *Ccr2*$^{-/-}$ $CD45.2^+$ mice at the age of 6 weeks. Mice were analyzed at 6 months of age.

Assessment of cell proliferation using EdU incorporation

One, two or three days after i.n. administration of CpG, C57BL/6 WT or *Ccr2*$^{-/-}$ mice were injected i.p. with EdU (1 mg in 400 µl). Mice were sacrificed 24 hours later and incorporation of EdU was assessed by flow cytometry.

***Ex vivo* stimulation of tissue monocytes with CpG and LPS**

Lung and splenic monocytes were sorted by FACS according to the gating strategy described in Figure 1a and by Swirski and collaborators (Swirski et al., 2009), respectively. Two hundred thousands ($2x10^5$) cells were cultured in RPMI medium supplemented with 10% FBS and additives (L-glutamine 8 mM, MEAA 0.1 mM, Pyruvate Na 1mM, Penicillin/streptomycin 50 UI ml^{-1}, β-mercaptoethanol 0.5 mM), with or without CpG (7 µg ml^{-1}) or LPS (10 ng ml^{-1}) in a 24-well plate. Twenty-four, 36, 48 and 54 hours later, cells were harvested and phenotyped. ViaProbe (7-AAD) cell viability solution was used to discriminate between dead and living cells.

Western blot

Five hundred thousands lung monocytes were sorted by FACS from naive *Ccr2*$^{-/-}$ mice and were cultured in RPMI medium supplemented with 10% FBS and additives (L-glutamine 8mM, MEAA 0.1 mM, Pyruvate Na 1mM, Penicillin/streptomycin 50UI ml^{-1}, β-mercaptoethanol 0.5mM) in a 12-well plate. Cells were treated with or without ODN or CpG-DNA (7 µg ml^{-1}) for 30 minutes. Cells were then harvested, centrifuged and pellets were lysed in radioimmunoprecipitation assay (RIPA) lysis buffer with 1 mM Na3VO4, 10 mM NaF and complete protease inhibitor (Roche Diagnostics). Protein extracts were added to Laemmli buffer, boiled and run on a 10% polyacrylamide-SDS gel; after electrophoresis, gels were electro-transferred onto a polyvinylidene difluoride membrane (PVDF) for western-blotting. Nonspecific binding was blocked in 20 mM Tris, pH 7.5, 500 mM NaCl, 0.2% Tween 20 (TBS-Tween), and 5% dry milk during 1 h. Membranes were then incubated with rabbit anti-phospho-p44/42 MAPK (Erk1/2), anti-p44/42 MAPK (Erk1/2) or anti-β-Actin antibodies (1:1,000; Cell Signaling Technology) overnight at 4°C, rinsed with TBS-Tween and further incubated with horseradish peroxidase (HRP)-conjugated goat anti-rabbit IgG (1:5,000; Kirkegaard & Perry Laboratories) for 60 min at room temperature. Result was visualized using an enhanced chemiluminescence system (ECL kit; Amersham) followed by autoradiography with Fuji x-ray films.

mRNA isolation, microarray and Gene Set Enrichment Analyses

Singlet living Ly-$6C^{hi}CD64^{lo}$ cells from *Ccr2*$^{-/-}$ or WT mice, and AMs, SS IMs and CpG IMs

from WT mice were directly sorted in Trizol® (Life Technologies). The 4 cell populations were sorted in duplicate (CpG IMs) or triplicate (all the others), yielding a total of 11 samples. Total RNA was purified using Direct-zol® kit (Zymo Research) following manufacturer's recommendations. For each cell type, total RNAs were eluted in a total of 175 µl of water. Eluted RNAs were incubated with DNase for 10 min at room temperature in a total volume of 200 µl using the RNase-Free DNase Set from Qiagen (Venlo), followed by purification on RNeasy® Micro columns (Qiagen) and final elution in 50µl water. RNAs were quantitatively and qualitatively verified using Agilent RNA 6000 Pico Kit run on an Agilent 2100 Bioanalyzer. Concentrations were around 1ng/µl and RNA Integrity Numbers were above 8.

1.5ng RNA was used to generate fragmented and biotin-labeled ssDNA targets using GeneChip® WT Pico Reagent Kit (Affymetrix). The fragmented and labeled targets were hybridized to GeneChip® Mouse Gene 1.0 ST Arrays following standard Affymetrix protocol, which includes overnight hybridization at 45°C and 60 rpm in an Affymetrix GeneChip Hybridization Oven 645. The arrays were then washed and stained in an Affymetrix GeneChip Fluidics Station 450.

Microarrays were analyzed using R (version 3.3.1) and Bioconductor (Huber et al., 2015). Raw data were background-corrected and quantile-normalized using "Robust Multichip Average algorithm" (RMA) from "oligo" package. Normalized data were then annotated using "mogene10sttranscriptcluster.db" annotation package.

Differential expression analysis between Ly-6C^{hi} monocytes from *Ccr2*$^{-/-}$ mice and Ly-6C^{hi} monocytes from WT mice was performed using "Linear Models for Microarray Data" (Limma) package in Bioconductor, with thresholds as following: Benjamini Hochberg adjusted *P* value (adj *P* value) < 0.05 AND Fold Change (FC) > 2 or < 0.5, and after having filtered out non annotated probes. Differential expression analysis between SS IMs and CpG IMs was performed identically, excepted for adj *P* value threshold set to 0.05. Volcano plot of differences between Ly-6C^{hi} monocytes from *Ccr2*$^{-/-}$ mice and Ly-6C^{hi} monocytes from WT mice was obtained by plotting $\log_2$ (FC) on the x axis and $-\log_{10}$ (adj *P* value) on the y axis for all probes present in the Affymetrix GeneChip® Mouse Gene 1.0 ST Array, including non annotated ones.

Heatmaps were generated by plotting normalized expression values of relevant samples and genes using "heatmap.2" function from "gplots" package.

Principal Component Analysis (PCA) was performed using "prcomp" function on normalized expression values of AMs, SS IMs and CpG IMs. Values of principal components 1, 2 and 3 were then tridimensionnally plotted using "plot3d" function of "rgl" package. Percentages shown on each axis indicate the % of variability explained, with PC1 explaining the most variability.

In order to identify biological signatures of CpG IMs compared to SS IMs, we decided to employ the commonly used non-parametric, rank based tool, Gene Set Enrichment Analysis (GSEA version 2.2.2) (Subramanian et al., 2005). Microarray normalized expression data of SS IMs (3 samples) and CpG IMs (2 samples) were used by GSEA as dataset to rank genes between the two cell types. Since (i) CpG IM class contains 2 samples and (ii) RMA normalized data are in log scale, « Diff_of_Classes » method was chosen to rank genes in the dataset. Enrichment analysis was then performed using hallmark gene sets of MsigDB database.

Real-time PCR analysis

Singlet living lung Ly-6C^{hi} cells from *Ccr2*$^{-/-}$ mice, and lung IMs, AMs and splenic monocytes from WT mice were directly sorted in Trizol® (Life Technologies). Total RNA was isolated using Direct-zol® kit (Zymo Research) following manufacturer's recommendations. Complementary DNA was obtained using RevertAid First Strand cDNA Synthesis Kit (Thermo Fisher Scientific). Quantitative real-time PCR were performed in duplicates using ABsolute Blue qPCR SYBR Green ROX Mix (Thermo Fisher Scientific) and ABI 7900HT Fast Real-Time PCR System (Applied Biosystems) under the following conditions: (1) initial denaturation at 95°C for 15 min followed by (2) 40 cycles of 95°C 15 s and 60°C 1 min. Primer sequences were as followed :. 5'-AGCTGAACATGAACGGCATCT-3' and 5'- GATCGGCCAGCCATCTGA-3' for *Tlr9*, 5'-AGCCCAGTGTTACCACCAAG-3' and 5'-ACCCAAGAACAAGCACAAGG-3' for the housekeeping gene *Ubc*, 5'-CATGGCTCGCTCGGTGACC-3' and 5'-AATGTGAGGCGGGTGGAACTG-3' for the housekeeping gene *B2m*, 5'-AGCTACTGTAATGATCAGTCAACG-3' and 5'-AGAGGTCCTTTTCACCAGCA-3' for the housekeeping gene *Hprt*. Expression levels of TLR9 were normalized relative to three control genes (*Ubc*, *B2m* and *Hprt*) using qBase+ software (Biogazelle).

s.c. and i.p. CpG treatments

WT mice were injected s.c. or i.p. with 100 µl saline or 200 µl (i.p.) or 100 µl (s.c.) saline containing 50 µg CpG. Mice were analyzed 7 days later.

Splenectomy

Ccr2$^{-/-}$ mice were anesthetized by intraperitoneal injection of ketamine (75 mg kg^{-1}), xylazine (10 mg kg^{-1}) and buprenorphine (0.05 mg kg^{-1}). A transversal incision was made on the left lower back of the mice to expose the spleen. Spleen was resected and vessels were cauterized. The incision was sutured. Sham-operated mice underwent the same procedure without removal of the spleen.

Chemokine array

Lightly isoflurane anesthetized WT mice were instilled i.n. with 50 µl saline or 50 µl saline containing either CpG (50 µg) or LPS (10 µg). Eight hours later, mice were sacrificed and lungs were harvested without being perfused. Lungs were homogenized with an UltraTurrax homogenizer (IKA) in 2 ml saline containing complete protease inhibitor (Roche Diagnostics). Samples were then centrifuged for 10 minutes at 16,000 x g and supernatants were tested for the presence of chemokines using a chemokine antibody array (Abcam) according to manufacturer instructions. Membranes were developed and digitized for analysis using ImageJ. Each sample spot density was measured, averaged and normalized to membrane reference spots.

Chemokine inhibition

Ccr2$^{-/-}$ mice were injected i.p. with neutralizing anti-CCL2 (200 µg), anti-CCL5 (50 µg), anti-CCL9 (50 µg) antibodies or a combination of these 3 antibodies, 30 minutes before an i.n. administration of CpG. Control mice received the appropriate isotype controls. The numbers

of lung monocytes and CpG IMs were analyzed 1 day and 7 days after CpG administration, respectively.

Statistical Analysis

Statistical analyses were performed using R (version 3.2.4). Data from independent experiments were pooled for analysis in each data panel, unless otherwise indicated. Raw data was transformed when needed and was back-transformed for graphical presentation. Respect of the assumptions of normal distribution of residuals and homoscedasticity was verified using diagnostic plots. We considered a *P*-value lower than 0.05 as significant. *, $P<0.05$; **, $P<0.01$, ***, $P<0.001$; ns, not significant.

Supplemental References

Andrade, E.B., Alves, J., Madureira, P., Oliveira, L., Ribeiro, A., Cordeiro-da-Silva, A., Correia-Neves, M., Trieu-Cuot, P., and Ferreira, P. (2013). TLR2-induced IL-10 production impairs neutrophil recruitment to infected tissues during neonatal bacterial sepsis. J. Immunol. *191*, 4759-4768.

Bouabe, H., Liu, Y., Moser, M., Bosl, M.R., and Heesemann, J. (2011). Novel highly sensitive IL-10-beta-lactamase reporter mouse reveals cells of the innate immune system as a substantial source of IL-10 in vivo. J. Immunol. *187*, 3165-3176.

Chen, H., Wu, S., Lu, R., Zhang, Y.G., Zheng, Y., and Sun, J. (2014). Pulmonary permeability assessed by fluorescent-labeled dextran instilled intranasally into mice with LPS-induced acute lung injury. PloS One *9*, e101925.

Chen, Y.G., Zhang, Y., Deng, L.Q., Chen, H., Zhang, Y.J., Zhou, N.J., Yuan, K., Yu, L.Z., Xiong, Z.H., Gui, X.M.*, et al.* (2016). Control of Methicillin-Resistant Staphylococcus aureus Pneumonia Utilizing TLR2 Agonist Pam3CSK4. PloS One *11*, e0149233.

Errea, A., Gonzalez Maciel, D., Hiriart, Y., Hozbor, D., and Rumbo, M. (2015). Intranasal administration of TLR agonists induces a discriminated local innate response along murine respiratory tract. Immunol. Lett. *164*, 33-39.

Gueders, M.M., Paulissen, G., Crahay, C., Quesada-Calvo, F., Hacha, J., Van Hove, C., Tournoy, K., Louis, R., Foidart, J.M., Noel, A., and Cataldo, D.D. (2009). Mouse models of asthma: a comparison between C57BL/6 and BALB/c strains regarding bronchial responsiveness, inflammation, and cytokine production. Inflamm. Res. *58*, 845-854.

Hemmi, H., Takeuchi, O., Kawai, T., Kaisho, T., Sato, S., Sanjo, H., Matsumoto, M., Hoshino, K., Wagner, H., Takeda, K., and Akira, S. (2000). A Toll-like receptor recognizes bacterial DNA. Nature *408*, 740-745.

Hickey, A.J., Lin, J.S., Kummer, L.W., Szaba, F.M., Duso, D.K., Tighe, M., Parent, M.A., and Smiley, S.T. (2013). Intranasal prophylaxis with CpG oligodeoxynucleotide can protect against Yersinia pestis infection. Infect. Immun. *81*, 2123-2132.

Hiroshima, Y., Hsu, K., Tedla, N., Chung, Y.M., Chow, S., Herbert, C., and Geczy, C.L. (2014). S100A8 induces IL-10 and protects against acute lung injury. J. Immunol. *192*, 2800-2811.

Huber, W., Carey, V.J., Gentleman, R., Anders, S., Carlson, M., Carvalho, B.S., Bravo, H.C., Davis, S., Gatto, L., Girke, T.*, et al.* (2015). Orchestrating high-throughput genomic analysis with Bioconductor. Nat. Methods *12*, 115-121.

LeMessurier, K.S., Hacker, H., Chi, L., Tuomanen, E., and Redecke, V. (2013). Type I interferon protects against pneumococcal invasive disease by inhibiting bacterial transmigration across the lung. PLoS Pathog. *9*, e1003727.

Marichal, T., Bedoret, D., Mesnil, C., Pichavant, M., Goriely, S., Trottein, F., Cataldo, D., Goldman, M., Lekeux, P., Bureau, F., and Desmet, C.J. (2010). Interferon response factor 3 is essential for house dust mite-induced airway allergy. J. Allergy Clin. Immunol. *126*, 836-844.

Marichal, T., Ohata, K., Bedoret, D., Mesnil, C., Sabatel, C., Kobiyama, K., Lekeux, P., Coban, C., Akira, S., Ishii, K.J., *et al.* (2011). DNA released from dying host cells mediates aluminum adjuvant activity. Nat. Med. *17*, 996-1002.

Marino, R., Thuraisingam, T., Camateros, P., Kanagaratham, C., Xu, Y.Z., Henri, J., Yang, J., He, G., Ding, A., and Radzioch, D. (2011). Secretory leukocyte protease inhibitor plays an important role in the regulation of allergic asthma in mice. J. Immunol. *186*, 4433-4442.

Munoz, N., Van Maele, L., Marques, J.M., Rial, A., Sirard, J.C., and Chabalgoity, J.A. (2010). Mucosal administration of flagellin protects mice from Streptococcus pneumoniae lung infection. Infect. Immun. *78*, 4226-4233.

Reppe, K., Radunzel, P., Dietert, K., Tschernig, T., Wolff, T., Hammerschmidt, S., Gruber, A.D., Suttorp, N., and Witzenrath, M. (2015). Pulmonary immunostimulation with MALP-2 in influenza virus-infected mice increases survival after pneumococcal superinfection. Infect. Immun. *83*, 4617-4629.

Subramanian, A., Tamayo, P., Mootha, V.K., Mukherjee, S., Ebert, B.L., Gillette, M.A., Paulovich, A., Pomeroy, S.L., Golub, T.R., Lander, E.S., and Mesirov, J.P. (2005). Gene set enrichment analysis: a knowledge-based approach for interpreting genome-wide expression profiles. P. Natl. Acad. Sci. U.S.A *102*, 15545-15550.

Swirski, F.K., Nahrendorf, M., Etzrodt, M., Wildgruber, M., Cortez-Retamozo, V., Panizzi, P., Figueiredo, J.L., Kohler, R.H., Chudnovskiy, A., Waterman, P., *et al.* (2009). Identification of splenic reservoir monocytes and their deployment to inflammatory sites. Science *325*, 612-616.

Van, L.P., Bardel, E., Gregoire, S., Vanoirbeek, J., Schneider, E., Dy, M., and Thieblemont, N. (2011). Treatment with the TLR7 agonist R848 induces regulatory T-cell-mediated suppression of established asthma symptoms. Eur. J Immunol. *41*, 1992-1999.

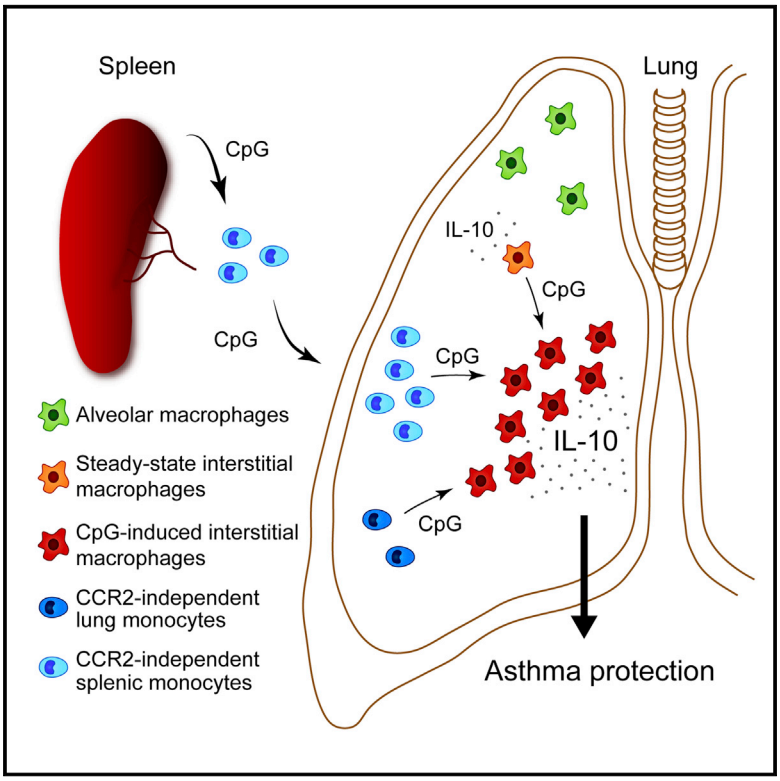
Vogel, A.J., and Brown, D.M. (2015). Single-Dose CpG Immunization Protects Against a Heterosubtypic Challenge and Generates Antigen-Specific Memory T Cells. Front. Immunol. *6*, 327.

Article

Immunity

Exposure to Bacterial CpG DNA Protects from Airway Allergic Inflammation by Expanding Regulatory Lung Interstitial Macrophages

Graphical Abstract



Authors

Catherine Sabatel, Coraline Radermecker, Laurence Fievez, ..., Florent Ginhoux, Thomas Marichal, Fabrice Bureau

Correspondence

t.marichal@ulg.ac.be (T.M.), fabrice.bureau@ulg.ac.be (F.B.)

In Brief

Exposure to unmethylated CpG DNA (CpG) from bacteria is associated with a reduced risk of developing asthma. Sabatel et al. find that CpG exposure leads to higher numbers of lung interstitial macrophages that prevent allergic inflammation through the production of the regulatory cytokine interleukin-10.

Highlights

- Exposure to bacterial CpG DNA (CpG) expands regulatory lung interstitial macrophages (IMs)
- Transfer of WT but not *Il10*$^{-/-}$ IMs protects from allergen-induced airway inflammation
- CpG-induced IMs arise from local and splenic reservoir monocytes
- Migration of regulatory IM precursors to the lung does not require CCR2

Accession Numbers

E-MTAB-5012

Sabatel et al., 2017, Immunity *46*, 457–473
March 21, 2017 © 2017 Elsevier Inc.
http://dx.doi.org/10.1016/j.immuni.2017.02.016

CellPress

Immunity
Article

Exposure to Bacterial CpG DNA Protects from Airway Allergic Inflammation by Expanding Regulatory Lung Interstitial Macrophages

Catherine Sabatel,[1,2,11] Coraline Radermecker,[1,2,11] Laurence Fievez,[1,11] Genevieve Paulissen,[1] Svetoslav Chakarov,[3] Claudia Fernandes,[1] Sabine Olivier,[1] Marie Toussaint,[4] Dimitri Pirottin,[1,2] Xue Xiao,[2,5] Pascale Quatresooz,[6] Jean-Claude Sirard,[7] Didier Cataldo,[8] Laurent Gillet,[2,5] Hicham Bouabe,[9] Christophe J. Desmet,[1] Florent Ginhoux,[3] Thomas Marichal,[1,2,*] and Fabrice Bureau[1,2,10,12,*]

[1]Laboratory of Cellular and Molecular Immunology, GIGA Research, University of Liège, 4000 Liège, Belgium
[2]Faculty of Veterinary Medicine, University of Liège, 4000 Liège, Belgium
[3]Singapore Immunology Network, Agency for Science, Technology, and Research, Singapore 138648, Singapore
[4]Airway Disease Infection Section, National Heart and Lung Institute, Imperial College London, London W2 1PG, UK
[5]Laboratory of Immunology-Vaccinology, Fundamental and Applied Research for Animals & Health, University of Liège, 4000 Liège, Belgium
[6]Centre de Recherche sur les Protéines Prion, Department of Human Histology, University of Liège, 4000 Liège, Belgium
[7]INSERM U1019, CNRS UMR 8204, Center for Infection and Immunity of Lille, University of Lille, CHU Lille, Institut Pasteur de Lille, 59000 Lille, France
[8]Laboratory of Tumor and Developmental Biology, GIGA Research, University of Liège, 4000 Liège, Belgium
[9]Laboratory of Lymphocyte Signalling and Development, Babraham Institute, Cambridge CB22 3AT, UK
[10]Walloon Excellence in Life Sciences and Biotechnology, Wallonia, Belgium
[11]Co-first author
[12]Lead Contact
*Correspondence: t.marichal@ulg.ac.be (T.M.), fabrice.bureau@ulg.ac.be (F.B.)
http://dx.doi.org/10.1016/j.immuni.2017.02.016

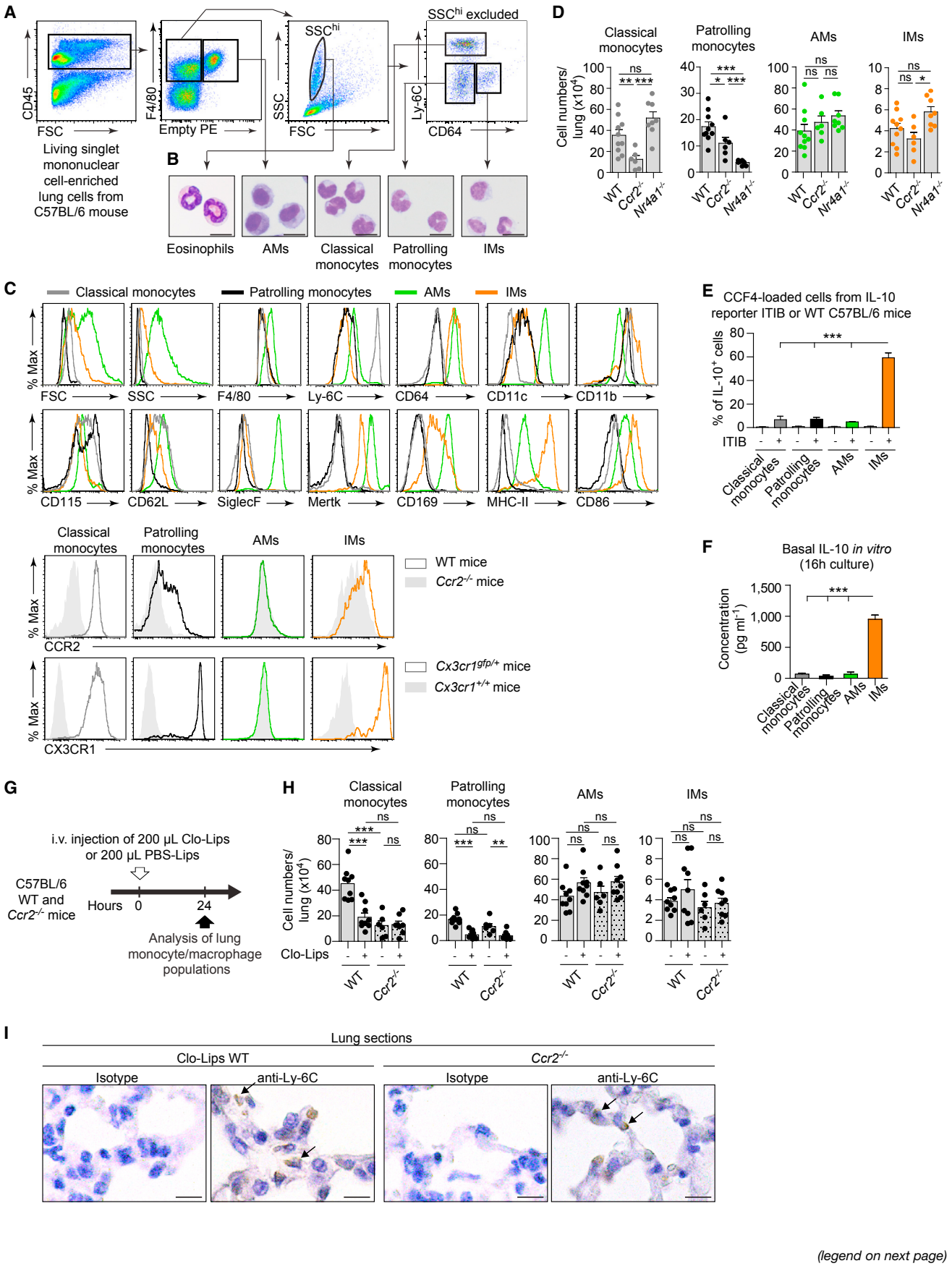
SUMMARY

Living in a microbe-rich environment reduces the risk of developing asthma. Exposure of humans or mice to unmethylated CpG DNA (CpG) from bacteria reproduces these protective effects, suggesting a major contribution of CpG to microbe-induced asthma resistance. However, how CpG confers protection remains elusive. We found that exposure to CpG expanded regulatory lung interstitial macrophages (IMs) from monocytes infiltrating the lung or mobilized from the spleen. Trafficking of IM precursors to the lung was independent of CCR2, a chemokine receptor required for monocyte mobilization from the bone marrow. Using a mouse model of allergic airway inflammation, we found that adoptive transfer of IMs isolated from CpG-treated mice recapitulated the protective effects of CpG when administered before allergen sensitization or challenge. IM-mediated protection was dependent on IL-10, given that *Il10*$^{-/-}$ CpG-induced IMs lacked regulatory effects. Thus, the expansion of regulatory lung IMs upon exposure to CpG might underlie the reduced risk of asthma development associated with a microbe-rich environment.

INTRODUCTION

The increased prevalence of allergic asthma over the past few decades points to alterations in the environment (Eder et al., 2006). The hygiene hypothesis postulates that decreased exposure to environmental and commensal microbes or their products, partly because of changes associated with urban lifestyles, is responsible for this rise (Strachan, 1989; von Mutius, 2016). In line with this hypothesis, epidemiological studies associate growing up on a farm, where exposure to bacterial endotoxin (lipopolysaccharide [LPS]) is high, with reduced risk of allergic sensitization (Braun-Fahrländer et al., 2002; von Mutius, 2016). However, whether LPS mediates the aforementioned protective effects is uncertain. Indeed, concurrent studies in non-rural environments have suggested that exposure to LPS is instead a risk factor for increased asthma prevalence and severity (Thorne et al., 2005). Moreover, although LPS has demonstrated protective effects in some animal models (Schuijs et al., 2015), it has also been shown to promote experimental asthma (Eisenbarth et al., 2002; Hammad et al., 2009).

Another candidate for mediating the protective effects of microbe-rich environments is bacterial DNA, which contains unmethylated CpG motifs with immunomodulatory properties (Krieg, 2006). Bacterial DNA, like LPS, is present in high amounts in dust from rural homes (Roy et al., 2003), and treatment with synthetic CpG DNA (CpG) consistently prevents allergic sensitization in animal models (Kline et al., 1998; Sur et al., 1999). Moreover, CpG is able to reverse established asthma in animals (Broide et al., 1998; Kline et al., 2002) and has shown efficacy in attenuating allergic disorders in human clinical trials (Beeh et al., 2013; Creticos et al., 2006; Krieg, 2006). How CpG exerts these immunomodulatory effects remains unclear. It was initially proposed that CpG, which is often co-administered with allergens, redirects allergen-specific T helper 2 (Th2) cell responses toward Th1 or regulatory T cell responses (Broide et al., 1998; Kline et al., 2002; Kline et al., 1998; Krieg, 2012). However,



(legend on next page)

CpG is capable of conferring protection in the absence of allergens (Beeh et al., 2013; Broide et al., 1998; Krieg, 2012), suggesting that it acts independently of the adaptive immune system.

In 2009, we identified a small population of regulatory macrophages in the lung interstitium of mice (Bedoret et al., 2009). These lung interstitial macrophages (IMs), also found in humans (Hoppstädter et al., 2010), spontaneously produce the immunosuppressive cytokine interleukin-10 (IL-10), a hallmark of regulatory macrophages (Mosser and Edwards, 2008). Moreover, when exposed to low doses of LPS, IMs, which are located in the vicinity of lung dendritic cells (DCs), can counteract the capacity of LPS-activated DCs to induce Th2 responses against harmless antigens (Bedoret et al., 2009). In agreement with this, mice lacking functional IMs, but not wild-type (WT) mice, develop overt asthmatic reactions when exposed to low doses of a mixture of allergen and LPS (Bedoret et al., 2009). However, the immunosuppressive effects of IMs are overwhelmed when the airways are exposed to high levels of allergens and LPS, given that 100% of WT mice develop asthma upon exposure to high doses of house dust mite (HDM) extracts, a phenomenon that requires Toll-like receptor 4 (TLR4) activation by HDM-borne LPS (Hammad et al., 2009). We therefore reasoned that pathogen-associated molecular patterns (PAMPs) other than LPS could improve the immunosuppressive effects of IMs and thereby explain how a microbe-rich environment reduces the risk of asthma development.

Here, we found that CpG is able to robustly expand the IM population. CpG-induced IMs (CpG IMs) developed from local and splenic reservoir monocytes and were able, by producing IL-10, to confer protection against allergic inflammation even when mice were sensitized and challenged with high doses of HDM. Our findings reveal a role for regulatory IMs shed in the protective effect of CpG exposure in allergic airway inflammation and suggest that similar mechanisms might underlie the reduced risk of human asthma development that is associated with exposure to a microbe-rich environment.

RESULTS

A Simplified Flow Cytometry Strategy Discriminates Lung Monocyte and Macrophage Subsets in Mice

In order to identify the monocyte and macrophage populations associated with the lung at steady state, we set up a simplified six-step, five-color flow cytometry staining procedure on mononuclear-cell-enriched lung cells isolated from whole, non-lavaged, perfused lungs of naive C57BL/6 WT mice. To encompass all monocyte and macrophage populations, we gated sequentially on living singlet cells (step 1), $CD45^+$ immune cells (step 2), and cells positive for the pan-monocyte and -macrophage marker F4/80 (step 3) (Figure 1A). Alveolar macrophages (AMs), the most abundant lung phagocytic cells present in the airways (Figure S1A), were identified as large (FSC^{hi}) autofluorescent $CD11c^{hi}SiglecF^{hi}CD64^+Mertk^+CD169^+$ cells (step 4) (Figures 1A–1C). F4/80-expressing lung-resident eosinophils (Mesnil et al., 2016) were excluded on the basis of their high granularity (SSC^{hi}) (step 5). The remaining $CD45^+F4/80^+$ cells were further separated into three populations according to their expression of the monocyte and macrophage markers Ly-6C (Geissmann et al., 2003) and CD64 (Gautier et al., 2012) (step 6) (Figures 1A and 1B).

Ly-$6C^{hi}CD64^{lo}$ cells were classical monocytes, given that they exhibited a monocytic morphology, expressed the typical markers of classical monocytes (Ly-$6C^{hi}CCR2^+CX3CR1^{int}$ $CD62L^+$), and were less abundant in *Ccr2*$^{-/-}$ mice (Figure 1B–1D), in which classical monocyte emigration from the bone marrow (BM) is compromised (Serbina and Pamer, 2006). Ly-$6C^{lo}CD64^{lo}$ cells also displayed a monocytic morphology, expressed the characteristic markers of patrolling monocytes (Ly-$6C^{lo}CCR2^{lo}CX3CR1^{hi}CD62L^-$), and were significantly reduced in mice lacking NR4A1 (Figure 1B–1D), a transcription factor controlling differentiation and survival of patrolling monocytes (Hanna et al., 2011), demonstrating that these cells were patrolling monocytes.

Finally, Ly-$6C^{lo}CD64^{hi}$ cells were identified as IMs. Indeed, these cells were absent in the broncho-alveolar lavage fluid (BALF) (Figure S1A) and were positive for MHC-II and the macrophage markers Mertk and CD169 (Figure 1C). IMs were already present after birth (Figure S1B), expressed low levels of CCR2, and were found in similar numbers in 6- to 10-week-old *Ccr2*$^{-/-}$, *Nr4a1*$^{-/-}$, and WT mice (Figure 1D). However, their numbers were significantly lower in 1-year-old *Ccr2*$^{-/-}$ mice than in age-matched controls (Figure S1C), suggesting that IMs represent a heterogeneous population and are partially maintained by classical monocytes in adults, as reported by others (Tan and Krasnow, 2016). To test this, we sutured $CD45.1^+$ WT and $CD45.2^+$ *Ccr2*$^{-/-}$ mice together for 6 months and analyzed the enrichment in WT partner cells within the *Ccr2*$^{-/-}$ host (Figure S1D). Parabiotic mice efficiently exchanged their circulation, as attested by the percentage of enrichment in blood B cells that

Figure 1. Identification of Monocyte and Macrophage Populations in the Mouse Lung

(A) Gating strategy.

(B) Photographs of FACS-sorted populations gated in (A).

(C and D) Surface phenotype (C) and absolute numbers (D) of the indicated populations in the lungs of WT (C and D), *Ccr2*$^{-/-}$ (D), and *Nr4a1*$^{-/-}$ (D) mice.

(E) Percentage of IL-10^+ cells within the cell populations as assessed by detection of 450 nm florescence (blue product) in CCF4-substrate-loaded cells isolated from IL-10-β-lactamase reporter ITIB or WT mice.

(F) Basal IL-10 concentration in culture supernatants of primary cell culture.

(G) Experimental outline for data in (H).

(H) Absolute numbers of the indicated populations in the lungs of WT and *Ccr2*$^{-/-}$ mice treated with i.v. PBS-Lips or Clo-Lips.

(I) Representative anti-Ly-6C immunostainings of lung sections from Clo-Lip-treated WT mice and *Ccr2*$^{-/-}$ mice.

Data in (A)–(C) and (I) represent one of at least six mice from at least three independent experiments. Data in (D) and (H) show the mean + SEM pooled from three independent experiments (n = 6–10 per group). Data in (E) and (F) show the mean + SEM from one of three independent experiments (n = 3–4 per group). p values were calculated with a one-way (D–F) or two-way (H) ANOVA followed by Tukey's post hoc tests (*$p < 0.05$; **$p < 0.01$; ***$p < 0.001$; ns, not significant). Scale bars, 10 μm. See also Figure S1 for additional information regarding the phenotype, localization, and IL-10 production by lung monocytes and macrophages.

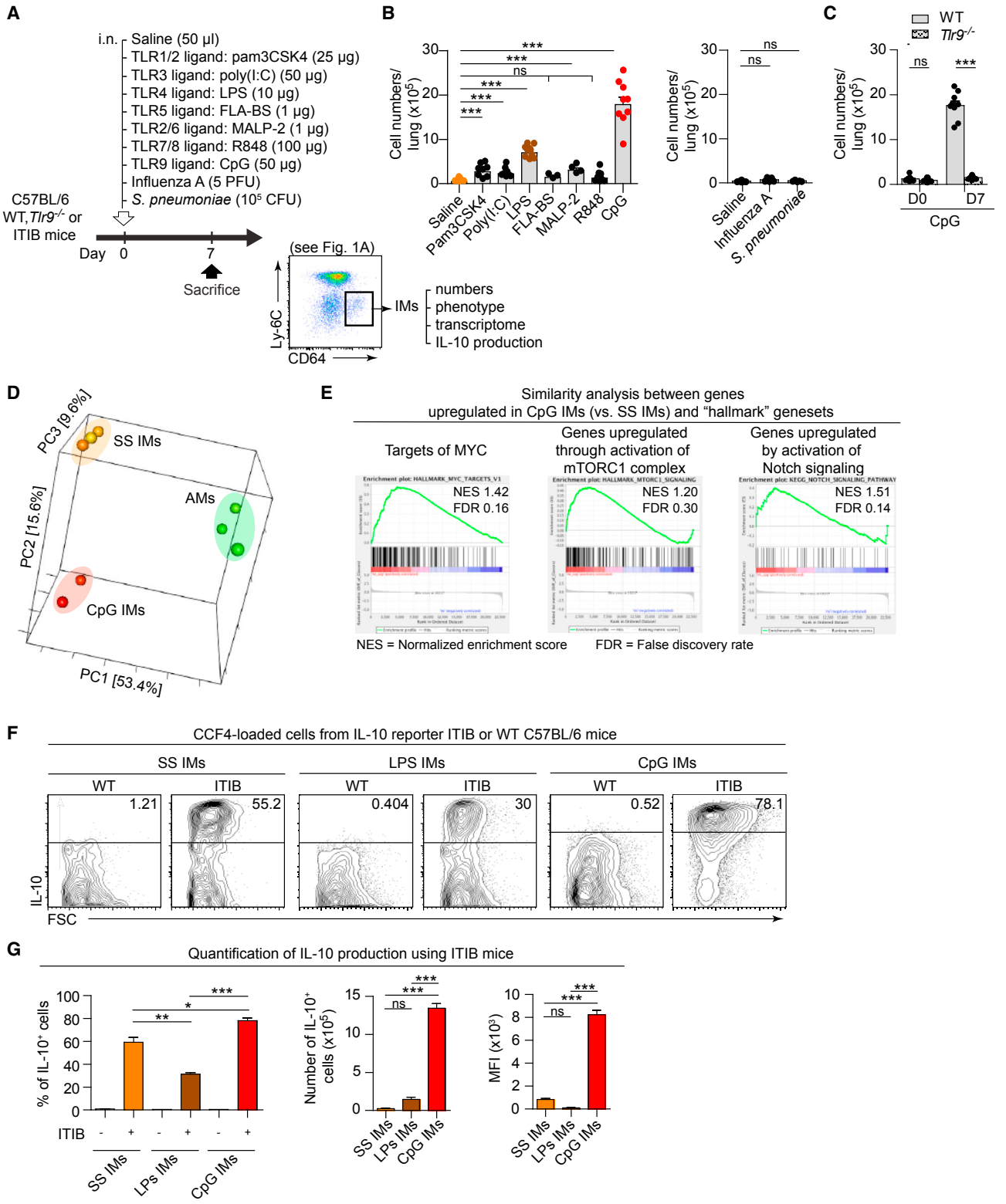


Figure 2. TLR9-Dependent Expansion of IL-10-Producing IMs upon Intranasal CpG Treatment

(A) Experimental outline.

(B and C) Absolute numbers of IMs in the lungs of WT mice 7 days after i.n. stimulation with the indicated TLR ligands or i.n. infection with influenza A or *S. pneumoniae* (B) and *Tlr9*$^{-/-}$ and control mice before and 7 days after i.n. injection of CpG (C). Data show mean + SEM and are pooled from three independent experiments (n = 6–12 per group).

(legend continued on next page)

reached 50%. Conversely, because CCR2 is required for the egress of classical monocytes from the BM, WT monocytes constituted more than 90% of the monocytes present in the blood of *Ccr2*$^{-/-}$ mice. Lung AMs were not enriched in WT cells, confirming that AMs can self-renew by local proliferation at steady state (Hashimoto et al., 2013). However, 35% of the IM pool was constituted by WT partner cells after 6 months of parabiosis, strongly supporting that IMs are, at least in part, replenished by circulating blood monocytes in adults, a feature shared with gut macrophages (Bain et al., 2014).

IMs constitutively expressed IL-10, as quantified in vivo by the use of IL-10-β-lactamase reporter ITIB mice (Bouabe et al., 2011) and ex vivo by ELISA (Figures 1E and 1F; Figure S1E). Notably, a spontaneous IM-derived IL-10 production was dependent on the adaptor molecule MYD88 but independent of TLR9 (Figure S1F), concordant with the fact that LPS, which mediates signaling through MYD88, sustains IM-derived IL-10 at steady state (Bedoret et al., 2009). Upon CpG or LPS stimulation, the increased ability of IMs to produce IL-10 relied on TLR9 and MyD88 or only MyD88, respectively (Figure S1F).

When applied to the lungs during HDM-induced airway allergy, the flow cytometry strategy identified similar cell populations (Figure S1G).

To determine which cells were truly located in the lung tissue, we depleted blood-vessel-associated monocytes and macrophages by injecting clodronate-containing liposomes (Clo-Lips) intravenously 24 hr before analysis (Figure 1G). This regimen had no effect on AMs or IMs but efficiently depleted patrolling monocytes and a substantial part (≈60%) of Ly-6C^{hi} monocytes (Figure 1H), showing that most monocytes, except some Ly-6C^{hi} monocytes, were associated with the lung vasculature. Concordant with this, combined in vivo and ex vivo anti-CD45 stainings confirmed that AMs, IMs, and only a fraction of Ly-6C^{hi} monocytes were truly located in the lungs of WT mice (Figures S1H and S1I). Anti-Ly-6C immunostaining of lung sections from Clo-Lip-treated WT and *Ccr2*$^{-/-}$ mice confirmed that the Ly-6C^{+} cells were located in the lung parenchyma (Figure 1I). Notably, in *Ccr2*$^{-/-}$ mice, Clo-Lip injection did not affect the amount of Ly-6C^{hi} monocytes, whose numbers and localization were similar to those from Clo-Lip-treated WT mice (Figures 1H and 1I), indicating that these monocytes established in the lung independently of CCR2. In the following sections, we refer to these CCR2-independent, lung-infiltrating monocytes, which were already present at the age of 3 days (Figure S1J), as lung monocytes. To assess whether lung monocytes represented a monocyte population distinct from classical CCR2-dependent blood monocytes, we performed a transcriptomic comparison of Ly-6C^{hi} monocytes recovered from perfused lung of WT mice (≈60% of CCR2-dependent classical blood monocytes and ≈40% of lung monocytes) and *Ccr2*$^{-/-}$ mice (more than 95% of lung monocytes). This analysis revealed only one differentially expressed gene, namely *Ccr2* (Figures S1K and S1L), showing that lung monocytes fully corresponded to classical Ly-6C^{hi} monocytes.

CpG Induces TLR9-Dependent IM Expansion

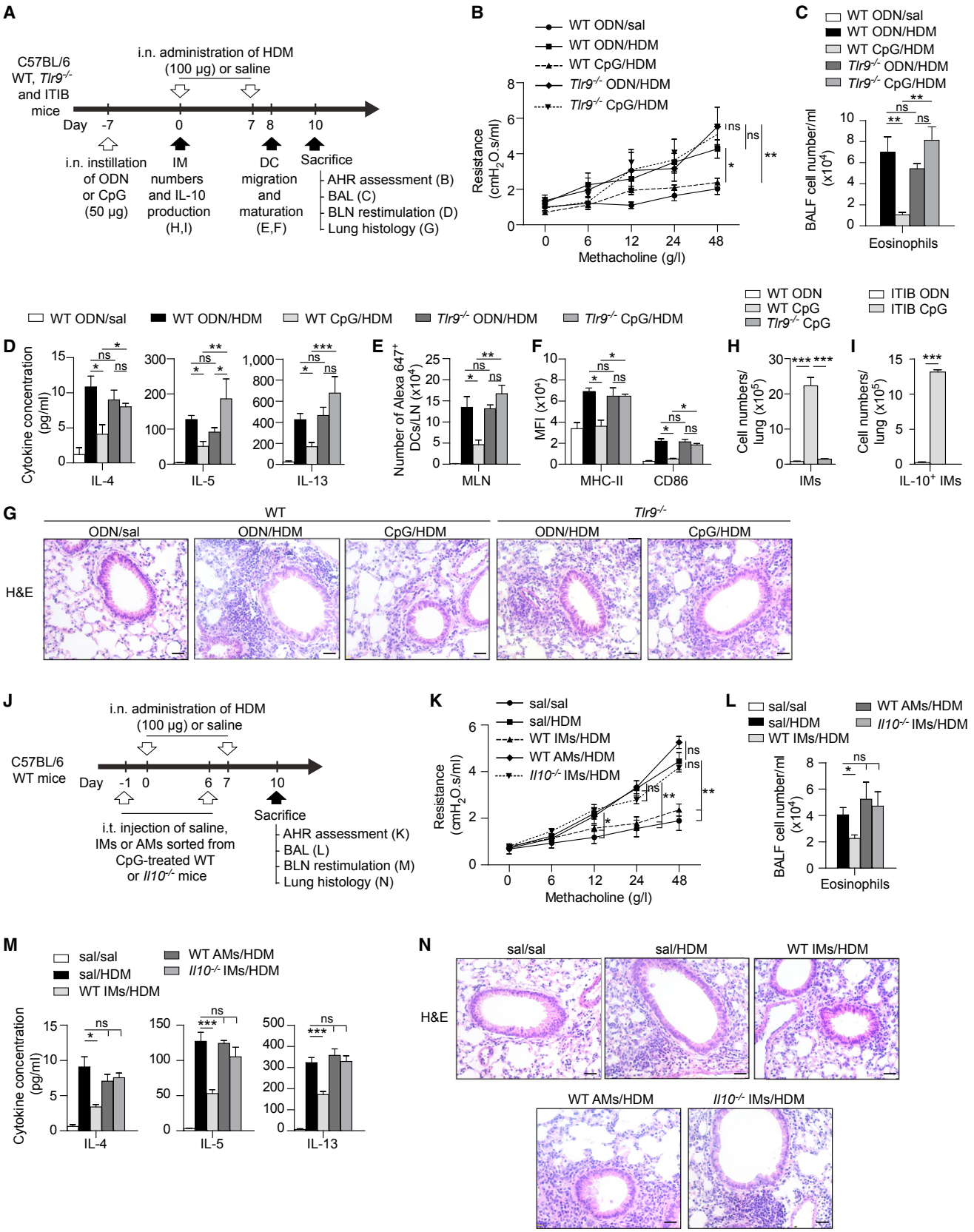
We hypothesized that exposure to certain PAMPs, such as LPS or CpG, might protect against asthma by enhancing the immunosuppressive potential of IMs. First, we confirmed expression of most TLRs on IMs (Figure S2A) and assessed how local exposure to PAMPs, especially TLR ligands, or a local infection would quantitatively affect IMs (Figure 2A; Figure S2B). Although several PAMPs, including LPS, were able to significantly expand IMs, CpG was by far the most potent in increasing IM numbers 1 week after a single intranasal (i.n.) exposure (42.5-fold with an average of 1.7×10^6 cells) (Figure 2B; Figure S2C), a phenomenon that was dependent on signaling through TLR9 (Figure 2C). Such expansion persisted up to 8 weeks after treatment, was also observed to a lesser extent when CpG was administered by a systemic route, and was associated with the presence of a small fraction of CpG IMs into the BALF (Figures S2D–S2G). Conversely, pulmonary infection with *Influenza A virus* (PR8) or *Streptococcus pneumoniae* did not have any significant effect on IM numbers 7 days after infection (Figure 2B). Of note, AM counts remained unchanged after CpG treatment and were moderately increased after LPS treatment (Figures S2H and S2I).

We compared gene expression profiles between CpG IMs and steady-state IMs (SS IMs). Principal-component analysis (PCA) revealed that CpG IMs clustered more closely with SS IMs than with AMs (Figure 2D), but 285 genes were differentially regulated between CpG IMs and SS IMs (fold change > 2, $p < 0.01$). Among genes upregulated in CpG IMs, gene-set enrichment analysis (GSEA) revealed a significant enrichment of genes implicated in macrophage activation and differentiation, such as targets of c-MYC (Aziz et al., 2009) or genes upregulated by activation of mTORC1 or NOTCH signaling (Covarrubias et al., 2016; Monsalve et al., 2009) (Figure 2E).

Protein expression of several surface markers was comparable between CpG IMs and SS IMs, except for CD11b and CD115, which were upregulated in CpG IMs, and for CD62L, SiglecF, and CD169, which were downregulated (Figure S2J).

Functionally, in comparison with SS IMs, CpG IMs exhibited a hypersuppressive profile. Indeed, the percentage of IL-10^{+} cells within CpG IMs was increased, leading to a 55-fold increase in the numbers of IL-10-producing IMs upon CpG treatment (Figures 2F and 2G). Furthermore, the level of IL-10 expression within CpG IMs was substantially greater than that in SS IMs (Figures 2F and 2G), leading to a global 550-fold increase in

(D) PCA comparing SS IMs, CpG IMs, and AMs. Percentages indicate the variability explained by each component.
(E) GSEA between CpG IMs and defined gene sets.
(F) Density plots showing IL-10 expression of IMs as assessed by detection of 450 nm fluorescence (blue product) in CCF4-substrate-loaded cells isolated from IL-10-β-lactamase reporter ITIB or WT mice. Numbers indicate the percentage of IL-10^{+} cells within the population, quantified in (G).
(G) Percentages (left), numbers (middle), and geometric mean fluorescence intensity (MFI, right) of IL-10^{+} cells within the cell populations. Data show the mean + SEM and represent one of two independent experiments (n = 3–4 per group).
p values were calculated with a one-way (B and G) or two-way (C) ANOVA followed by Tukey's post hoc tests (*$p < 0.05$; **$p < 0.01$; ***$p < 0.001$; ns, not significant). Abbreviations: D, day; PFU, plaque-forming units; and CFU, colony-forming units. See also Figure S2 for additional information regarding IM numbers, localization, phenotype, and AM numbers.



(legend on next page)

the amount of IM-derived IL-10 expressed in the lungs after CpG treatment. LPS stimulation did not promote such an enhanced suppressive profile (Figures 2F and 2G).

All together, our data show that IMs specifically expanded in response to CpG exposure and that CpG IMs acquired distinct transcriptomic, phenotypic, and functional features.

CpG-Induced IMs Prevent Allergic Sensitization to Inhaled Allergens

We wondered whether the hypersuppressive profile of CpG IMs might contribute to the protective effects of CpG on asthmatic sensitization. First, we developed a mouse model of asthma prevention by CpG, during which WT mice were intranasally exposed to CpG 7 days before two weekly i.n. instillations of 100 μg HDM (Figure 3A). This regimen of HDM exposure bypassed the regulatory functions of SS IMs, given that 100% of HDM-exposed WT mice developed airway hyperreactivity (AHR), BALF eosinophilia, HDM-specific lymph node (LN) Th2 responses, peribronchial inflammation, and increased mucus production, as well as increased activation of lung DCs and enhanced DC migration to the LNs (Figures 3B–3G; Figures S3A and S3B). In this model, CpG pre-exposure promoted robust expansion of IL-10-producing CpG IMs (Figures 3H and 3I) and protected WT mice, but not *Tlr9*$^{-/-}$ mice, from HDM-induced asthmatic features and DC activation (Figures 3B–3G; Figures S3A and S3B).

Second, to test whether CpG IMs were sufficient to confer such protection, we performed adoptive-transfer experiments (Figure 3J). AHR, eosinophilia, HDM-specific Th2 responses, lung inflammation, and mucus production were significantly reduced when CpG IMs sorted from lungs of CpG-treated WT mice were transferred before HDM exposures (Figures 3K–3N; Figures S3C and S3D). Such protection was specific to CpG IMs and relied on CpG-IM-derived IL-10, given that transfer of WT AMs or *Il10*$^{-/-}$ CpG IMs failed to improve the characteristic features of asthma (Figures 3J–3N; Figures S3C and S3D).

These results demonstrate that IL-10-producing IMs were essential for the protective effects of CpG against sensitization to inhaled allergens.

CpG-Induced IMs Mediate the Immunotherapeutic Effects of CpG on Established Asthma

CpG has already proven its efficacy in attenuating established asthma in animal models and in human clinical trials. Here, we developed a model of immunotherapy based on CpG treatment of HDM-sensitized WT mice before HDM challenge (Figure 4A).

CpG was more potent in expanding IL-10-producing CpG IMs and in decreasing AHR, eosinophilic inflammation, HDM-specific Th2 responses, mucus production, and DC activation than in sham-treated asthmatic counterparts, features that were not observed in *Tlr9*$^{-/-}$ mice (Figures 4B–4I; Figures S4A and S4B). Moreover, CpG IMs were sufficient to confer protection, given that adoptive transfer of CpG IMs before HDM challenge markedly decreased airway allergy in HDM-sensitized mice, an effect that was not observed when WT AMs or *Il10*$^{-/-}$ CpG IMs were transferred (Figures 4J–4N; Figures S4C and S4D). Importantly, the expansion of IL-10-producing IMs and the immunotherapeutic effects of CpG persisted up to 8 weeks after CpG treatment (Figures S4E–S4L). Moreover, similar CpG-induced IM-mediated protection was observed in an asthma model based on systemic sensitization with ovalbumin and alum (Figures S4M–S4Q).

CpG Expands IMs Mainly from CCR2-Independent Monocytes

Given the crucial contribution of CpG IMs to asthma prevention and treatment in our models, we sought to determine the origin of these macrophages. In adult tissues, macrophages are maintained or expanded by local proliferation or differentiation from CCR2-dependent BM-derived classical monocytes (Ginhoux and Guilliams, 2016).

First, to assess the proliferative ability of IMs, we analyzed the incorporation of EdU by IMs after CpG treatment. CpG exposure did not increase the percentage of EdU^{+} IMs at the time points analyzed, providing no support for local proliferation of IMs after CpG treatment (Figure 5A).

Second, we quantified the numbers of CpG IMs in *Ccr2*$^{-/-}$ mice. Surprisingly, CpG IM numbers were only slightly decreased in *Ccr2*$^{-/-}$ mice (Figure 5B), whereas LPS IM numbers were robustly reduced (Figure S5A), supporting the idea that CpG IMs, unlike LPS IMs, developed mostly from monocytes that were recruited independently of the BM. To test this, we used mixed BM competitive CD45.1/2 chimeras engrafted with CD45.1^{+} WT and CD45.2^{+} *Ccr2*$^{-/-}$ BM cells (Figure 5C). 8 weeks after reconstitution, >85% of blood Ly-6C^{hi} monocytes were of CD45.1^{+} WT origin, whereas B lymphocytes and neutrophils had a 1:1 ratio of CD45.1^{+} WT to CD45.2^{+} *Ccr2*$^{-/-}$ cells (Figures 5D and 5E). 8 and 12 weeks after reconstitution, the numbers of lung AMs and IMs were comparable with those before irradiation (Figures S5B and S5C) and originated mainly from CD45.1^{+} WT donor cells, showing that the depleted niches were repopulated by CCR2-dependent classical monocytes after irradiation (Figures 5D–5F). 7 days after CpG treatment, BM-competitive chimeras exhibited increased IM numbers (Figures S5B and S5C), and this expansion was associated with a drastic enrichment of CD45.2^{+} *Ccr2*$^{-/-}$ donor

Figure 3. Contribution of CpG IMs to the Prevention of Experimental Asthma

(A–I) Experimental outline (A), dynamic airway resistance upon methacholine inhalation (B), BALF eosinophil counts (C), cytokine concentrations in culture supernatants of bronchial LN (BLN) cells restimulated with HDM (D), quantification of lung DC migration to the BLN (E) and expression of MHC-II and CD86 at day 8 (F), H&E staining of lung sections (G), and numbers of CpG IMs (H) and IL-10^{+} CpG IMs (I) at day 0.

(J–N) Experimental outline (J), dynamic airway resistance upon methacholine inhalation (K), BALF eosinophil counts (L), cytokine concentrations in culture supernatants of BLN cells restimulated with HDM (M), and H&E staining of lung sections (N).

Data show the mean + SEM (B and K) or mean + SEM and are pooled from at least three independent experiments (n = 6–16 per group) (C–F, H, I, L, and M) or represent one of two independent experiments (n = 4 per group) (H and I). p values were calculated with one-way ANOVA followed by Tukey's post hoc tests (B–F, H, and K–M) or a two-tailed Student's t test (I) (*$p < 0.05$; **$p < 0.01$; ***$p < 0.001$; ns, not significant). Data in (G) and (N) represent one of at least six mice from at least two independent experiments. Scale bars, 32 μm. See also Figure S3 for periodic-acid-Schiff (PAS) stainings.

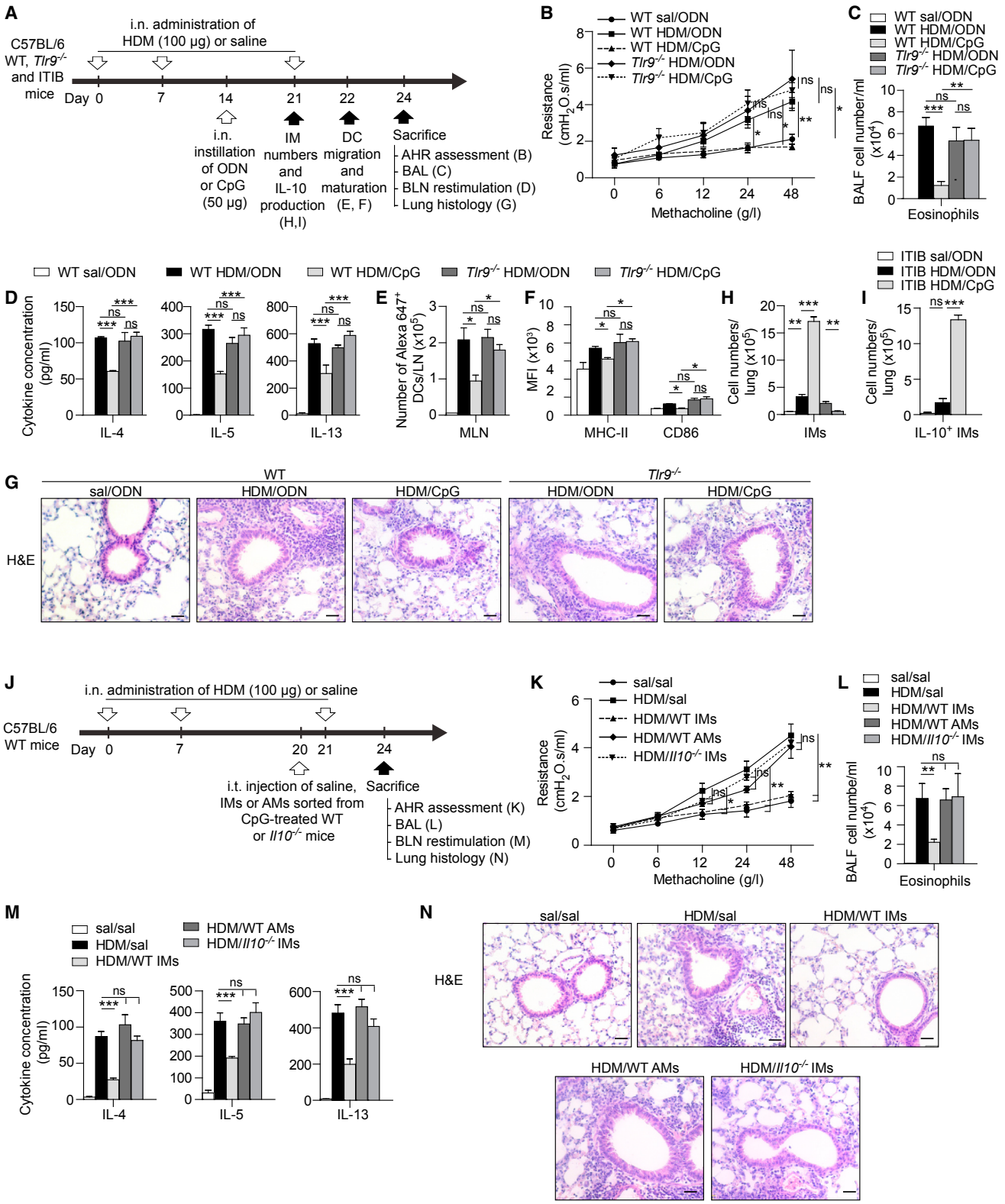


Figure 4. Contribution of CpG IMs to the Treatment of Experimental Asthma

(A–I) Experimental outline (A), dynamic airway resistance upon methacholine inhalation (B), BALF eosinophil counts (C), cytokine concentrations in culture supernatants of BLN cells restimulated with HDM (D), quantification of lung DC migration to the BLN (E) and expression of MHC-II and CD86 at day 22 (F), H&E staining of lung sections (G), and numbers of CpG IMs (H) and IL-10$^+$ CpG IMs (I) at day 21.

(legend continued on next page)

cells to the level of that observed in blood B lymphocytes, namely 100% of CCR2 independence when mice were analyzed at 12 weeks of age (Figures 5D–5F). These results demonstrate that CpG IMs mainly arose from CCR2-independent precursors. Notably, when chimeric mice were exposed to LPS, IM chimerism was not substantially affected and was similar to that of blood Ly-6C^{hi} monocytes, demonstrating that LPS IMs arose from BM-derived classical monocytes (Figures S5D and S5E).

All together, these results support that CpG IMs neither expanded through local proliferation nor substantially differentiated from CCR2-dependent BM-derived classical monocytes but instead mainly originated from CCR2-independent cells.

Lung and Splenic Monocytes Are the Precursors of CpG IMs

Earlier in this article, we defined lung monocytes as CCR2-independent classical monocytes infiltrating the lung parenchyma (Figure 6A). Given that IM expansion upon CpG sensing was mainly independent of CCR2, we hypothesized that lung monocytes could act as a local reservoir for CpG IMs.

First, we validated the CCR2 independence of lung monocytes by conducting parabiosis and mixed-BM-chimera experiments. CD45.1^{+} WT and CD45.2^{+} *Ccr2*$^{-/-}$ mice exchanged their circulation for 6 months, and the enrichment of WT and *Ccr2*$^{-/-}$ partner cells within the *Ccr2*$^{-/-}$ and WT hosts, respectively, was analyzed 24 hr after intravenous (i.v.) Clo-Lip treatment (Figure 6B). Notably, for lung monocytes, a comparable enrichment of partner cells was observed in WT and *Ccr2*$^{-/-}$ hosts (Figure 6B), indicating that these cells were continually replenished by circulating cells independently of CCR2. In BM-reconstituted competitive chimeras, lung monocytes were also repopulated with CCR2-independent engrafted cells, consistent with our findings in parabiotic mice (Figures 6C–6E; Figures S6A and S6B).

Our data so far are consistent with the idea that a precursor-product relationship could exist between lung monocytes and CpG IMs. When we analyzed the kinetics of the appearance of CpG IMs in vivo, we observed a differentiation pattern from Ly-6C^{hi}CD64^{lo} to Ly-6C^{lo}CD64^{hi} cells in both WT and *Ccr2*$^{-/-}$ mice (Figure 6F). With the progressive acquisition of CD64 and the subsequent loss of Ly-6C, the Ly-6C/CD64 plot looked like a waterfall (arrows in Figure 6F), suggesting that lung monocytes might give rise to CpG IMs.

Next, we tested whether lung monocytes could respond to CpG and differentiate into IM-like cells ex vivo. Lung monocytes sorted via fluorescence-activated cell sorting (FACS) expressed higher levels of *Tlr9* than did AMs or IMs (Figure 6G) and were able to respond to CpG, as shown by increased phosphorylation of Erk kinase (Häcker et al., 1999) (Figure 6H). Ex vivo CpG treatment of lung monocytes promoted their survival and triggered the same waterfall over time as in vivo treatment did (Figures 6I and 6J), a phenomenon that was dependent on TLR9 (Figure S6C). Of note, this waterfall was not observed in LPS-stimulated lung monocytes (Figure S6D). Our data thus support that lung monocytes can differentiate into CpG IMs. Nevertheless, the quantity of lung Ly-6C^{hi} cells and CpG IMs 1 and 7 days after CpG treatment, respectively (Figures 6K and 5B), largely exceeded the number of lung monocytes present at steady state (Figure 1H). We thus tested whether such lung monocytes were able to proliferate in situ, but no increase in EdU incorporation was detected 1 day after CpG treatment (Figure 6L; Figure S6E), when their numbers were >10-fold higher than on day 0 in both WT and *Ccr2*$^{-/-}$ mice (Figure 6K). Of note, after LPS treatment, this increased number of Ly-6C^{hi} cells was seen only in WT mice and not in *Ccr2*$^{-/-}$ mice, adding further support to the BM origin of LPS IMs (Figure S6F). These results suggest that, specifically upon CpG stimulation, additional CCR2-independent monocytes were recruited from a distal reservoir and differentiated into CpG IMs.

Interestingly, the spleen has been shown to constitute a reservoir of CCR2-independent monocytes, which were already present in 3-day-old mice (Figure S7A) and which can migrate to inflammatory tissues in an angiotensin II type 1 (AT-1)-receptor-dependent manner (Swirski et al., 2009). Splenic monocytes expressed higher levels of *Tlr9* than did AMs (Figure 7A), and, like for lung monocytes, ex vivo CpG stimulation promoted their survival and differentiation into CpG-IM-like cells (Figure 7B), showing that they can respond to CpG. Notably, 1 day after i.n. CpG treatment, splenic monocyte numbers were significantly decreased, which was associated with an increase in Ly-6C^{hi} monocytes in the lungs of both WT mice and mice lacking AT-1 receptor (*Agtr1a*$^{-/-}$) (Figures 7C and 7D). To assess the exact contribution of splenic monocytes to the pool of lung monocytes and CpG IMs, we quantified their numbers 1 and 7 days after CpG treatment, respectively, in splenectomized *Ccr2*$^{-/-}$ mice. As shown in Figures 7E and 7F, the pools of lung monocytes and CpG IMs were significantly reduced when the spleen was absent. SS IM numbers were unaffected by splenectomy (Figure 7F). Thus, the spleen constitutes a reservoir of monocytes that can seed the lung independently of angiotensin signaling and differentiate into CpG IMs.

Of note, when injected subcutaneously in *Ccr2*$^{-/-}$ mice, CpG induced recruitment of monocytes not only in the lung but also in other organs such as the heart and liver. However, except in the lung, this was not associated with an increase in macrophage numbers 7 days later. Conversely, i.n. CpG injection in *Ccr2*$^{-/-}$ mice promoted the recruitment of monocytes in the lung, but not in the heart or liver (Figures 7G and 7H). All together, these data suggest that CpG could mobilize CCR2-independent monocytes but that additional lung-specific signals directed their seeding into the lung and their differentiation into regulatory IMs.

(J–N) Experimental outline (J), dynamic airway resistance upon methacholine inhalation (K), BALF eosinophil counts (L), cytokine concentrations in culture supernatants of BLN cells restimulated with HDM (M), and H&E staining of lung sections (N).

Data show the mean + SEM (B and K) or mean + SEM and are pooled from at least three independent experiments (n = 6–16 per group) (C–F, H, I, L, and M) or represent one of two independent experiments (n = 4 per group) (H and I). p values were calculated with one-way ANOVA followed by Tukey's post hoc tests (*$p < 0.05$; **$p < 0.01$; ***$p < 0.001$; ns, not significant). Data in (G) and (N) represent one of at least six mice from at least two independent experiments. Scale bars, 32 μm. See also Figure S4 for PAS stainings, the long-term therapeutic model, and the assessment of the protective effects of CpG IMs in an ovalbumin and alum model.

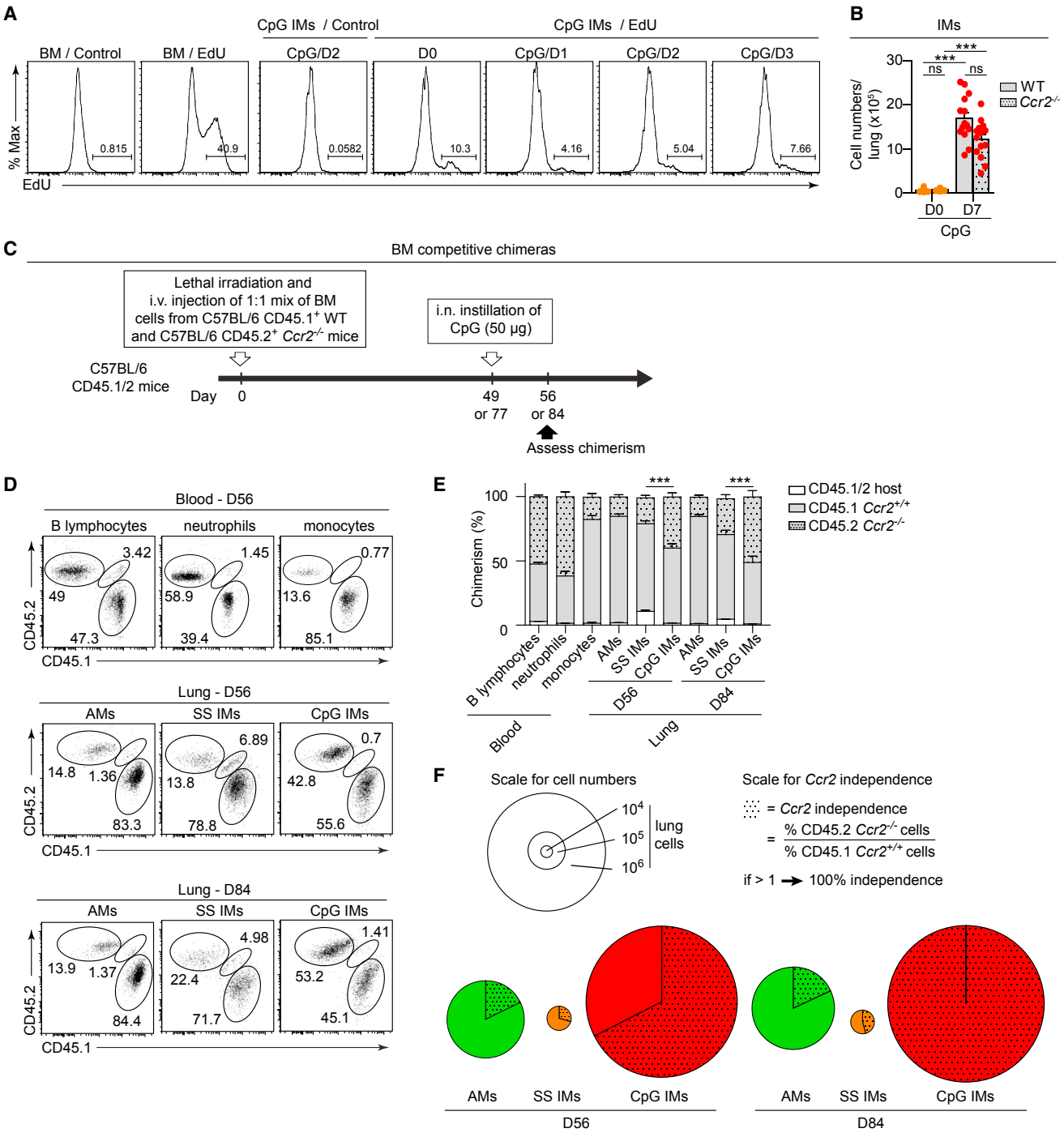


Figure 5. Level of Dependence of CpG IMs on CCR2

(A) IM incorporation of i.p. EdU injection 24 hr before each time point was assessed at day 0 and 1, 2, or 3 days after i.n. CpG treatment of WT mice. BM cells were used as controls. Numbers indicate the percentage of EdU^+ cells. Results represent one of at least five mice from two independent experiments.

(B) Absolute numbers of IMs in the lungs of WT and $Ccr2^{-/-}$ mice before and 7 days after i.n. CpG treatment (50 µg).

(C) Experimental outline for experiments using mixed BM competitive chimeras shown in (D)–(F).

(D) Dot plots showing the percentage of WT and $Ccr2^{-/-}$ BM-derived cells and host radio-resistant cells within the indicated populations.

(E) Percentage of BM chimerism and radio-resistance of the indicated populations.

(F) Pie charts depicting the average absolute cell number (surface area) and the CCR2 independence (dotted area) in the indicated cell populations.

(legend continued on next page)

In an attempt to identify the chemokines involved in splenic monocyte recruitment, we performed a chemokine array on lung extracts and found that CpG instillation induced increased levels of several chemokines, an effect that was, however, also observed with LPS (Figures 7I and 7J). Among those chemokines, CCL2 (MCP-1), CCL5 (RANTES), and CCL9 (MIP-1γ) were not only the most prominent ones but also the ones whose receptors (i.e., CCR2, CCR5, and CCR1, respectively) were the most expressed in Ly-6C^{hi} monocytes (Figures 7I–7K). To assess the potential role of these chemokines, we used neutralizing antibodies in vivo. Individual or combined inhibition of CCL2, CCL5, and CCL9, however, did not influence the numbers of lung monocytes in *Ccr2*$^{-/-}$ mice 1 day after CpG treatment (Figures S7B–S7D), suggesting that splenic monocytes were attracted to the lung independently of those signals.

DISCUSSION

We have shown that IMs substantially expanded in response to CpG, which, unlike LPS, has demonstrated consistent anti-allergic effects in humans and animals (Beeh et al., 2013; Broide et al., 1998; Creticos et al., 2006; Krieg, 2006; Sur et al., 1999). Not only were CpG IMs 42 times more numerous than SS IMs, but their overall IL-10 production was also increased 550-fold. This increased regulatory capacity of CpG IMs was associated with protection against asthma sensitization and exacerbation in experimental models in which the suppressive activity of SS IMs was overcome. Using WT mice adoptively transferred with WT or *Il10*$^{-/-}$ CpG IMs and *Tlr9*$^{-/-}$ mice, in which CpG-mediated IM expansion was abolished, we further demonstrated that CpG IMs were not only necessary but also sufficient for mediating the protective effects of CpG through the production of IL-10. Finally, we showed that the number of CpG IMs remained elevated for at least 8 weeks after CpG administration, which, in addition to the fact that CpG has been reported to induce sustained epigenetic modifications in macrophages (Ostuni et al., 2013), could account for the long-lasting innate effects of CpG. Given that SS IMs exert their suppressive activity by inhibiting maturation and migration of lung DCs (Bedoret et al., 2009), which are essential for both development and restimulation of Th2 cells (Lambrecht et al., 2000; van Rijt et al., 2005), and that DC activation was dampened in CpG-treated HDM-challenged mice, we speculate that CpG durably reinforces the ability of IMs to control DC function and, therefore, to break the link between innate and adaptive immunity. This study thus provides a possible mechanism, i.e., induction of hypersuppressive IMs, by which CpG exerts its immunotherapeutic effects in animals and humans and by which exposure to the environmental microbiome, especially to farm dust, which is known to be rich in bacterial DNA (Roy et al., 2003), protects from asthma (Braun-Fahrländer et al., 2002; von Mutius, 2016).

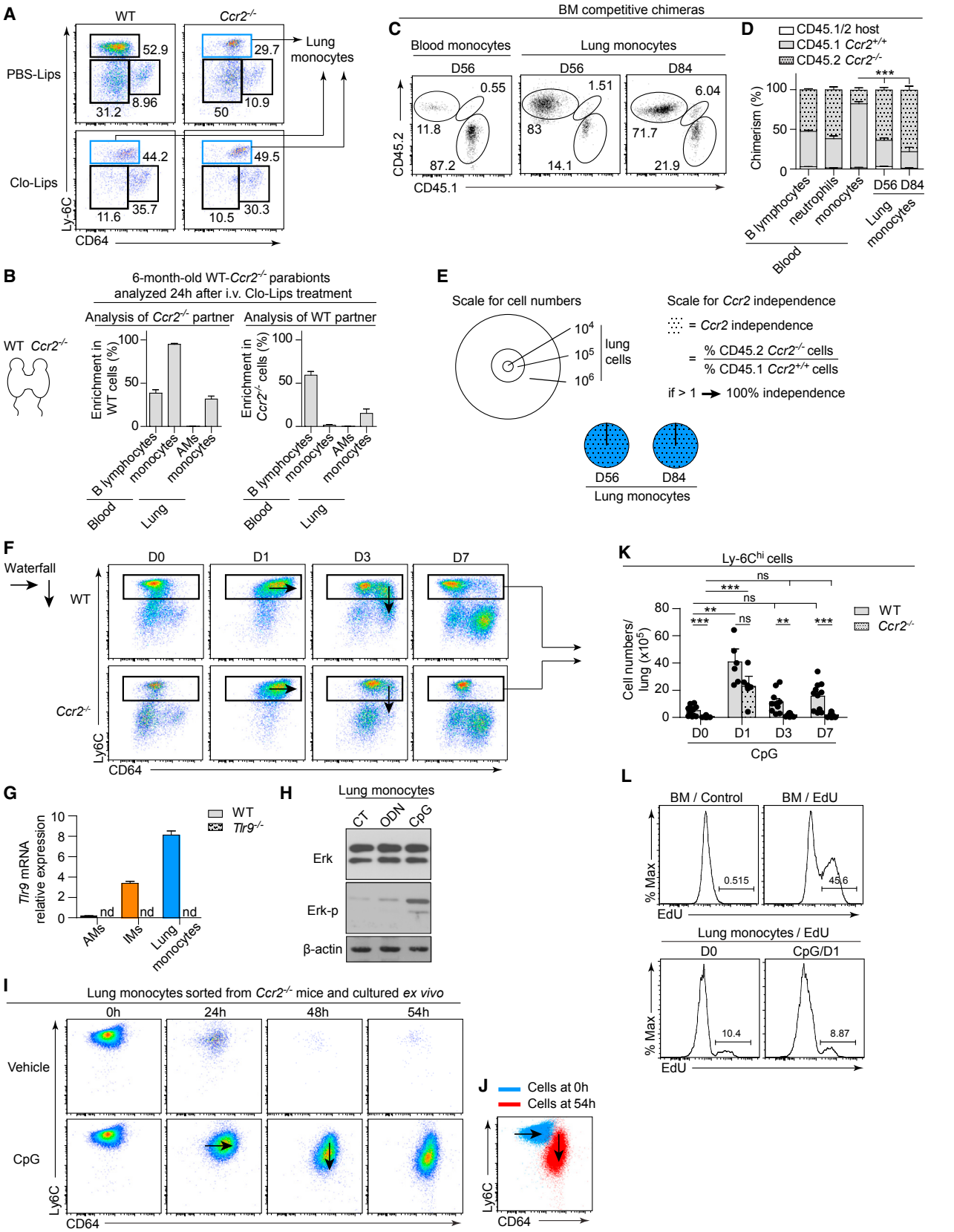
The "mononuclear phagocyte system" model, proposed in 1968 by van Furth and collaborators (van Furth and Cohn, 1968), postulates that tissue-resident macrophages are maintained from a constant supply of blood monocytes that extravasate into tissues. However, this model has been challenged by recent studies demonstrating that, under normal conditions, most macrophages arise from embryonic progenitors and self-renew in tissues throughout adulthood (Ginhoux and Guilliams, 2016; Gomez Perdiguero et al., 2015). The only exceptions are gut, dermis, and heart macrophages that, in accordance with the model of van Furth, rely on the constant recruitment of CCR2-dependent classical monocytes to maintain their population (Bain et al., 2014; Epelman et al., 2014; Tamoutounour et al., 2013). Our data from parabiotic mice support that IMs are also, at least in part, maintained by circulating monocytes in adults, as reported recently (Tan and Krasnow, 2016). During inflammation, macrophages expand through the same mechanisms, namely local proliferation and differentiation from recruited CCR2-dependent BM-derived classical monocytes (Davies et al., 2013). Our results from experiments in *Ccr2*$^{-/-}$, clodronate-treated, chimeric, parabiotic, and splenectomized mice are consistent with an unexpected model in which most CpG IMs can expand from CCR2-independent lung and splenic reservoir monocytes after CpG stimulation. In this model, CpG exerts multiple functions. First, it promotes the mobilization of splenic reservoir monocytes to the lung independently of MCP-1, RANTES, and MIP-1γ. Second, it triggers differentiation of not only these recruited monocytes but also the herein identified CCR2-independent, lung-infiltrating monocytes into IMs with a hypersuppressive profile.

Noteworthy, CpG and LPS appeared to have distinct effects on the recruitment of monocytes to the lung and their differentiation into suppressive IMs. First, CpG induced a substantial mobilization of monocytes from the spleen (i.e., a CCR2-independent reservoir), whereas LPS mainly triggered mobilization from the BM (i.e., a CCR2-dependent reservoir). Second, CpG acted directly on monocytes in vitro to promote their differentiation into macrophages, whereas LPS did not. Third, CpG exposure was able to strikingly increase IM ability to produce IL-10, which was not the case for LPS. Because CpG and LPS are known to act via distinct TLRs, which are expressed at different levels on different structural and immune cells, CpG and LPS most likely induce distinct biological responses in the spleen, BM, lungs, and monocytes themselves, creating a specific microenvironment tailoring IM origin, differentiation, and function.

Given that the numbers of lung reservoir monocytes were identical in WT and *Ccr2*$^{-/-}$ mice, it was tempting to speculate that these cells were different from classical monocytes. However, both cell types had indistinguishable transcriptomes, attesting that lung reservoir monocytes are actually classical monocytes. Although classical monocytes are thought to depend on CCR2 to leave the BM, our results indicate that a fraction of classical monocytes might exit the BM in a CCR2-independent manner to seed the pulmonary and splenic monocyte

(E and F) The percentages of chimerism and of CCR2 independence of blood B lymphocytes, neutrophils (i.e., 50% chimerism and 100% CCR2 independence), and monocytes (i.e., ≈10% chimerism and ≈20% CCR2 independence) were used as controls.

Data in (B) and (E) show the mean + SEM and are pooled from three independent experiments (n = 12–15 per group). p values were calculated with a two-way (B) or one-way (E) ANOVA followed by Tukey's post hoc tests (*p < 0.05; **p < 0.01; ***p < 0.001; ns, not significant). D, day. See also Figure S5 for the CCR2 dependence of LPS IMs and numbers of AMs, SS IMs, LPS IMs, and CpG IMs before irradiation and after BM reconstitution.



(legend on next page)

reservoirs. Identifying the network of chemokine(s) and chemokine receptor(s) orchestrating the traffic of these cells will require additional work.

It has been suggested that the anti-allergic properties of CpG were mediated by plasmacytoid DCs (pDCs), which are known to not only express TLR9 but also play a key role in preventing experimental asthma (de Heer et al., 2004; Krieg, 2006). However, lung pDCs, unlike the other pDC subsets, lack TLR9 expression and therefore cannot account for the role of CpG in regulating lung immune responses (Chen et al., 2006). We have shown here that lung and splenic reservoir monocytes expressed TLR9, which was required for differentiation of CCR2-independent monocytes into IMs after CpG stimulation. Our study thus identifies those reservoir monocytes as the TLR9-expressing cells mediating the immunomodulatory effects of CpG in the lung. Of note, it has been demonstrated that human IMs express TLR9 and are able to increase their production of IL-10 upon bacterial DNA stimulation (Hoppstädter et al., 2010), suggesting that our findings in mice are relevant to humans. Moreover, polymorphisms in the TLR9 promoter region have been associated with an increased risk of asthma development (Lazarus et al., 2003; Smit et al., 2009), supporting the idea that environmental CpG exerts a protective role in humans and that loss of functional TLR9 in human IMs might contribute to asthma development.

In conclusion, our study shows that lung and splenic reservoir monocytes use TLR9 to specifically sense bacterial CpG and massively differentiate into IMs endowed with enhanced anti-allergic properties. These findings are of pathophysiological importance because they provide a possible mechanistic explanation for the hygiene hypothesis and for the protective effects of synthetic CpG in experimental models and human clinical trials. Moreover, they reinforce the idea that therapeutic strategies aimed at ameliorating the inhibitory properties of IMs could help control asthma.

EXPERIMENTAL PROCEDURES

A full description of the experimental procedures can be found in the Supplemental Information.

Mice

WT, *Cx3cr1*$^{GFP/+}$, *Ccr2*$^{-/-}$, *Nr4a1*$^{-/-}$, *Myd88*$^{-/-}$, *Il10*$^{-/-}$, and *Agtr1a*$^{-/-}$ C57BL/6 mice were from the Jackson Laboratory. *Tlr9*$^{-/-}$ and IL-10-β-lactamase reporter (ITIB) mice were generated by others (see Supplemental Information). All mice were used at 6–10 weeks of age unless otherwise indicated. All experimental procedures and protocols were approved by the local ethics committee. Additional information can be found in the Supplemental Information.

Reagents and Antibodies

Mouse non-CpG DNA (ODN, 5′-GCTTGATGACTCAGCCGGAA-3′; reference no. HC4034) and CpG DNA (5′-TCCATGACGTTCCTGATGCT-3′; reference no. HC4033) were from Sanbio. HDM extracts (HDM from *Dermatophagoides farinae*) were from Greer Laboratories. Additional reagents and antibodies are described in the Supplemental Information.

Cell Isolation, Staining, and Flow Cytometry

To obtain single-lung-cell suspensions, we perfused lungs with 10 mL of PBS through the right ventricle, cut them into small pieces, and digested them for 1 hr at 37°C in HBSS containing 1 mg/mL collagenase A (Roche) and 0.05 mg/mL DNase I (Roche). We then enriched single-cell suspensions in mononuclear cells by harvesting cells from the 1.080:1.038 g/mL interface with a density gradient (Easycoll from VWR).

Cell phenotyping and sorting were performed on a FACSCANTO II and a FACSARIA III (BD Biosciences), respectively. Additional information can be found in the Supplemental Information.

Vascular Monocyte and Macrophage Depletion

WT or *Ccr2*$^{-/-}$ mice were injected intravenously with 200 μL of Clo-Lips or empty liposomes (PBS-Lips), and lung cells were harvested 24 hr later.

HDM-Induced Model of Asthma and CpG Treatments

Lightly isoflurane-anesthetized WT, *Tlr9*$^{-/-}$, or ITIB mice were sensitized by two weekly i.n. instillations of vehicle (LPS-free saline) or HDM extracts (100 μg in 50 μL) on days 0 and 7. In experiments shown in Figure 3, mice received i.n. installation of 50 μL saline containing 50 μg ODN or 50 μg CpG 7 days before the first HDM treatment (day −7) and were sacrificed at day 10. In experiments shown in Figure 4, mice received i.n. installation of 50 μL saline containing 50 μg ODN or 50 μg CpG 7 days after the second HDM treatment (day 14). Mice were then challenged by an i.n. instillation of vehicle or HDM (100 μg in 50 μL) and were sacrificed at day 24. For adoptive-transfer experiments, WT mice were transferred intratracheally with 1.5 × 10^6 AMs or CpG IMs sorted from CpG-treated WT or *Il10*$^{-/-}$ mice or with vehicle (50 μL saline) 24 hr before HDM administrations.

Figure 6. CpG-Induced Differentiation of IMs from TLR9-Responsive CCR2-Independent Lung Monocytes

(A) Dot plots of lung-associated classical monocytes (Ly-6C^{hi}), patrolling monocytes (Ly-6C^{lo}CD64^{lo}), and IMs (Ly-6C^{lo}CD64^{hi}) in the indicated groups (same strategy as in Figure 1A). The gate in blue represents lung monocytes. Numbers indicate the percentages of gated cells in the subpopulation.

(B) Analysis of 6-month-old WT *Ccr2*$^{-/-}$ parabionts 24 hr after i.v. Clo-Lip treatment. The percentage of enrichment in partner cells within each host is shown. Bar graphs (mean + SEM) show summary data pooled from two pairs of parabionts.

(C–E) Mixed BM competitive chimeras were analyzed at day 56 or 84, 24 hr after i.v. injection of Clo-Lip. (C) Dot plots showing the percentage of WT and *Ccr2*$^{-/-}$ BM-derived cells and host radio-resistant cells within the indicated populations. (D) Percentage of BM chimerism and radio-resistance of the indicated populations. (E) Pie charts depicting the average absolute cell number and the CCR2 independence (dotted area) in the indicated cell populations.

(F) Waterfall (i.e., differentiation pattern from Ly-6C^{hi}CD64^{lo} to Ly-6C^{lo}CD64^{hi} cells) after i.n. CpG treatment in vivo.

(G) *Tlr9* mRNA expression in AMs, IMs, and lung monocytes sorted from WT or *Tlr9*$^{-/-}$ mice.

(H) Western blot of Erk and phospho-Erk (Erk-p) in lung monocytes sorted from *Ccr2*$^{-/-}$ mice and stimulated ex vivo with saline (CT), ODN, or CpG.

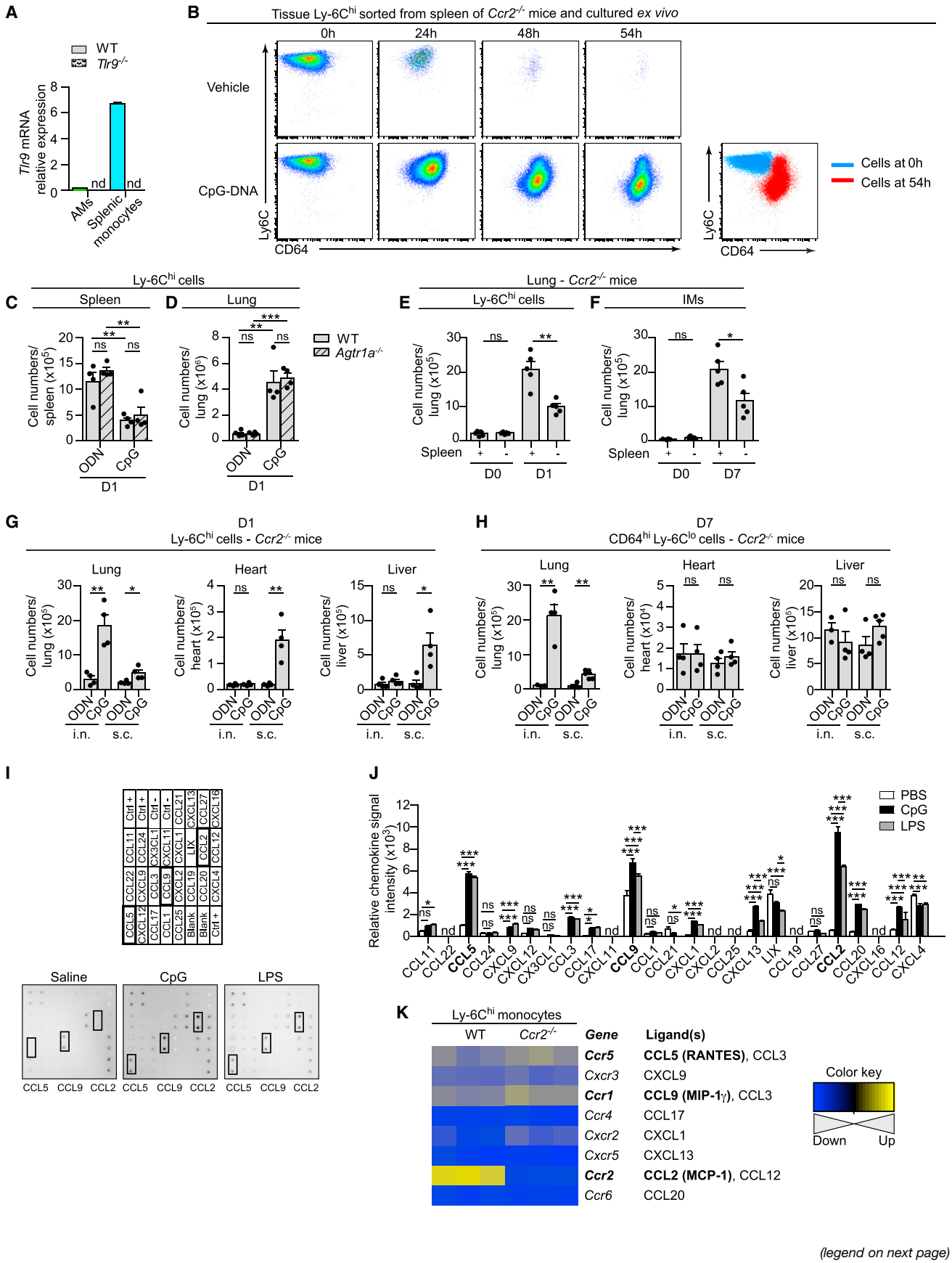
(I) Waterfall of lung monocytes sorted from *Ccr2*$^{-/-}$ mice and stimulated ex vivo with vehicle or CpG.

(J) Superposition of dot plots of living lung monocytes before and 54 hr after stimulation with CpG.

(K) Absolute numbers of lung monocytes in WT and *Ccr2*$^{-/-}$ mice before and 1, 3, and 7 days after i.n. CpG instillation.

(L) Incorporation of i.p. EdU injection 24 hr before was assessed at day 0 and 1 day after i.n. CpG instillation in *Ccr2*$^{-/-}$ mice. WT BM cells were used as controls. Numbers indicate the percentage of EdU$^+$ cells.

Data in (A), (F), (H), (I), and (L) represent one of at least six samples from three independent experiments. Data in (D), (G), and (K) show the mean + SEM and are pooled from three independent experiments (n = 6–15 per group) (D and K) or two independent sorting experiments (n = 4 samples per group) (G). p values were calculated with a one-way (D) or two-way (K) ANOVA followed by Tukey's post hoc tests (*$p < 0.05$; **$p < 0.01$; ***$p < 0.001$; ns, not significant). D, day. See also Figure S6 for numbers of lung monocytes before irradiation and after BM reconstitution, as well as after LPS treatment, and ex vivo differentiation of LPS- or CpG-stimulated lung monocytes from WT or *Tlr9*$^{-/-}$ mice, respectively.



(legend on next page)

We estimated AHR by assessing dynamic airway resistance in anesthetized animals with a FlexiVent small animal ventilator (SCIREQ). Mice were sacrificed, and BALF, lung, and LN cells were harvested and analyzed as described previously (Marichal et al., 2010).

Additional details can be found in the Supplemental Information.

Additional Methods

Methodological details regarding cytologic examination, immunohistochemistry, microarrays, GSEAs, IL-10 detection, generation of mixed BM chimeras and parabiotic mice, EdU incorporation, ex vivo stimulation of tissue monocytes with CpG and LPS, western blot, real-time PCR, splenectomy, chemokine detection, and inhibition are described in the Supplemental Information.

Statistical Analyses

Statistical analyses were performed with R (version 3.2.4). Data from independent experiments were pooled for analysis in each data panel unless otherwise indicated. Raw data were transformed when needed and were back-transformed for graphical presentation. Assumptions of the normal distribution of residuals and homoscedasticity were verified with diagnostic plots. We considered a p value lower than 0.05 to be significant (*$p < 0.05$; **$p < 0.01$; ***$p < 0.001$; ns, not significant).

ACCESSION NUMBERS

The accession number for the microarray data reported in this paper is Array Express: E-MTAB-5012.

SUPPLEMENTAL INFORMATION

Supplemental Information include Supplemental Experimental Procedures and seven figures and can be found with this article online at http://dx.doi.org/10.1016/j.immuni.2017.02.016.

AUTHOR CONTRIBUTIONS

F.B. conceived the project; C.S., C.R., L.F., C.J.D., T.M., and F.B. designed the experiments with help from F.G.; T.M. and F.B. supervised the project; C.S., C.R., and L.F. did most of the experiments and compiled the data; C.F., S.O., and M.T. participated in several experiments; S.C. performed the experiments with parabiotic mice; J.-C.S. provided the *S. pneumonia* clinical isolate; G.P. performed the immunohistochemistry and helped with histological examinations; X.X., D.P., and L.G. performed the microarray analyses; T.M. and L.F. performed splenectomies; H.B. provided the ITIB mice and helped with experiments involving such mice; D.C. and P.Q. made their equipment and facilities available for AHR measurement and microbial infection, respectively; C.S. and L.F. prepared the figures; T.M. and F.B. wrote the manuscript; and all authors provided feedback on the manuscript.

ACKNOWLEDGMENTS

We thank Dr. François Trottein (Institut Pasteur de Lille) for providing *Influenza A virus*; Prof. Hans Nauwynck (Ghent University) for advice; Dr. Natalia Kosovilka from the Stanford PAN facility; Dr. Sandra Ormenese and Raafat Stephan from the Cell Imaging and Flow Cytometry GIGA Platform; Dr. Pierre Drion and other staff members from the Mouse Facility and Transgenics GIGA Platform; Dr. Chantal Humblet from the GIGA Immunohistology Platform; and Raja Fares, Cédric François, and Ilham Sbai for excellent technical and secretarial assistance. The Laboratory of Cellular and Molecular Immunology is supported by the F.R.S.-FNRS for the FRFS-WELBIO under grant CR-2012S-01R, by the Belgian Program on Interuniversity Attraction Poles (IUAP; T-TIME; P7/39), and by an "Action de Recherche Concertée de la Fédération Wallonie-Bruxelles de Belgique" (12/07-03-ITPKC). C.S. and C.R. are research fellows of the F.R.S.-FNRS, L.F. is supported by the FRFS-WELBIO (CR-2012S-01R), T.M. is supported by the Acteria Foundation, and C.D. and T.M. are research associates of the F.R.S.-FNRS.

Received: August 9, 2016
Revised: December 21, 2016
Accepted: January 24, 2017
Published: March 21, 2017

REFERENCES

Aziz, A., Soucie, E., Sarrazin, S., and Sieweke, M.H. (2009). MafB/c-Maf deficiency enables self-renewal of differentiated functional macrophages. Science *326*, 867–871.

Bain, C.C., Bravo-Blas, A., Scott, C.L., Gomez Perdiguero, E., Geissmann, F., Henri, S., Malissen, B., Osborne, L.C., Artis, D., and Mowat, A.M. (2014). Constant replenishment from circulating monocytes maintains the macrophage pool in the intestine of adult mice. Nat. Immunol. *15*, 929–937.

Bedoret, D., Wallemacq, H., Marichal, T., Desmet, C., Quesada Calvo, F., Henry, E., Closset, R., Dewals, B., Thielen, C., Gustin, P., et al. (2009). Lung interstitial macrophages alter dendritic cell functions to prevent airway allergy in mice. J. Clin. Invest. *119*, 3723–3738.

Beeh, K.M., Kanniess, F., Wagner, F., Schilder, C., Naudts, I., Hammann-Haenni, A., Willers, J., Stocker, H., Mueller, P., Bachmann, M.F., and Renner, W.A. (2013). The novel TLR-9 agonist QbG10 shows clinical efficacy in persistent allergic asthma. J. Allergy Clin. Immunol. *131*, 866–874.

Bouabe, H., Liu, Y., Moser, M., Bösl, M.R., and Heesemann, J. (2011). Novel highly sensitive IL-10-beta-lactamase reporter mouse reveals cells of the innate immune system as a substantial source of IL-10 in vivo. J. Immunol. *187*, 3165–3176.

Braun-Fahrländer, C., Riedler, J., Herz, U., Eder, W., Waser, M., Grize, L., Maisch, S., Carr, D., Gerlach, F., Bufe, A., et al.; Allergy and Endotoxin

Figure 7. Mobilization of CCR2-Independent Spleen Reservoir Monocytes to the Lung and Differentiation into CpG IMs

(A) *Tlr9* mRNA expression in splenic monocytes and AMs sorted from WT or $Tlr9^{-/-}$ mice.

(B) Waterfall of splenic monocytes sorted from $Ccr2^{-/-}$ mice and stimulated ex vivo with vehicle or CpG. The right panel shows the superposition of dot plots of living lung monocytes before and 54 hr after stimulation with CpG. Data represent one of at least four samples from two independent experiments.

(C and D) Absolute numbers of Ly-$6C^{hi}$ monocytes in the spleen (C) and lung (D) of WT and $Agtr1a^{-/-}$ mice 1 day after i.n. CpG treatment. Data show the mean + SEM and represent one of two independent experiments (n = 4 per group).

(E and F) Absolute numbers of Ly-$6C^{hi}$ monocytes (E) or IMs (F) in splenectomized and sham-operated mice before (day 0) and 1 day (E) or 7 days (F) after i.n. CpG treatment.

(G and H) Absolute numbers of Ly-$6C^{hi}$ monocytes (G) and Ly-$6C^{lo}CD64^{hi}$ macrophages (H) 1 day (G) and 7 days (H) after i.n. or subcutaneous ODN or CpG treatment of $Ccr2^{-/-}$ mice.

(I and J) Chemokine array was performed on whole lung proteins extracted 8 hr after i.n. PBS, LPS, or CpG treatment of WT mice. (I) Representative blots depicting the detected signals; the boxes show the most induced chemokines. (J) Quantification of chemokine signal intensity.

(K) Heatmap showing gene expression of the receptors for chemokines that were significantly induced by CpG in (J).

Data in (A), (E)–(H), and (J) show the mean + SEM and are pooled from two (A, F–H, and J) or three (E) independent experiments (n = 3–6 per group). p values were calculated with a two-way ANOVA followed by Tukey's post hoc tests (*$p < 0.05$; **$p < 0.01$; ***$p < 0.001$; ns, not significant). Ctrl, control; D, day. See also Figure S7 for the numbers of spleen monocytes in $Ccr2^{-/-}$ mice and in vivo chemokine neutralization experiments.

Study Team (2002). Environmental exposure to endotoxin and its relation to asthma in school-age children. N. Engl. J. Med. *347*, 869–877.

Broide, D., Schwarze, J., Tighe, H., Gifford, T., Nguyen, M.D., Malek, S., Van Uden, J., Martin-Orozco, E., Gelfand, E.W., and Raz, E. (1998). Immunostimulatory DNA sequences inhibit IL-5, eosinophilic inflammation, and airway hyperresponsiveness in mice. J. Immunol. *161*, 7054–7062.

Chen, L., Arora, M., Yarlagadda, M., Oriss, T.B., Krishnamoorthy, N., Ray, A., and Ray, P. (2006). Distinct responses of lung and spleen dendritic cells to the TLR9 agonist CpG oligodeoxynucleotide. J. Immunol. *177*, 2373–2383.

Covarrubias, A.J., Aksoylar, H.I., Yu, J., Snyder, N.W., Worth, A.J., Iyer, S.S., Wang, J., Ben-Sahra, I., Byles, V., Polynne-Stapornkul, T., et al. (2016). Akt-mTORC1 signaling regulates Acly to integrate metabolic input to control of macrophage activation. eLife *5*, e11612.

Creticos, P.S., Schroeder, J.T., Hamilton, R.G., Balcer-Whaley, S.L., Khattignavong, A.P., Lindblad, R., Li, H., Coffman, R., Seyfert, V., Eiden, J.J., and Broide, D.; Immune Tolerance Network Group (2006). Immunotherapy with a ragweed-toll-like receptor 9 agonist vaccine for allergic rhinitis. N. Engl. J. Med. *355*, 1445–1455.

Davies, L.C., Rosas, M., Jenkins, S.J., Liao, C.T., Scurr, M.J., Brombacher, F., Fraser, D.J., Allen, J.E., Jones, S.A., and Taylor, P.R. (2013). Distinct bone marrow-derived and tissue-resident macrophage lineages proliferate at key stages during inflammation. Nat. Commun. *4*, 1886.

de Heer, H.J., Hammad, H., Soullié, T., Hijdra, D., Vos, N., Willart, M.A., Hoogsteden, H.C., and Lambrecht, B.N. (2004). Essential role of lung plasmacytoid dendritic cells in preventing asthmatic reactions to harmless inhaled antigen. J. Exp. Med. *200*, 89–98.

Eder, W., Ege, M.J., and von Mutius, E. (2006). The asthma epidemic. N. Engl. J. Med. *355*, 2226–2235.

Eisenbarth, S.C., Piggott, D.A., Huleatt, J.W., Visintin, I., Herrick, C.A., and Bottomly, K. (2002). Lipopolysaccharide-enhanced, toll-like receptor 4-dependent T helper cell type 2 responses to inhaled antigen. J. Exp. Med. *196*, 1645–1651.

Epelman, S., Lavine, K.J., Beaudin, A.E., Sojka, D.K., Carrero, J.A., Calderon, B., Brija, T., Gautier, E.L., Ivanov, S., Satpathy, A.T., et al. (2014). Embryonic and adult-derived resident cardiac macrophages are maintained through distinct mechanisms at steady state and during inflammation. Immunity *40*, 91–104.

Gautier, E.L., Shay, T., Miller, J., Greter, M., Jakubzick, C., Ivanov, S., Helft, J., Chow, A., Elpek, K.G., Gordonov, S., et al.; Immunological Genome Consortium (2012). Gene-expression profiles and transcriptional regulatory pathways that underlie the identity and diversity of mouse tissue macrophages. Nat. Immunol. *13*, 1118–1128.

Geissmann, F., Jung, S., and Littman, D.R. (2003). Blood monocytes consist of two principal subsets with distinct migratory properties. Immunity *19*, 71–82.

Ginhoux, F., and Guilliams, M. (2016). Tissue-Resident Macrophage Ontogeny and Homeostasis. Immunity *44*, 439–449.

Gomez Perdiguero, E., Klapproth, K., Schulz, C., Busch, K., Azzoni, E., Crozet, L., Garner, H., Trouillet, C., de Bruijn, M.F., Geissmann, F., and Rodewald, H.R. (2015). Tissue-resident macrophages originate from yolk-sac-derived erythro-myeloid progenitors. Nature *518*, 547–551.

Häcker, H., Mischak, H., Häcker, G., Eser, S., Prenzel, N., Ullrich, A., and Wagner, H. (1999). Cell type-specific activation of mitogen-activated protein kinases by CpG-DNA controls interleukin-12 release from antigen-presenting cells. EMBO J. *18*, 6973–6982.

Hammad, H., Chieppa, M., Perros, F., Willart, M.A., Germain, R.N., and Lambrecht, B.N. (2009). House dust mite allergen induces asthma via Toll-like receptor 4 triggering of airway structural cells. Nat. Med. *15*, 410–416.

Hanna, R.N., Carlin, L.M., Hubbeling, H.G., Nackiewicz, D., Green, A.M., Punt, J.A., Geissmann, F., and Hedrick, C.C. (2011). The transcription factor NR4A1 (Nur77) controls bone marrow differentiation and the survival of Ly6C- monocytes. Nat. Immunol. *12*, 778–785.

Hashimoto, D., Chow, A., Noizat, C., Teo, P., Beasley, M.B., Leboeuf, M., Becker, C.D., See, P., Price, J., Lucas, D., et al. (2013). Tissue-resident macrophages self-maintain locally throughout adult life with minimal contribution from circulating monocytes. Immunity *38*, 792–804.

Hoppstädter, J., Diesel, B., Zarbock, R., Breinig, T., Monz, D., Koch, M., Meyerhans, A., Gortner, L., Lehr, C.M., Huwer, H., and Kiemer, A.K. (2010). Differential cell reaction upon Toll-like receptor 4 and 9 activation in human alveolar and lung interstitial macrophages. Respir. Res. *11*, 124.

Kline, J.N., Waldschmidt, T.J., Businga, T.R., Lemish, J.E., Weinstock, J.V., Thorne, P.S., and Krieg, A.M. (1998). Modulation of airway inflammation by CpG oligodeoxynucleotides in a murine model of asthma. J. Immunol. *160*, 2555–2559.

Kline, J.N., Kitagaki, K., Businga, T.R., and Jain, V.V. (2002). Treatment of established asthma in a murine model using CpG oligodeoxynucleotides. Am. J. Physiol. Lung Cell. Mol. Physiol. *283*, L170–L179.

Krieg, A.M. (2006). Therapeutic potential of Toll-like receptor 9 activation. Nat. Rev. Drug Discov. *5*, 471–484.

Krieg, A.M. (2012). CpG still rocks! Update on an accidental drug. Nucleic Acid Ther. *22*, 77–89.

Lambrecht, B.N., De Veerman, M., Coyle, A.J., Gutierrez-Ramos, J.C., Thielemans, K., and Pauwels, R.A. (2000). Myeloid dendritic cells induce Th2 responses to inhaled antigen, leading to eosinophilic airway inflammation. J. Clin. Invest. *106*, 551–559.

Lazarus, R., Klimecki, W.T., Raby, B.A., Vercelli, D., Palmer, L.J., Kwiatkowski, D.J., Silverman, E.K., Martinez, F., and Weiss, S.T. (2003). Single-nucleotide polymorphisms in the Toll-like receptor 9 gene (TLR9): frequencies, pairwise linkage disequilibrium, and haplotypes in three U.S. ethnic groups and exploratory case-control disease association studies. Genomics *81*, 85–91.

Marichal, T., Bedoret, D., Mesnil, C., Pichavant, M., Goriely, S., Trottein, F., Cataldo, D., Goldman, M., Lekeux, P., Bureau, F., and Desmet, C.J. (2010). Interferon response factor 3 is essential for house dust mite-induced airway allergy. J. Allergy Clin. Immunol. *126*, 836–844.e13.

Mesnil, C., Raulier, S., Paulissen, G., Xiao, X., Birrell, M.A., Pirottin, D., Janss, T., Starkl, P., Ramery, E., Henket, M., et al. (2016). Lung-resident eosinophils represent a distinct regulatory eosinophil subset. J. Clin. Invest. *126*, 3279–3295.

Monsalve, E., Ruiz-García, A., Baladrón, V., Ruiz-Hidalgo, M.J., Sánchez-Solana, B., Rivero, S., García-Ramírez, J.J., Rubio, A., Laborda, J., and Díaz-Guerra, M.J. (2009). Notch1 upregulates LPS-induced macrophage activation by increasing NF-kappaB activity. Eur. J. Immunol. *39*, 2556–2570.

Mosser, D.M., and Edwards, J.P. (2008). Exploring the full spectrum of macrophage activation. Nat. Rev. Immunol. *8*, 958–969.

Ostuni, R., Piccolo, V., Barozzi, I., Polletti, S., Termanini, A., Bonifacio, S., Curina, A., Prosperini, E., Ghisletti, S., and Natoli, G. (2013). Latent enhancers activated by stimulation in differentiated cells. Cell *152*, 157–171.

Roy, S.R., Schiltz, A.M., Marotta, A., Shen, Y., and Liu, A.H. (2003). Bacterial DNA in house and farm barn dust. J. Allergy Clin. Immunol. *112*, 571–578.

Schuijs, M.J., Willart, M.A., Vergote, K., Gras, D., Deswarte, K., Ege, M.J., Madeira, F.B., Beyaert, R., van Loo, G., Bracher, F., et al. (2015). Farm dust and endotoxin protect against allergy through A20 induction in lung epithelial cells. Science *349*, 1106–1110.

Serbina, N.V., and Pamer, E.G. (2006). Monocyte emigration from bone marrow during bacterial infection requires signals mediated by chemokine receptor CCR2. Nat. Immunol. *7*, 311–317.

Smit, L.A., Siroux, V., Bouzigon, E., Oryszczyn, M.P., Lathrop, M., Demenais, F., and Kauffmann, F.; Epidemiological Study on the Genetics and Environment of Asthma, Bronchial Hyperresponsiveness, and Atopy (EGEA) Cooperative Group (2009). CD14 and toll-like receptor gene polymorphisms, country living, and asthma in adults. Am. J. Respir. Crit. Care Med. *179*, 363–368.

Strachan, D.P. (1989). Hay fever, hygiene, and household size. BMJ *299*, 1259–1260.

Sur, S., Wild, J.S., Choudhury, B.K., Sur, N., Alam, R., and Klinman, D.M. (1999). Long term prevention of allergic lung inflammation in a mouse model of asthma by CpG oligodeoxynucleotides. J. Immunol. *162*, 6284–6293.

Swirski, F.K., Nahrendorf, M., Etzrodt, M., Wildgruber, M., Cortez-Retamozo, V., Panizzi, P., Figueiredo, J.L., Kohler, R.H., Chudnovskiy, A., Waterman, P., et al. (2009). Identification of splenic reservoir monocytes and their deployment to inflammatory sites. Science *325*, 612–616.

Tamoutounour, S., Guilliams, M., Montanana Sanchis, F., Liu, H., Terhorst, D., Malosse, C., Pollet, E., Ardouin, L., Luche, H., Sanchez, C., et al. (2013). Origins and functional specialization of macrophages and of conventional and monocyte-derived dendritic cells in mouse skin. Immunity *39*, 925–938.

Tan, S.Y., and Krasnow, M.A. (2016). Developmental origin of lung macrophage diversity. Development *143*, 1318–1327.

Thorne, P.S., Kulhánková, K., Yin, M., Cohn, R., Arbes, S.J., Jr., and Zeldin, D.C. (2005). Endotoxin exposure is a risk factor for asthma: the national survey of endotoxin in United States housing. Am. J. Respir. Crit. Care Med. *172*, 1371–1377.

van Furth, R., and Cohn, Z.A. (1968). The origin and kinetics of mononuclear phagocytes. J. Exp. Med. *128*, 415–435.

van Rijt, L.S., Jung, S., Kleinjan, A., Vos, N., Willart, M., Duez, C., Hoogsteden, H.C., and Lambrecht, B.N. (2005). In vivo depletion of lung CD11c+ dendritic cells during allergen challenge abrogates the characteristic features of asthma. J. Exp. Med. *201*, 981–991.

von Mutius, E. (2016). The microbial environment and its influence on asthma prevention in early life. J. Allergy Clin. Immunol. *137*, 680–689.

Immunity, Volume *46*

Supplemental Information

Exposure to Bacterial CpG DNA Protects from Airway Allergic Inflammation by Expanding Regulatory Lung Interstitial Macrophages

Catherine Sabatel, Coraline Radermecker, Laurence Fievez, Genevieve Paulissen, Svetoslav Chakarov, Claudia Fernandes, Sabine Olivier, Marie Toussaint, Dimitri Pirottin, Xue Xiao, Pascale Quatresooz, Jean-Claude Sirard, Didier Cataldo, Laurent Gillet, Hicham Bouabe, Christophe J. Desmet, Florent Ginhoux, Thomas Marichal, and Fabrice Bureau

Supplemental Figures and Legends

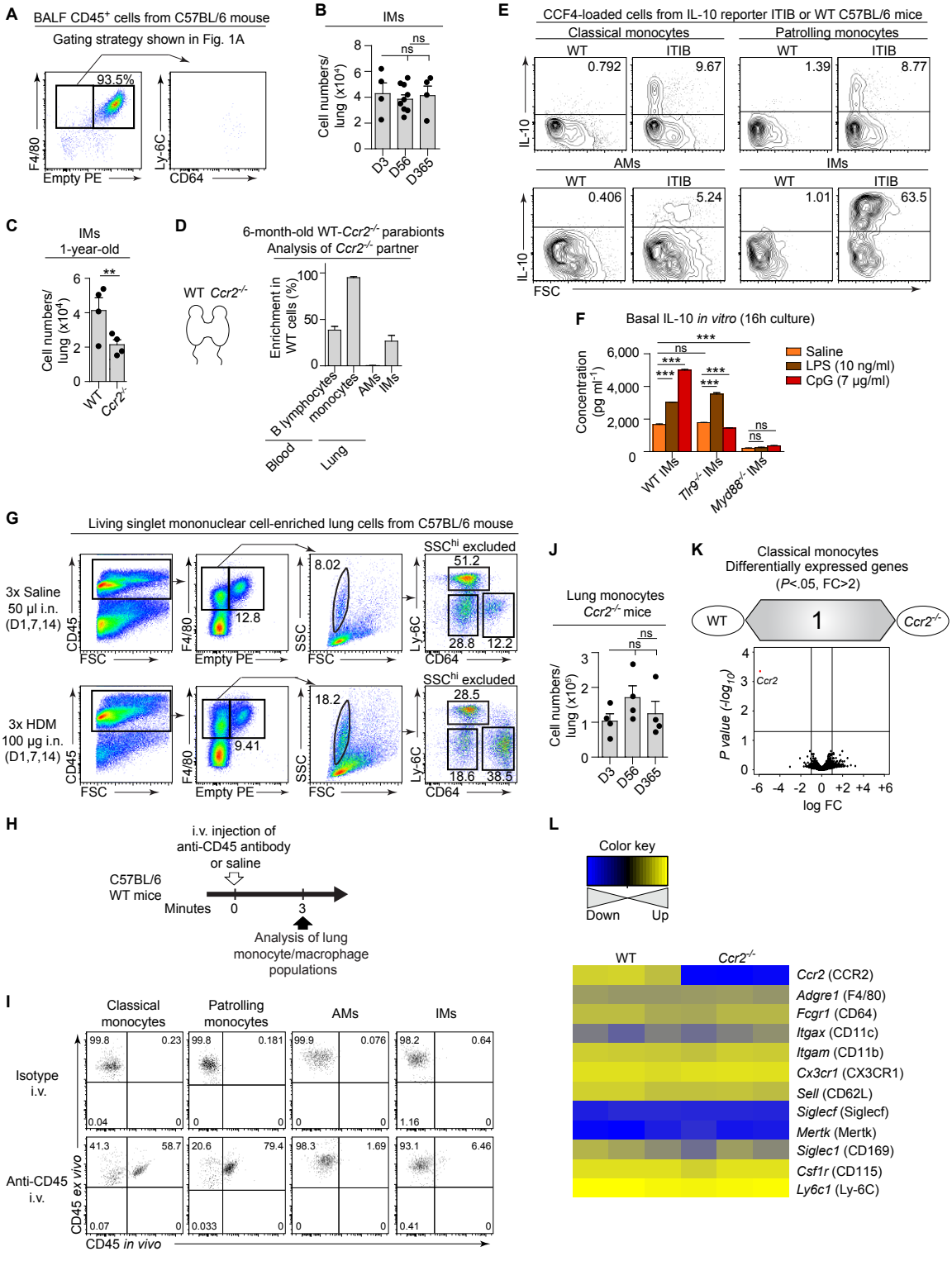


Figure S1, related to Figure 1. Identification of monocyte and macrophage populations in the mouse lung: additional analyses. (A) Analysis of steady-state BALF $CD45^+$ cells using the gating strategy shown in Figure 1A. >90% of cells are identified as AMs at steady-state. (B-C) Absolute numbers of IMs (B) at different time points after birth in WT mice and (C) in 1-year-old WT and *Ccr2*$^{-/-}$ mice. (D) WT and *Ccr2*$^{-/-}$ mice were sutured together for 6 months. The % of enrichment in WT partner cells within the *Ccr2*$^{-/-}$ host is shown. (E) Density plots showing steady-state IL-10 expression as assessed by detection of 450 nm fluorescence (blue fluorescent product of the CCF4 substrate) in CCF4 substrate-loaded cells isolated from IL-10-β-lactamase reporter ITIB or WT control mice. Numbers indicate % of $IL\text{-}10^+$ cells within the cell populations. (F) IL-10 concentration in culture supernatants of FACS-sorted IMs from WT, *Tlr9*$^{-/-}$ or *Myd88*$^{-/-}$ mice stimulated with LPS (10 ng ml^{-1}) or CpG (7 µg ml^{-1}) for 16 hours. (G) Gating strategy identifying monocytes and macrophages in the mouse lung (developed in Figure 1A) applied at day 17 to WT mice having received 3 weekly i.n. instillations of saline (50µL) or HDM (100 µg in 50 µL). (H) Experimental outline for data shown in I. Briefly, APC-conjugated anti-CD45 antibodies were given i.v. 3 minutes before euthanasia, and the indicated cell populations were analyzed by flow cytometry. (I) Representative dot plots showing binding of anti-CD45 *in vivo vs.* anti-CD45 *ex vivo* staining on the indicated populations. (J) Absolute numbers of lung monocytes at different time points after birth in *Ccr2*$^{-/-}$ mice. (K) Summary of differentially expressed genes (DE) ($P<0.05$, FC >2) showing DE genes in red in volcano plot and the total number of DE genes in the middle of the bidirectional arrows. (L) Heatmap showing relative expression of DE genes of cell surface markers displayed in Figure 1C. (A,E,G,I) Results are representative of 1 of ≥5 mice coming from ≥2 independent experiments, each of them giving similar results. (D) Bar graphs (mean + SEM) showing summary data pooled from two pairs of parabionts. (B,C,J) Data shown mean + SEM and are pooled from 2 independent experiments (n=4-9/group). (F) Data show mean + SEM and are representative of 1 of 2 independent sorting experiments. *P* values were calculated using (B,J) a one-way or (F) a two-way ANOVA followed by Tukey's post hoc tests, or (C) a two-tailed Student's *t* test. D, day.

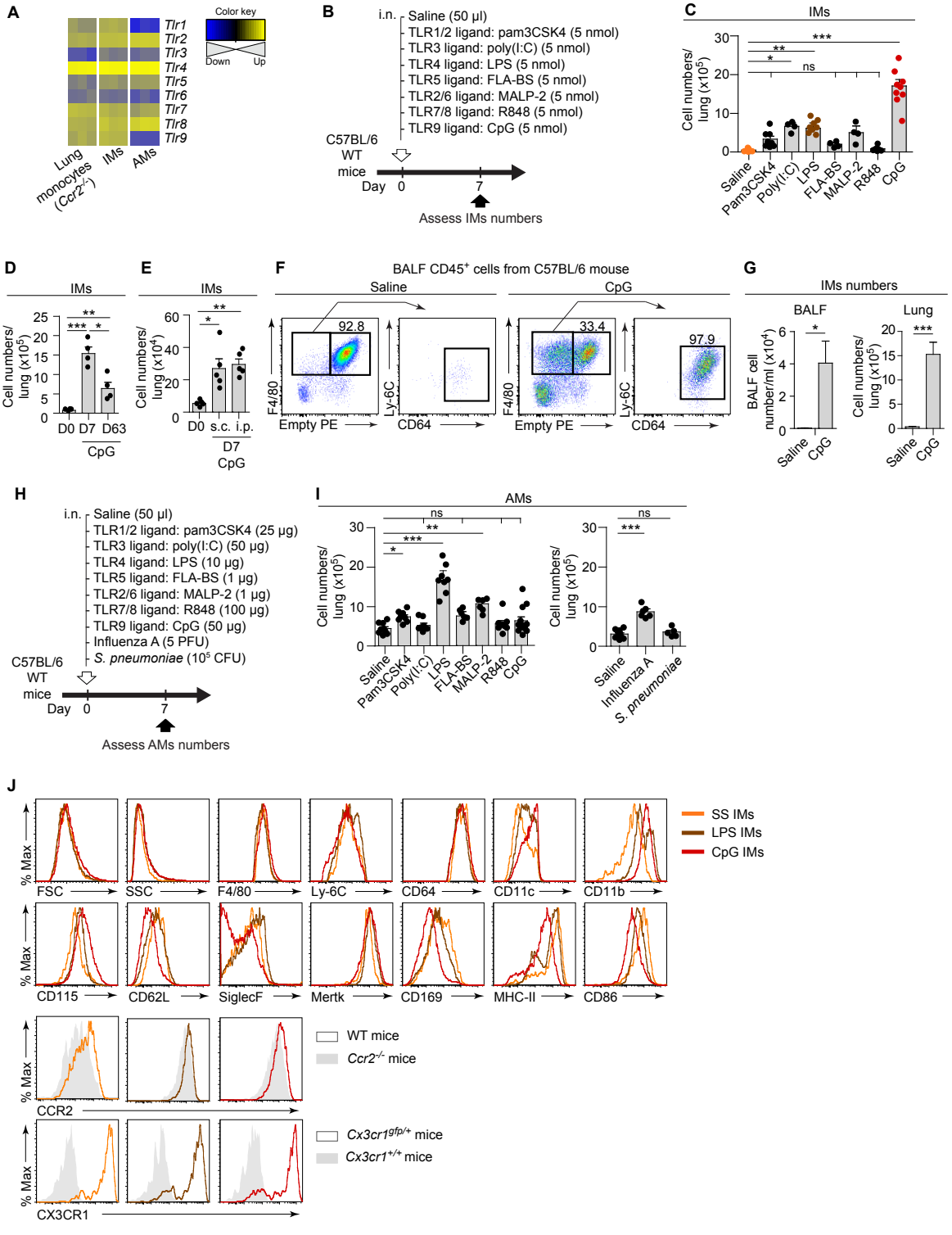

A
Color key
Down
Up
Tlr1
Tlr2
Tlr3
Tlr4
Tlr5
Tlr6
Tlr7
Tlr8
Tlr9
Lung monocytes (Ccr2-/-)
IMs
AMs
B
i.n.
Saline (50 µl)
TLR1/2 ligand: pam3CSK4 (5 nmol)
TLR3 ligand: poly(I:C) (5 nmol)
TLR4 ligand: LPS (5 nmol)
TLR5 ligand: FLA-BS (5 nmol)
TLR2/6 ligand: MALP-2 (5 nmol)
TLR7/8 ligand: R848 (5 nmol)
TLR9 ligand: CpG (5 nmol)
C57BL/6 WT mice
Day 0
7
Assess IMs numbers
C
IMs
Cell numbers/ lung (x10^5)
***
**
*
ns
Saline
Pam3CSK4
Poly(I:C)
LPS
FLA-BS
MALP-2
R848
CpG
D
IMs
Cell numbers/ lung (x10^5)
D0 D7 D63
CpG
E
IMs
Cell numbers/ lung (x10^4)
D0 s.c. i.p.
D7
CpG
F
BALF CD45+ cells from C57BL/6 mouse
Saline
CpG
92.8
33.4
97.9
F4/80
Empty PE
Ly-6C
CD64
G
IMs numbers
BALF
Lung
BALF cell number/ml (x10^4)
Cell numbers/ lung (x10^5)
Saline
CpG
H
i.n.
Saline (50 µl)
TLR1/2 ligand: pam3CSK4 (25 µg)
TLR3 ligand: poly(I:C) (50 µg)
TLR4 ligand: LPS (10 µg)
TLR5 ligand: FLA-BS (1 µg)
TLR2/6 ligand: MALP-2 (1 µg)
TLR7/8 ligand: R848 (100 µg)
TLR9 ligand: CpG (50 µg)
Influenza A (5 PFU)
S. pneumoniae (10^5 CFU)
C57BL/6 WT mice
Day 0
7
Assess AMs numbers
I
AMs
Cell numbers/ lung (x10^5)
ns
**
***
*
Saline
Pam3CSK4
Poly(I:C)
LPS
FLA-BS
MALP-2
R848
CpG
Influenza A
S. pneumoniae
J
% Max
FSC
SSC
F4/80
Ly-6C
CD64
CD11c
CD11b
CD115
CD62L
SiglecF
Mertk
CD169
MHC-II
CD86
SS IMs
LPS IMs
CpG IMs
CCR2
WT mice
Ccr2-/- mice
CX3CR1
Cx3cr1gfp/+ mice
Cx3cr1+/+ mice

Figure S2, related to Figure 2. Quantification of IM and AM numbers, and localization and surface phenotype of IMs upon exposure to TLR ligands. (A) Heatmap showing relative expression of *Tlr* on lung monocytes sorted from *Ccr2*$^{-/-}$ mice, and AMs and IMs sorted from WT mice. (B) Experimental outline for data shown in C. (C) Absolute numbers of IMs in the lungs of WT mice 7 days following i.n. stimulation with the indicated doses of TLR ligands (i.e. 5 nmol) (D) Absolute numbers of CpG IMs before and 7 or 63 days after i.n. CpG instillation. (E) C57BL/6 WT mice were injected s.c. or i.p. with 50 µg CpG (in 100 µl and 200 µl, respectively). Seven days later (D7), numbers of IMs were determined in the lung and compared with mice analyzed at D0. (F-G) Quantification of IMs in the BALF of mice i.n. instilled with saline or CpG 7 days earlier. (F) Representative dot plot of BALF CD45^{+} cells using the gating strategy shown in Figure 1A. Numbers indicate the % within the CD45^{+} BALF cells. (G) Absolute BALF and lung IM numbers. (H) Experimental outline for data shown in I. Briefly, WT C57BL/6 mice were instilled i.n. with 50 µl saline, or 50 µl saline containing the indicated stimulants or pathogens (doses used are shown in brackets). (I) Absolute numbers of AMs in the lungs of C57BL/6 WT mice 7 days after i.n. stimulation with the indicated TLR ligands and i.n. infection with influenza A virus (PR8 strain) or *S. pneumoniae* (serotype 1). (J) Surface phenotype of lung IMs at steady-state (SS IMs) or 7 days after i.n. LPS (LPS IMs) or CpG-DNA (CpG IMs) instillations. (C,E,I) Data show mean + SEM and are pooled from 2-3 independent experiments (n=3-12/group). *P* values were calculated using a one-way ANOVA followed by Tukey's post hoc tests. (D,G) Data show mean + SEM and are representative of 1 of 2 independent experiments (n=4/group). *P* values were calculated using (D) a one-way ANOVA followed by Tukey's post hoc tests and (G) a two-tailed unpaired Student's *t* test. (F,J) Data are representative of 1 of ≥6 mice coming from (F) 2 or (J) ≥3 independent experiments, each of them giving comparable results. D, day.

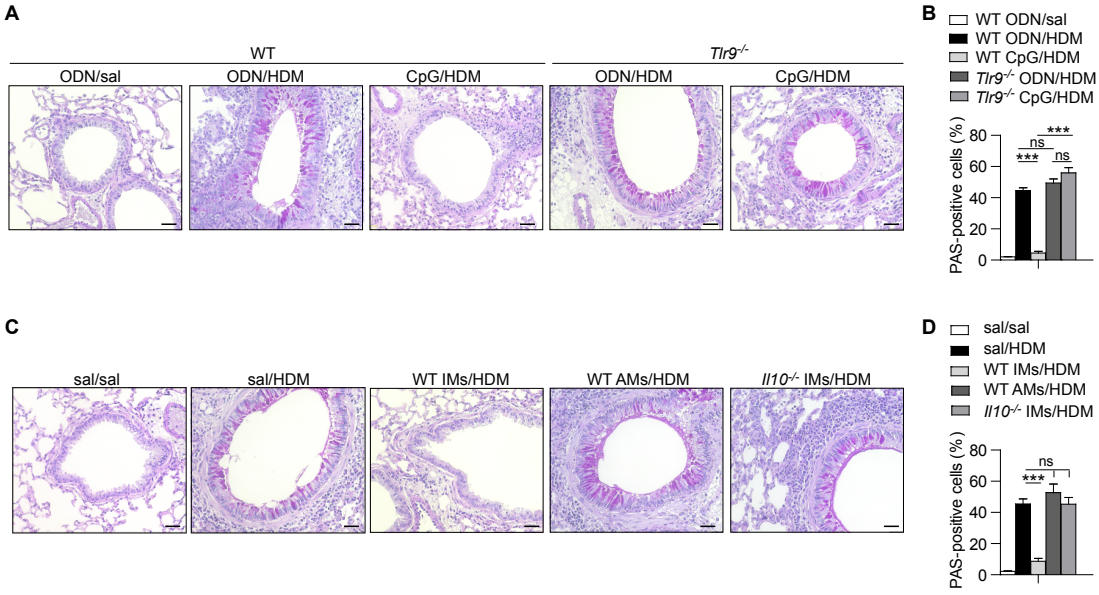

A
WT
Tlr9-/-
ODN/sal
ODN/HDM
CpG/HDM
ODN/HDM
CpG/HDM
B
WT ODN/sal
WT ODN/HDM
WT CpG/HDM
Tlr9-/- ODN/HDM
Tlr9-/- CpG/HDM
PAS-positive cells (%)
0
20
40
60
80
ns
***
***
ns
C
sal/sal
sal/HDM
WT IMs/HDM
WT AMs/HDM
Il10-/- IMs/HDM
D
sal/sal
sal/HDM
WT IMs/HDM
WT AMs/HDM
Il10-/- IMs/HDM
PAS-positive cells (%)
0
20
40
60
80
ns
***

Figure S3, related to Figure 3. Contribution of CpG IMs to the prevention of experimental asthma: mucus production. (A-B) Experimental outline is shown in Figure 3A. Briefly, WT C57BL/6 and *Tlr9*$^{-/-}$ mice were instilled i.n. with 50 µg ODN or 50 µg CpG, were sensitized 7 and 14 days later with 100 µg HDM or saline and were sacrificed 3 days later. (A) Representative Periodic Acid-Schiff (PAS) staining of lung sections of the indicated groups of mice. (B) Quantification of mucus production as the % positivity of PAS-stained goblet cells per total epithelial cells. (C-D) Experimental outline is shown in Figure 3J. Briefly, WT C57BL/6 were transferred i.t. on day -1 and 6 with saline or $1.5.10^6$ AMs or CpG IMs sorted from WT or *Il10*$^{-/-}$ mice, sensitized 1 day later with 100 µg HDM or saline and sacrificed 3 days after the second sensitization. (C) PAS staining of lung sections of the indicated groups of mice. (D) Quantification of mucus production as the % positivity of PAS-stained goblet cells per total epithelial cells. (A and C) Data are representative of one of ≥6 mice analyzed, each of them giving comparable results. (B and D) Data show mean + SEM and are pooled from 2 independent experiments (n=4-6 mice/group). *P* values were calculated using a one-way ANOVA followed by Tukey's post hoc tests. Scale bar: 32 µm.

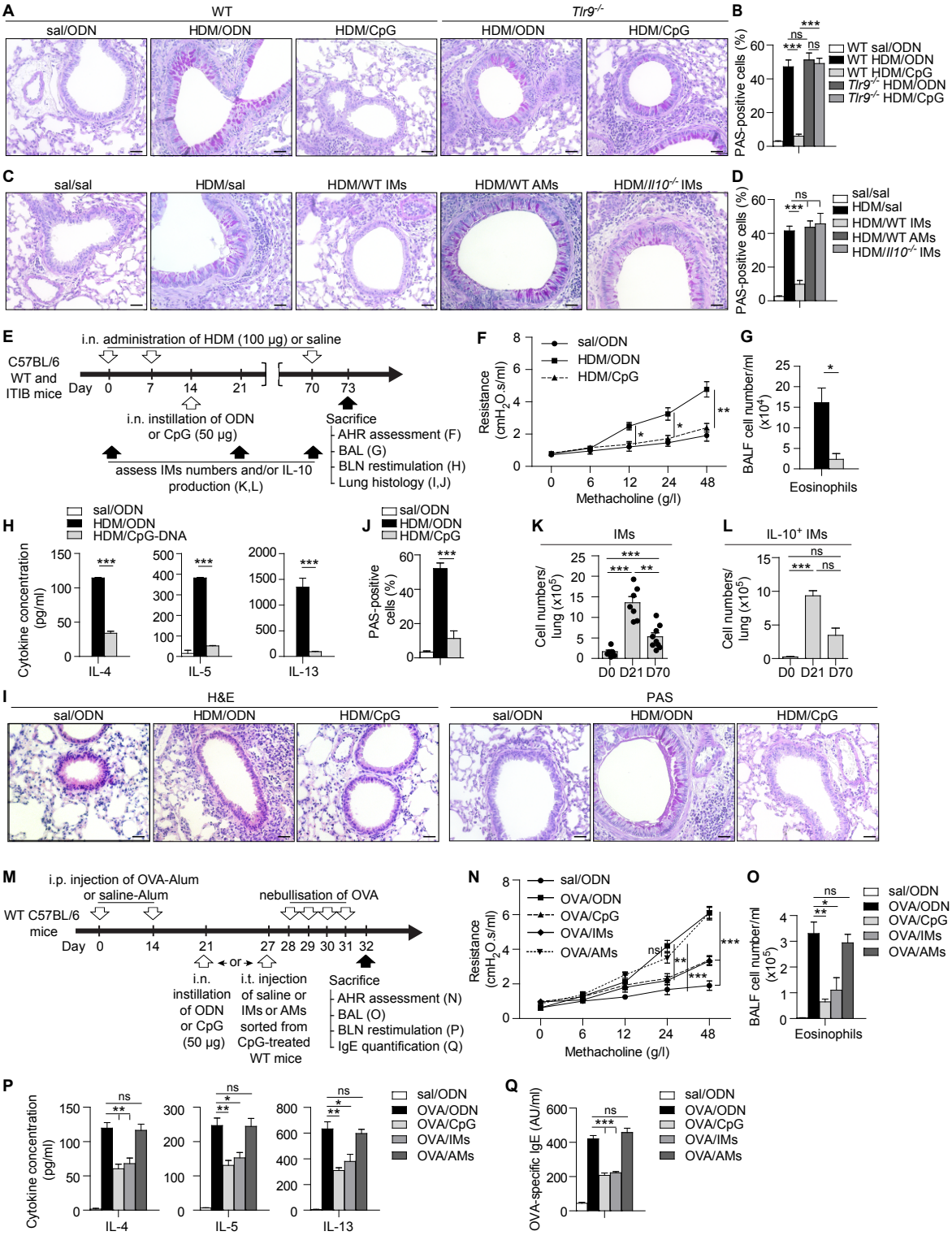

A
WT
Tlr9-/-
sal/ODN
HDM/ODN
HDM/CpG
HDM/ODN
HDM/CpG
B
PAS-positive cells (%)
WT sal/ODN
WT HDM/ODN
WT HDM/CpG
Tlr9-/- HDM/ODN
Tlr9-/- HDM/CpG
C
sal/sal
HDM/sal
HDM/WT IMs
HDM/WT AMs
HDM/Il10-/- IMs
D
sal/sal
HDM/sal
HDM/WT IMs
HDM/WT AMs
HDM/Il10-/- IMs
E
i.n. administration of HDM (100 µg) or saline
C57BL/6 WT and ITIB mice
Day 0 7 14 21 70 73
i.n. instillation of ODN or CpG (50 µg)
Sacrifice
AHR assessment (F)
BAL (G)
BLN restimulation (H)
Lung histology (I,J)
assess IMs numbers and/or IL-10 production (K,L)
F
sal/ODN
HDM/ODN
HDM/CpG
Resistance (cmH2O.s/ml)
Methacholine (g/l)
G
BALF cell number/ml (x10^4)
Eosinophils
H
sal/ODN
HDM/ODN
HDM/CpG-DNA
Cytokine concentration (pg/ml)
IL-4
IL-5
IL-13
J
sal/ODN
HDM/ODN
HDM/CpG
PAS-positive cells (%)
K
IMs
Cell numbers/ lung (x10^5)
D0 D21 D70
L
IL-10+ IMs
Cell numbers/ lung (x10^5)
D0 D21 D70
I
H&E
PAS
sal/ODN
HDM/ODN
HDM/CpG
M
i.p. injection of OVA-Alum or saline-Alum
nebullisation of OVA
WT C57BL/6 mice
Day 0 14 21 27 28 29 30 31 32
or
i.n. instillation of ODN or CpG (50 µg)
i.t. injection of saline or IMs or AMs sorted from CpG-treated WT mice
Sacrifice
AHR assessment (N)
BAL (O)
BLN restimulation (P)
IgE quantification (Q)
N
sal/ODN
OVA/ODN
OVA/CpG
OVA/IMs
OVA/AMs
Resistance (cmH2O.s/ml)
Methacholine (g/l)
O
BALF cell number/ml (x10^5)
Eosinophils
P
Cytokine concentration (pg/ml)
IL-4
IL-5
IL-13
Q
OVA-specific IgE (AU/ml)

Figure S4, related to Figure 4. Contribution of CpG IMs to the treatment of experimental asthma: mucus production, long-lasting effects of CpG on IM numbers and HDM-induced experimental asthma, and contribution of CpG and CpG IMs in the protection against OVA-induced experimental asthma. (A-B) Experimental outline is shown in Figure 4A. Briefly, WT C57BL/6 and *Tlr9*$^{-/-}$ mice were instilled i.n. with 100 µg HDM or saline at days 0 and 7, were exposed to CpG or ODN at day 14 and challenged with HDM at day 21. Mice were sacrificed 3 days after the HDM challenge. (A) Representative Periodic Acid-Schiff (PAS) staining of lung sections of the indicated groups of mice. (B) Quantification of mucus production as the % positivity of PAS-stained goblet cells per total epithelial cells. (C-D) Experimental outline is shown in Figure 4J. Briefly, WT mice previously sensitized with 2 i.n. administrations of HDM were transferred i.t. with saline or $1.5.10^6$ AMs or CpG IMs sorted from WT or *Il10*$^{-/-}$ mice, challenged 1 day later with 100 µg HDM and sacrificed 3 days later. (C) PAS staining of lung sections of the indicated groups of mice. (D) Quantification of mucus production as the % positivity of PAS-stained goblet cells per total epithelial cells. (A and C) Data are representative of one of ≥6 mice analyzed, each of them giving comparable results. (B and D) Data show mean + SEM and are pooled from 2 independent experiments (n=4-6 mice/group). *P* values were calculated using a one-way ANOVA followed by Tukey's post hoc tests. Scale bar: 32 µm. (E) Experimental outline for data shown in F-L. Briefly, C57BL/6 WT or ITIB mice (panel J) mice were sensitized with 2 weekly i.n. administrations of HDM (100 µg) or saline and instilled 7 days later (D14) i.n. with CpG or ODN. On D56, mice were challenged with 100 µg HDM and were sacrificed on D73. IM numbers were assessed at the indicated time points. (F) Dynamic airway resistance upon methacholine inhalation. (G) BALF eosinophil counts. (H) Cytokine concentrations in culture supernatants of BLN cells restimulated with HDM. (I) Hematoxylin and eosin (H&E) and Periodic Acid Schiff (PAS) stainings of lung sections. (J) Quantification of mucus production as the % positivity of PAS-stained goblet cells per total epithelial cells. (K,L) Numbers of (K) CpG IMs and (L) IL-10$^+$ CpG IMs at D0, 21 and 70. (F) Data show mean + SEM and are representative of 1 of 3 independent experiments (n=4/group), each of them giving similar results. (G,H,K) Data show mean + SEM and are pooled from 3 independent experiments (n=6-12/group), each of them giving comparable results. (L) Data show mean + SEM and are pooled from 2 independent experiments (n=4/group). (I) Data are representative of one of ≥6 mice analyzed, each of them giving comparable results. (J) Data show mean + SEM and are pooled from 2 independent experiments (n=4-6 mice/group). (F-H;K,L,J) *P* values were calculated using a one-way ANOVA followed by Tukey's post hoc tests. Scale bars: 32 µm. (M) Experimental outline for data shown in N-Q. Briefly, C57BL/6 WT mice were sensitized i.p. with OVA admixed with alum at D0 and 14 and instilled 7 days later (D21) i.n. with CpG or ODN. Alternatively, mice were transferred on D27 with $1.5.10^6$ AMs or CpG IMs sorted from WT mice. From D28 to D31, mice were challenged with inhalations of OVA 1% (1 hour/day). Mice were sacrificed on D32. (N) Dynamic airway resistance upon methacholine inhalation. (O) BALF eosinophil counts. (P) Cytokine concentrations in culture supernatants of BLN cells restimulated with OVA. (Q) Quantification of serum OVA-specific IgE. (N-Q) Data shown mean + SEM and are representative of 1 of 2 independent experiments (n=4-6/group), each of them giving similar results. *P* values were calculated using a one-way ANOVA followed by Tukey's post hoc tests.

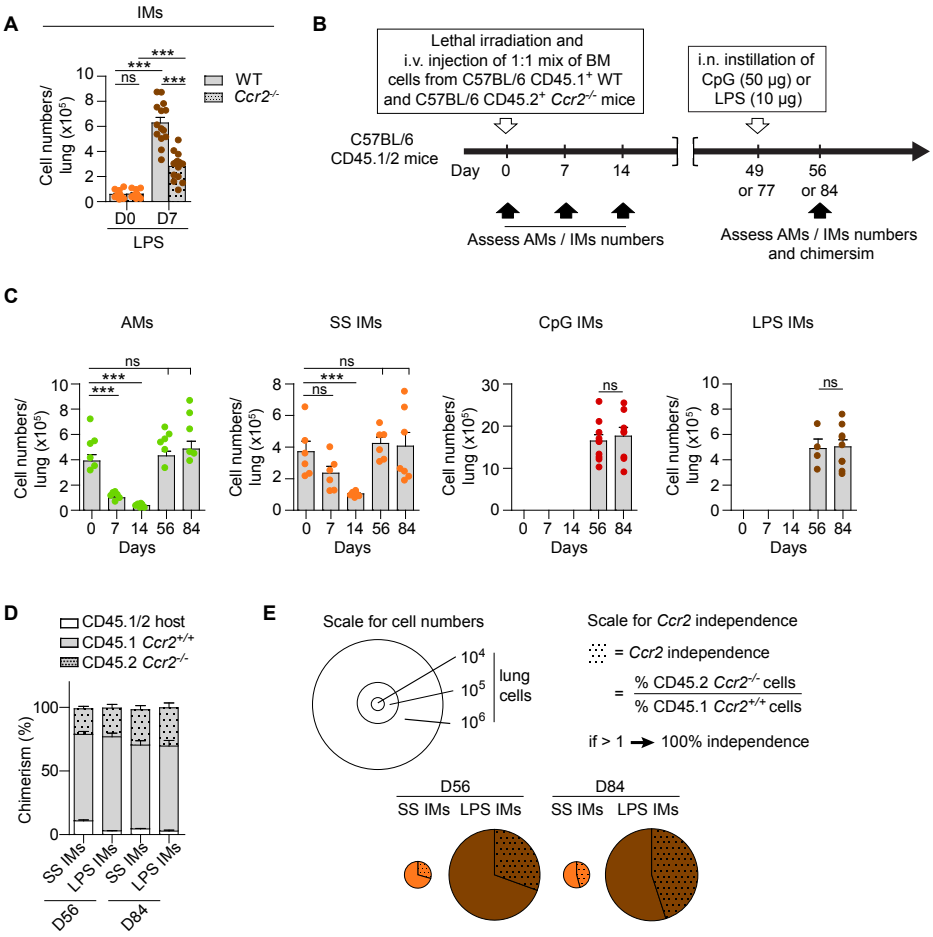

A
IMs
Cell numbers/ lung (x10⁵)
WT
Ccr2-/-
D0
D7
LPS
B
Lethal irradiation and i.v. injection of 1:1 mix of BM cells from C57BL/6 CD45.1+ WT and C57BL/6 CD45.2+ Ccr2-/- mice
i.n. instillation of CpG (50 µg) or LPS (10 µg)
C57BL/6 CD45.1/2 mice
Day 0 7 14
49 or 77
56 or 84
Assess AMs / IMs numbers
Assess AMs / IMs numbers and chimersim
C
AMs
SS IMs
CpG IMs
LPS IMs
Days
D
CD45.1/2 host
CD45.1 Ccr2+/+
CD45.2 Ccr2-/-
Chimerism (%)
SS IMs
LPS IMs
D56
D84
E
Scale for cell numbers
lung cells
Scale for Ccr2 independence
= Ccr2 independence
% CD45.2 Ccr2-/- cells / % CD45.1 Ccr2+/+ cells
if > 1 → 100% independence

Figure S5, related to Figure 5. Dependence of LPS IMs on CCR2, and numbers of AMs and IMs before irradiation and following BM reconstitution. (A) Absolute numbers of IMs in the lungs of WT and *Ccr2*$^{-/-}$ mice before and 7 days after i.n. LPS treatment (10 µg). (B) Experimental outline for data shown in C-E. Briefly, CD45.1/2^{+} mice were lethally irradiated and reconstituted with equal amounts of CD45.1^{+} WT and CD45.2^{+}*Ccr2*$^{-/-}$ BM cells. Some mice were instilled with CpG or LPS at day 49 or 77 and analyzed 7 days later. (C) Macrophage numbers were assessed over time, as indicated. Absolute numbers of the indicated populations before (D0, day 0) irradiation, and 7, 14, 56 and 84 days after BM reconstitution. (D) The chimerism of SS IMs and LPS IMs was assessed at day 56 or 84. % of BM chimerism and radio-resistance of the indicated populations. (E) Pie charts depicting the average absolute cell number (surface area) and the CCR2 independence (dotted area) in the indicated cell populations. (D and E) The % of chimerism and the % of CCR2 independence of blood B lymphocytes, neutrophils (i.e., 50% chimerism, 100% CCR2 independence) and monocytes (i.e. ≈10% chimerism, ≈20% CCR2 independence) were used as controls and are shown in Figure 5, D-F. (A,C,D) Data show mean ± SEM and are pooled from (A,D) 3 independent experiments (n=10-15/group), or (C) 2 independent experiments (n=6-7/group), each of them giving similar results. *P* values were calculated using (A) a two-way ANOVA or (C,D) a one-way ANOVA followed by Tukey's test for multiple comparisons. D, day.

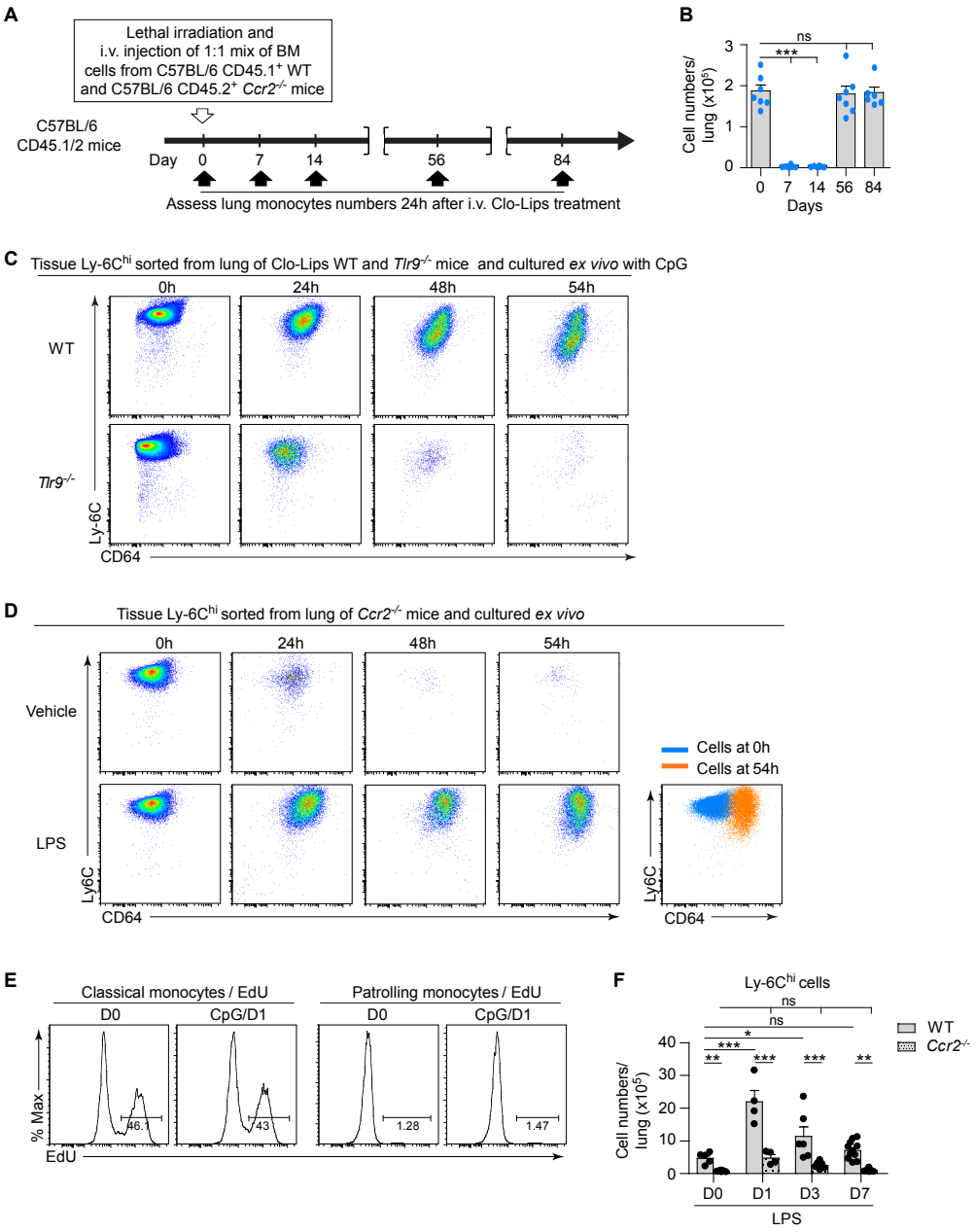

A
Lethal irradiation and
i.v. injection of 1:1 mix of BM
cells from C57BL/6 CD45.1+ WT
and C57BL/6 CD45.2+ Ccr2-/- mice
C57BL/6
CD45.1/2 mice
Day 0 7 14 56 84
Assess lung monocytes numbers 24h after i.v. Clo-Lips treatment
B
Cell numbers/ lung (x10^5)
ns
***
0 7 14 56 84
Days
C
Tissue Ly-6C^hi sorted from lung of Clo-Lips WT and Tlr9-/- mice and cultured ex vivo with CpG
0h 24h 48h 54h
WT
Tlr9-/-
Ly-6C
CD64
D
Tissue Ly-6C^hi sorted from lung of Ccr2-/- mice and cultured ex vivo
0h 24h 48h 54h
Vehicle
LPS
Ly6C
CD64
Cells at 0h
Cells at 54h
E
Classical monocytes / EdU
Patrolling monocytes / EdU
D0 CpG/D1 D0 CpG/D1
% Max
EdU
46.1
43
1.28
1.47
F
Ly-6C^hi cells
Cell numbers/ lung (x10^5)
D0 D1 D3 D7
LPS
WT
Ccr2-/-

Figure S6, related to Figure 6. Numbers of lung monocytes before irradiation and following BM reconstitution, differentiation of lung monocytes upon CpG or LPS stimulation *ex vivo*, monocyte EdU incorporation upon CpG treatment and numbers of lung monocytes in WT and *Ccr2*$^{-/-}$ mice before and 1, 3 and 7 days after i.n. LPS instillation. (A) Experimental outline for data shown in B. Briefly, CD45.1/2^{+} mice were lethally irradiated and reconstituted with equal amounts of CD45.1^{+} WT and CD45.2^{+} *Ccr2*$^{-/-}$ BM cells. Numbers of lung monocytes were assessed over time, as indicated. (B) Absolute numbers of lung monocytes before (D0, day 0) irradiation, and 7, 14, 56 and 84 days after BM reconstitution. Data show mean + SEM and are pooled from 2 independent experiments (n=6-7/group), each of them giving similar results. (C) Dot plots of living lung monocytes sorted from Clo-Lip-treated C57BL/6 WT and *Tlr9*$^{-/-}$ mice and cultured *ex vivo* before and 24, 48 or 54 hours after stimulation with vehicle or CpG. (D) Dot plots of living lung monocytes sorted from *Ccr2*$^{-/-}$ mice and cultured *ex vivo* before and 24, 48 or 54 hours after stimulation with vehicle or LPS. On the right panel, superposition of dot plots of living lung monocytes cultured *ex vivo* before (0h) and 54 hours (54h) after stimulation with LPS. (C-D) Data are representative of one of ≥5 samples coming from 3 independent experiments. (E) Incorporation of EdU (injected i.p. 24 hours before) in classical Ly-6C^{hi} and patrolling Ly-6C^{lo} lung associated monocytes was assessed at day 0 and 1 day after i.n. CpG instillation in WT mice. WT BM cells were used as controls (shown in Figure 6L). Numbers indicate % of EdU^{+} cells. Results are representative of one of ≥4 mice coming from 2 independent experiments. (F) Absolute numbers of lung monocytes in WT and *Ccr2*$^{-/-}$ mice before and 1, 3 and 7 days after i.n. LPS instillation. Data show mean + SEM and are pooled from 2 independent experiments (n=4-10/group). *P* values were calculated using (B) a one-way ANOVA or (F) a two-way ANOVA followed by Tukey's post hoc tests.

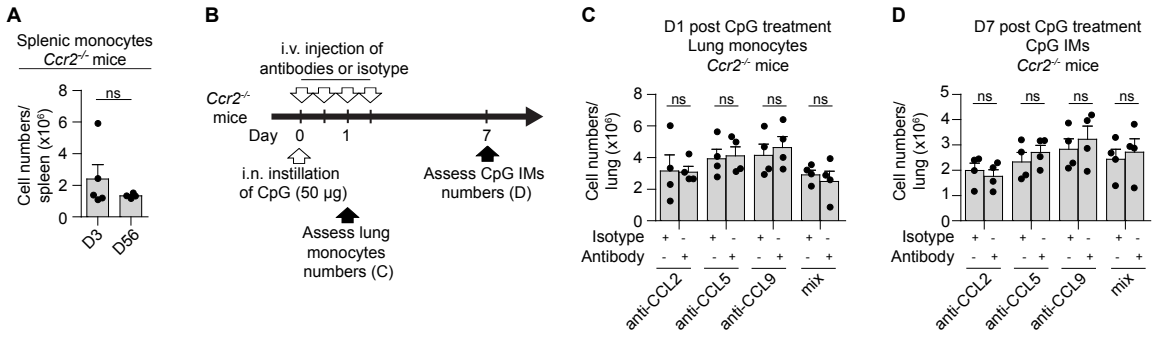

A
Splenic monocytes
Ccr2-/- mice
Cell numbers/ spleen (x10⁶)
ns
D3
D56
B
i.v. injection of antibodies or isotype
Ccr2-/- mice
Day 0 1 7
i.n. instillation of CpG (50 µg)
Assess CpG IMs numbers (D)
Assess lung monocytes numbers (C)
C
D1 post CpG treatment
Lung monocytes
Ccr2-/- mice
Cell numbers/ lung (x10⁶)
Isotype
Antibody
anti-CCL2
anti-CCL5
anti-CCL9
mix
D
D7 post CpG treatment
CpG IMs
Ccr2-/- mice

Figure S7, related to Figure 7. Analyses of *Ccr2*$^{-/-}$ mice: numbers of spleen monocytes, and numbers of monocytes and macrophages in the lung following chemokine neutralization and i.n. CpG treatment. (A) Absolute numbers of spleen monocytes at different time points after birth in *Ccr2*$^{-/-}$ mice. (B) Experimental outline for *in vivo* chemokine neutralization experiments shown in C-D. Absolute numbers of (C) lung monocytes 1 day or (D) CpG IMs 7 days after i.n. CpG instillation in *Ccr2*$^{-/-}$ mice which received i.p. injection of the indicated antibodies. Data show mean + SEM and are pooled from 2 independent experiments (n=4-5/group). *P* values were calculated using (A) a one-way or (C,D) a two-way ANOVA followed by Tukey's post hoc tests.

Supplemental Experimental Procedures

Mice

WT CD45.2$^+$ C57BL/6 and WT CD45.1$^+$ C57BL/6 mice were from the Jackson Laboratory. CD45.1/2$^+$ WT C57BL/6 mice were obtained by crossing CD45.1$^+$ with CD45.2$^+$ mice. *Agtr1a*$^{-/-}$, *Ccr2*$^{-/-}$, *Cx3cr1*$^{gfp/+}$, *Il-10*$^{-/-}$, *Myd88*$^{-/-}$ and *Nr4a1*$^{-/-}$ mice on the C57BL/6 background were from the Jackson Laboratory. *Tlr9*$^{-/-}$ (Hemmi et al., 2000) and IL-10-β-lactamase reporter (ITIB) (Bouabe et al., 2011) mice were described elsewhere. All mice, except parabiotic mice that were generated at the Singapore Immunology Network (SIgN, Singapore), were housed and bred in institutional specific pathogen-free facilities at the GIGA-Research center of the University of Liege (Belgium) and were used at 6-10 weeks of age, unless otherwise indicated. All experimental procedures and protocols were reviewed and approved by the Institutional Animal Care and Use Ethics Committee of the University of Liege (Belgium), except for experiments involving parabiotic mice that were approved by the local ethical committee at the Singapore Immunology Network (SIgN, Singapore).

The "Guide for the Care and Use of Laboratory Animals", prepared by the Institute of Laboratory Animal Resources, National Research Council, and published by the National Academy Press, as well as European and local legislations, were followed carefully.

Reagents and Antibodies

2.4G2 Fc receptor blocking antibodies were produced in house. Fluorogenic coumarin-cephalosporin-fluorescein (4)-acetoxymethyl (CCF4-AM) was from Invitrogen. Pam3CSK4, Poly(I:C), FLA-BS and R848 were from InvivoGen. MALP-2 was from Enzo Life Sciences. LPS from E. *coli* O55:B5 was from Sigma. Mouse non-CpG DNA (ODN, 5'-gcttgatgactcagccggaa-3'; Ref. HC4034) and CpG-DNA (5'-tccatgacgttcctgatgct-3'; Ref. HC4033) were from Sanbio. Clodronate-containing liposomes or control liposomes were from Foundation Clodronate Liposomes. 5-ethynyl-2'-deoxy-uridine (EdU) was from Jena Bioscience. HDM extracts (HDM from *Dermatophagoides farinae*) were from Greer Laboratories. OVA grade III and grade V were purchased from Sigma Aldrich. Fluorescent HDM was produced by labelling with the Alexa fluor 647 Protein Labelling kit (Molecular Probes).

PE-conjugated anti-B220 (clone RA3-6B2), APC-, FITC-, PerCP-Cy5.5- and V500-conjugated anti-CD45.2 (clone 104), PE-conjugated anti-CD64 (clone X54-5:7.1), PE-Cy7-conjugated anti-CD11b (clone M1/70), APC- and APC-Cy7-conjugated anti-CD11c (clone HL3), PerCP-Cy5.5-, BV421-conjugated anti-CD49b (clone DX5), FITC-conjugated anti-Ly6C (clone AL-21), PE- and PE-Cy7-conjugated anti-Ly6g (clone 1A8), APC-conjugated anti-MHCII (clone AF6-120.1), PE-conjugated anti-NK1.1 (clone PK136), PE-conjugated anti-SiglecF (clone E50-2440) were purchased from BD Pharmingen. APC-conjugated anti-CD45.1 (clone A20), FITC-conjugated anti-CD11b (clone M1/70), efluor660-conjugated anti-CD169 (clone SER-4), PerCP-Cy5.5-conjugated anti-CD19 (clone 1D3), PE-conjugated anti-CD115 (clone AFS98), efluor 450-conjugated anti-CD3 (clone 17A2), PerCP-Cy5.5-conjugated anti-CD62L (clone MEL-14), biotin-conjugated anti-CD86 (clone GL-1), efluor 660-, PerCP-efluor710-conjugated anti-CD90.2 (clone 30H12), PE-conjugated anti-F4/80 (clone BM8) were from eBioscience. BV421-conjugated anti-CD64 (clone X54-5:7.1) and

PerCP-Cy5.5-conjugated anti-MHCII (clone M5/M4.15.2) were from Biolegend. PE-conjugated anti-CCR2 (clone 475301), and APC-conjugated anti-merTK (clone 108928) were from R&D systems. Anti-CD11b MicroBeads were from Miltenyi Biotec. Appropriate isotype control antibodies were purchased from the same respective manufacturers.

Rabbit anti-phospho-p44/42 MAPK (Erk1/2) and anti-β-Actin (clone D6A8) antibodies were from Cell Signaling Technology. Horseradish peroxidase (HRP)-conjugated goat anti-rabbit IgG antibody was from Kirkegaard & Perry Laboratories.

Goat anti-CCL2, rat anti-CCL5 (clone 53405) and rat anti-CCL9 (clone 62105) neutralizing antibodies were from R&D Systems. Appropriate isotype control antibodies were purchased from the same manufacturer.

Cell isolation, staining and flow cytometry

To obtain single-lung-cell suspensions, lungs were perfused with 10 ml of PBS through the right ventricle, cut into small pieces, and digested for 1 h at 37°C in HBSS containing 1 mg ml^{-1} collagenase A (Roche) and 0.05 mg ml^{-1} DNase I (Roche). Single-cell suspensions were then enriched in mononuclear cells by harvesting cells from the 1.080:1.038 g ml^{-1} interface using a density gradient (Easycoll from VWR). Blood was collected and mixed with EDTA (100 mM), and red blood cells were lysed with RBC lysis buffer (eBioscience). To obtain single-heart and liver-cell suspensions, these organs were cut into small pieces and digested for 1 h at 37°C in HBSS containing 1 mg ml^{-1} collagenase A (Roche) and 0.05 mg ml^{-1} DNase I (Roche).

Cell phenotyping and sorting were performed on a FACSCANTO II and a FACSARIA III (BD Biosciences), respectively. Staining reactions were performed at 4°C after incubation with 2.4G2 Fc receptor blocking antibodies to reduce non-specific binding.

Regarding cell phenotyping and sorting, FSC-W and FSC-A discrimination was used to exclude doublet cells, and ViaProbe (7-AAD) cell viability solution (BD Biosciences) was used to discriminate between dead and living cells. In experiments aimed at isolating lung Ly-$6C^{hi}CD64^{lo}$ classical monocytes, Ly-$6C^{lo}CD64^{lo}$ patrolling monocytes, AMs, SS IMs, CpG IMs, or splenic monocytes, lung mononuclear cells and splenic cells were first enriched in CD11b-expressing cells by MACS using CD11b microbeads. Results were analyzed with FlowJo software (Tree Star).

Cytologic examination

Cytologic examination of FACS-sorted populations was performed on cytospin preparations stained with Hemacolor® (Merck KgaA). Sections were examined with a FSX100 microscope (Olympus).

Vascular monocytes/macrophage depletion

WT or *Ccr2*$^{-/-}$ mice were injected i.v. with 200 µl of clodronate-containing liposomes (Clo-Lips) or empty liposomes (PBS-Lips), and lung cells were harvested 24 hours later.

Assessment of IL-10 expression in ITIB mice and IL-10 production *ex vivo*

To assess IL-10 expression using IL-10-β-lactamase reporter ITIB mice (Bouabe et al., 2011), lung cells from IL-10-β-lactamase reporter ITIB and control WT mice were resuspended in a

CCF4-AM-containing solution supplemented with probenecid (Invitrogen), prepared according to the manufacturer's instructions, and incubated 90 min at 29°C. Briefly, CCF4-AM is a lipophilic ester derivative that consists of a cephalosporin core bridging a 7-hydroxycoumarin to a fluorescein. Once inside the cell, the ester groups are readily hydrolysed by cytoplasmic esterases, releasing the negatively charged form, CCF4, which is thus trapped in the cytosol (using inhibitor for anion transporters, such as probenecid, further increase trapping substrate/product within the cells). Exciting intact CCF4 at 405 nm induces fluorescence resonance energy transfer (FRET) from the coumarin to the fluorescein that subsequently emits green light. After cleavage of the ß-lactam ring of CCF4 by ß-lactamase, which is expressed under the control of the *Il10* gene promoter, the two fluorophores are separated, resulting in the disruption of FRET. Excitation at 409 nm now results in blue fluorescence detectable at 450 nm. CCF4-loaded cells were then classically stained and analyzed by flow cytometry. CCF4-loaded WT cells were used as negative controls.

For IL-10 production *ex vivo*, classical monocytes, patrolling monocytes, AMs and IMs were FACS-sorted from naive WT mice and $2x10^5$ cells were cultured in 200 µl of RPMI medium supplemented with 10% foetal bovine serum (FBS) and additives (L-glutamine 8mM, MEAA 0.1 mM, Pyruvate Na 1mM, Penicillin/streptomycin 50 UI ml^{-1}, β-mercaptoethanol 0.5mM) in a 96 well plate during 16 h. In some experiments, IMs isolated from WT, *Tlr9*$^{-/-}$ or *Myd88*$^{-/-}$ mice were cultured and stimulated during 16h with LPS (10 ng ml^{-1}) or CpG (7 µg ml^{-1}). Concentrations of IL-10 were measured by ELISA (eBioscience) in culture supernatants.

Quantification of monocytes/macrophages numbers

Lung cell numbers were counted following whole lung digestion and mononuclear cell enrichment by the use of a hemocytometer. The numbers of monocytes/macrophages were determined according to the gating strategy shown in Figure 1A.

Total BALF cell numbers were counted by the use of a hemacytometer. The numbers of SS IMs and CpG IMs were determined according to the gating strategy shown in Figure 1A.

Total splenic, cardiac, liver and bone marrow cell numbers were counted following tissue dissociation by the use of a hemacytometer. The numbers of splenic, cardiac, liver and bone marrow monocytes or macrophages were determined according to the gating strategy described by Swirski and collaborators (Swirski et al., 2009) or shown in Figure 1A, respectively.

Immunohistochemistry

Lungs were fixed in 4% formalin, paraffin-embedded and cut in 5 µm thick sections. Deparaffinized tissues were dewaxed and endogenous peroxides were blocked with hydrogen peroxide 3% (Merck). Tissue sections were then immersed in protein block serum free (Dako) for 10 min at room temperature. Mouse lung sections were stained with a rat anti-mouse Ly-6C (dilution 1/50) for 2 h at room temperature (Abcam) followed by a HRP-coupled rabbit anti-rat staining (dilution 1/400) for 40 min at room temperature (Abcam). Peroxidase activity was revealed using the 3,3'-diaminobenzidine hydrochloride kit (Dako), and tissues were then counter-colored with Carazzi's hematoxylin. Slides were mounted on Eukitt medium (Fluka Analytical).

In vivo labeling of vascular leukocytes

WT mice were injected i.v. with 0.5 µg of anti-CD45.2 antibodies. The antibody was allowed to circulate for 3 minutes prior to euthanasia in order to label all leukocytes in the vascular space. Lungs were then harvested without being perfused and the monocyte/macrophage populations were analyzed by flow cytometry.

Airway exposure to TLR ligands and pathogens

Lightly isoflurane anesthetized mice were instilled i.n. with 50 µl saline or 50 µl saline containing various TLR ligands (i.e. Pam3CSK4 25 µg; Poly(I:C) 50 µg; LPS 10 µg; FLA-BS 1 µg; MALP-2 1 µg; CpG-DNA 50 µg) or respiratory pathogens (i.e. influenza A 5 PFU; *S. pneumoniae* serotype 1, clinical isolate E1586, 10^5 CFU). The doses of TLR ligands used were chosen according to the ones found in the literature: Pam3CSK4 (Andrade et al., 2013; Chen et al., 2016); Poly(I :C) (Errea et al., 2015; LeMessurier et al., 2013); LPS (Chen et al., 2014; Hiroshima et al., 2014); FLA-BS (Errea et al., 2015; Munoz et al., 2010); MALP-2 (Reppe et al., 2015); R848 (Marino et al., 2011; Van et al., 2011); CpG (Hickey et al., 2013; Vogel and Brown, 2015). Influenza type A virus strain A/PR/8/34 (PR8) was provided by Dr François Trottein (Institut Pasteur de Lille, France). In experiments shown in Figure S2B and S2C, the concentration of the TLR ligands used was corresponding to 5 nmoles for each stimulant.

House dust mite-induced model of asthma and CpG treatments.

Lightly isoflurane anesthetized WT, ITIB or *Tlr9*$^{-/-}$ mice were sensitized by two weekly i.n. instillations of vehicle (LPS-free saline) or HDM extracts (100 µg in 50 µl) on day 0 and on day 7. In experiments shown in Figure 3E and 3F, mice were sensitized by HDM on day 0 and AlexaFluor-labeled HDM on day 7.

For assessing the effects of CpG in preventing asthma development (Figure 3), mice were instilled i.n. with 50 µl saline containing 50 µg ODN or 50 µg CpG 7 days before the first HDM treatment. Mice were sacrificed 3 days after the second HDM treatment (day 10). In adoptive transfer experiments, WT mice were transferred i.t. with $1.5x10^6$ AMs or CpG IMs sorted from CpG-treated WT or *Il-10*$^{-/-}$ mice (mortality rate varying between 40 and 60% in CpG-injected *Il-10*$^{-/-}$ mice, but not WT mice, unpublished observation), or vehicle (50 µl saline), 24 hours before each HDM treatment (days -1 and 6).

For assessing the curative effects of CpG on established asthma (Figure 4), mice were instilled i.n. with 50 µl saline containing 50 µg ODN or 50 µg CpG 7 days after the second HDM treatment (day 14). Seven days later (day 21), mice were challenged by an i.n. instillation of vehicle (LPS-free saline) or HDM (100 µg in 50 µl). In experiments shown in Figure 4E and 4F, mice were challenged by AlexaFluor-labeled HDM on day 21. Mice were sacrificed at day 24. In adoptive transfer experiments, WT mice were transferred i.t. with $1.5x10^6$ AMs or CpG IMs sorted from CpG-treated WT or *Il-10*$^{-/-}$ mice (mortality rate varying between 40 and 60% in CpG-injected *Il-10*$^{-/-}$ mice, but not WT mice, unpublished observation), or vehicle (50 µl saline), 24 hours before the last HDM challenge (day 20). In

experiments assessing the long-lasting effects of CpG on established asthma, mice were challenged with HDM 8 weeks after a single CpG instillation and were sacrificed 3 days later.

Assessment of the asthmatic response in HDM-exposed mice

AHR was estimated by assessing dynamic airway resistance in anesthetized animals subjected to increasing doses of methacholine using a FlexiVent small animal ventilator (SCIREQ), as previously described (Gueders et al., 2009). Mice were sacrificed and BALF, lungs and lymph node cells were harvested and analyzed as described previously (Marichal et al., 2010). Briefly, BALF eosinophilia was evaluated by total and differential cell counts, lung inflammation and mucus production were evaluated on H&E- and PAS-stained lung sections, respectively. Mucus production was also quantified as the percentage of PAS-stained goblet cells per total epithelial cells in randomly selected bronchi. Seven randomly selected sections were analyzed per murine lung. Bronchial lymph node cells were cultured *in vitro* in supplemented Click's medium (10% FBS, L-glutamine 8mM, modified essential amino acids 0.1 mM, sodium pyruvate 1mM, Penicillin/Streptomycin 50 UI ml^{-1} and β-mercaptoethanol 0.5mM) with or without HDM restimulation (30 μg ml^{-1}). Culture supernatants were assayed for cytokine production (IL-4, IL-5, IL-13) by ELISA (eBioscience) after 3 days of culture.

To assess DC maturation and migration, mice were injected i.n. with 100 μg of HDM labeled with Alexa fluor-647 or saline at day 7 (Figure 3E and 3F) or at day 21 (Figure 4E and 4F). Mice were sacrificed 24 hours later. BLN were minced, and total cell numbers were counted by the use of a hemacytometer. The number of antigen-positive DCs (i.e. $HDM^{+}CD11c^{hi}MHC\text{-}II^{hi}$ cells) was determined in the BLN by flow cytometry. The extent of lung DC maturation was determined by quantifying surface expression of the maturation markers CD86 and MHC-II on lung total DCs (i.e. non-autofluorescent $CD11c^{hi}MHC\text{-}II^{int/hi}$ cells) by flow cytometry.

OVA/Alum-induced model of asthma and CpG treatments

WT mice were sensitized on days 0 and 14 by i.p. injection of 100 μl saline containing 10 μg OVA (grade V) admixed with 100 μl Imject Alum (Pierce). Sham-immunized mice received 100 μl saline mixed with 100 μl Imject Alum. On days 28–31, mice were challenged by exposure to an aerosol of 1% OVA (w/v; grade III) in saline for 1 hour. For assessing the curative effects of CpG on established asthma, mice were instilled i.n. with 50 μl saline containing 50 μg ODN or 50 μg CpG 7 days before the aerosol challenge (day 21). Mice were sacrificed 24 hours after the last challenge (day 32). In adoptive transfer experiments, WT mice were transferred i.t. with $1.5x10^{6}$ of AMs or CpG IMs sorted from CpG-treated WT mice or vehicle (50 μl saline) 24 hours before the OVA challenge (day 27).

Read-outs used for assessment of the asthmatic response was performed similarly as for the HDM-induced asthma models, except that BLN were restimulated with OVA (50 μg ml^{-1}, grade V) and that a quantification of OVA-specific IgE was also performed, as described (Marichal et al., 2011).

Generation of bone marrow mixed chimeras and parabiotic mice

Twelve week-old $CD45.1/2^{+}$ WT C57BL/6 mice were lethally irradiated with two doses of 6 Gy 3 hours apart. Two hours after the second irradiation, these mice were injected i.v. with

$2x10^6$ BM cells consisting of a 1:1 mix of BM cells obtained from $CD45.1^+$ C57BL/6 and $CD45.2^+$ *Ccr2*$^{-/-}$ C57BL/6 mice. Mice were treated with antibiotics (Baytril, Bayer, 0.05 $mg.ml^{-1}$ in drinking water) from the day before irradiation until the time of sacrifice. Cell numbers were evaluated 7, 14, 56 and 84 days later and chimerism was assessed 56 and 84 days later. In some experiments, such BM mixed chimeras were instilled with CpG or LPS 7 days before the analysis.

Parabiotic mice were generated by suturing age- and weight-matched WT $CD45.1^+$ and *Ccr2*$^{-/-}$ $CD45.2^+$ mice at the age of 6 weeks. Mice were analyzed at 6 months of age.

Assessment of cell proliferation using EdU incorporation

One, two or three days after i.n. administration of CpG, C57BL/6 WT or *Ccr2*$^{-/-}$ mice were injected i.p. with EdU (1 mg in 400 µl). Mice were sacrificed 24 hours later and incorporation of EdU was assessed by flow cytometry.

***Ex vivo* stimulation of tissue monocytes with CpG and LPS**

Lung and splenic monocytes were sorted by FACS according to the gating strategy described in Figure 1a and by Swirski and collaborators (Swirski et al., 2009), respectively. Two hundred thousands ($2x10^5$) cells were cultured in RPMI medium supplemented with 10% FBS and additives (L-glutamine 8 mM, MEAA 0.1 mM, Pyruvate Na 1mM, Penicillin/streptomycin 50 UI ml^{-1}, β-mercaptoethanol 0.5 mM), with or without CpG (7 µg ml^{-1}) or LPS (10 ng ml^{-1}) in a 24-well plate. Twenty-four, 36, 48 and 54 hours later, cells were harvested and phenotyped. ViaProbe (7-AAD) cell viability solution was used to discriminate between dead and living cells.

Western blot

Five hundred thousands lung monocytes were sorted by FACS from naive *Ccr2*$^{-/-}$ mice and were cultured in RPMI medium supplemented with 10% FBS and additives (L-glutamine 8mM, MEAA 0.1 mM, Pyruvate Na 1mM, Penicillin/streptomycin 50UI ml^{-1}, β-mercaptoethanol 0.5mM) in a 12-well plate. Cells were treated with or without ODN or CpG-DNA (7 µg ml^{-1}) for 30 minutes. Cells were then harvested, centrifuged and pellets were lysed in radioimmunoprecipitation assay (RIPA) lysis buffer with 1 mM Na3VO4, 10 mM NaF and complete protease inhibitor (Roche Diagnostics). Protein extracts were added to Laemmli buffer, boiled and run on a 10% polyacrylamide-SDS gel; after electrophoresis, gels were electro-transferred onto a polyvinylidene difluoride membrane (PVDF) for western-blotting. Nonspecific binding was blocked in 20 mM Tris, pH 7.5, 500 mM NaCl, 0.2% Tween 20 (TBS-Tween), and 5% dry milk during 1 h. Membranes were then incubated with rabbit anti-phospho-p44/42 MAPK (Erk1/2), anti-p44/42 MAPK (Erk1/2) or anti-β-Actin antibodies (1:1,000; Cell Signaling Technology) overnight at 4°C, rinsed with TBS-Tween and further incubated with horseradish peroxidase (HRP)-conjugated goat anti-rabbit IgG (1:5,000; Kirkegaard & Perry Laboratories) for 60 min at room temperature. Result was visualized using an enhanced chemiluminescence system (ECL kit; Amersham) followed by autoradiography with Fuji x-ray films.

mRNA isolation, microarray and Gene Set Enrichment Analyses

Singlet living Ly-$6C^{hi}CD64^{lo}$ cells from *Ccr2*$^{-/-}$ or WT mice, and AMs, SS IMs and CpG IMs

from WT mice were directly sorted in Trizol® (Life Technologies). The 4 cell populations were sorted in duplicate (CpG IMs) or triplicate (all the others), yielding a total of 11 samples. Total RNA was purified using Direct-zol® kit (Zymo Research) following manufacturer's recommendations. For each cell type, total RNAs were eluted in a total of 175 µl of water. Eluted RNAs were incubated with DNase for 10 min at room temperature in a total volume of 200 µl using the RNase-Free DNase Set from Qiagen (Venlo), followed by purification on RNeasy® Micro columns (Qiagen) and final elution in 50µl water. RNAs were quantitatively and qualitatively verified using Agilent RNA 6000 Pico Kit run on an Agilent 2100 Bioanalyzer. Concentrations were around 1ng/µl and RNA Integrity Numbers were above 8.

1.5ng RNA was used to generate fragmented and biotin-labeled ssDNA targets using GeneChip® WT Pico Reagent Kit (Affymetrix). The fragmented and labeled targets were hybridized to GeneChip® Mouse Gene 1.0 ST Arrays following standard Affymetrix protocol, which includes overnight hybridization at 45°C and 60 rpm in an Affymetrix GeneChip Hybridization Oven 645. The arrays were then washed and stained in an Affymetrix GeneChip Fluidics Station 450.

Microarrays were analyzed using R (version 3.3.1) and Bioconductor (Huber et al., 2015). Raw data were background-corrected and quantile-normalized using "Robust Multichip Average algorithm" (RMA) from "oligo" package. Normalized data were then annotated using "mogene10sttranscriptcluster.db" annotation package.

Differential expression analysis between Ly-6C^{hi} monocytes from *Ccr2*$^{-/-}$ mice and Ly-6C^{hi} monocytes from WT mice was performed using "Linear Models for Microarray Data" (Limma) package in Bioconductor, with thresholds as following: Benjamini Hochberg adjusted *P* value (adj *P* value) < 0.05 AND Fold Change (FC) > 2 or < 0.5, and after having filtered out non annotated probes. Differential expression analysis between SS IMs and CpG IMs was performed identically, excepted for adj *P* value threshold set to 0.05. Volcano plot of differences between Ly-6C^{hi} monocytes from *Ccr2*$^{-/-}$ mice and Ly-6C^{hi} monocytes from WT mice was obtained by plotting $\log_2$ (FC) on the x axis and $-\log_{10}$ (adj *P* value) on the y axis for all probes present in the Affymetrix GeneChip® Mouse Gene 1.0 ST Array, including non annotated ones.

Heatmaps were generated by plotting normalized expression values of relevant samples and genes using "heatmap.2" function from "gplots" package.

Principal Component Analysis (PCA) was performed using "prcomp" function on normalized expression values of AMs, SS IMs and CpG IMs. Values of principal components 1, 2 and 3 were then tridimensionnally plotted using "plot3d" function of "rgl" package. Percentages shown on each axis indicate the % of variability explained, with PC1 explaining the most variability.

In order to identify biological signatures of CpG IMs compared to SS IMs, we decided to employ the commonly used non-parametric, rank based tool, Gene Set Enrichment Analysis (GSEA version 2.2.2) (Subramanian et al., 2005). Microarray normalized expression data of SS IMs (3 samples) and CpG IMs (2 samples) were used by GSEA as dataset to rank genes between the two cell types. Since (i) CpG IM class contains 2 samples and (ii) RMA normalized data are in log scale, « Diff_of_Classes » method was chosen to rank genes in the dataset. Enrichment analysis was then performed using hallmark gene sets of MsigDB database.

Real-time PCR analysis

Singlet living lung Ly-6C^{hi} cells from *Ccr2*$^{-/-}$ mice, and lung IMs, AMs and splenic monocytes from WT mice were directly sorted in Trizol® (Life Technologies). Total RNA was isolated using Direct-zol® kit (Zymo Research) following manufacturer's recommendations. Complementary DNA was obtained using RevertAid First Strand cDNA Synthesis Kit (Thermo Fisher Scientific). Quantitative real-time PCR were performed in duplicates using ABsolute Blue qPCR SYBR Green ROX Mix (Thermo Fisher Scientific) and ABI 7900HT Fast Real-Time PCR System (Applied Biosystems) under the following conditions: (1) initial denaturation at 95°C for 15 min followed by (2) 40 cycles of 95°C 15 s and 60°C 1 min. Primer sequences were as followed :. 5'-AGCTGAACATGAACGGCATCT-3' and 5'- GATCGGCCAGCCATCTGA-3' for *Tlr9*, 5'-AGCCCAGTGTTACCACCAAG-3' and 5'-ACCCAAGAACAAGCACAAGG-3' for the housekeeping gene *Ubc*, 5'-CATGGCTCGCTCGGTGACC-3' and 5'-AATGTGAGGCGGGTGGAACTG-3' for the housekeeping gene *B2m*, 5'-AGCTACTGTAATGATCAGTCAACG-3' and 5'-AGAGGTCCTTTTCACCAGCA-3' for the housekeeping gene *Hprt*. Expression levels of TLR9 were normalized relative to three control genes (*Ubc*, *B2m* and *Hprt*) using qBase+ software (Biogazelle).

s.c. and i.p. CpG treatments

WT mice were injected s.c. or i.p. with 100 µl saline or 200 µl (i.p.) or 100 µl (s.c.) saline containing 50 µg CpG. Mice were analyzed 7 days later.

Splenectomy

Ccr2$^{-/-}$ mice were anesthetized by intraperitoneal injection of ketamine (75 mg kg^{-1}), xylazine (10 mg kg^{-1}) and buprenorphine (0.05 mg kg^{-1}). A transversal incision was made on the left lower back of the mice to expose the spleen. Spleen was resected and vessels were cauterized. The incision was sutured. Sham-operated mice underwent the same procedure without removal of the spleen.

Chemokine array

Lightly isoflurane anesthetized WT mice were instilled i.n. with 50 µl saline or 50 µl saline containing either CpG (50 µg) or LPS (10 µg). Eight hours later, mice were sacrificed and lungs were harvested without being perfused. Lungs were homogenized with an UltraTurrax homogenizer (IKA) in 2 ml saline containing complete protease inhibitor (Roche Diagnostics). Samples were then centrifuged for 10 minutes at 16,000 x g and supernatants were tested for the presence of chemokines using a chemokine antibody array (Abcam) according to manufacturer instructions. Membranes were developed and digitized for analysis using ImageJ. Each sample spot density was measured, averaged and normalized to membrane reference spots.

Chemokine inhibition

Ccr2$^{-/-}$ mice were injected i.p. with neutralizing anti-CCL2 (200 µg), anti-CCL5 (50 µg), anti-CCL9 (50 µg) antibodies or a combination of these 3 antibodies, 30 minutes before an i.n. administration of CpG. Control mice received the appropriate isotype controls. The numbers

of lung monocytes and CpG IMs were analyzed 1 day and 7 days after CpG administration, respectively.

Statistical Analysis

Statistical analyses were performed using R (version 3.2.4). Data from independent experiments were pooled for analysis in each data panel, unless otherwise indicated. Raw data was transformed when needed and was back-transformed for graphical presentation. Respect of the assumptions of normal distribution of residuals and homoscedasticity was verified using diagnostic plots. We considered a *P*-value lower than 0.05 as significant. *, $P<0.05$; **, $P<0.01$, ***, $P<0.001$; ns, not significant.

Supplemental References

Andrade, E.B., Alves, J., Madureira, P., Oliveira, L., Ribeiro, A., Cordeiro-da-Silva, A., Correia-Neves, M., Trieu-Cuot, P., and Ferreira, P. (2013). TLR2-induced IL-10 production impairs neutrophil recruitment to infected tissues during neonatal bacterial sepsis. J. Immunol. *191*, 4759-4768.

Bouabe, H., Liu, Y., Moser, M., Bosl, M.R., and Heesemann, J. (2011). Novel highly sensitive IL-10-beta-lactamase reporter mouse reveals cells of the innate immune system as a substantial source of IL-10 in vivo. J. Immunol. *187*, 3165-3176.

Chen, H., Wu, S., Lu, R., Zhang, Y.G., Zheng, Y., and Sun, J. (2014). Pulmonary permeability assessed by fluorescent-labeled dextran instilled intranasally into mice with LPS-induced acute lung injury. PloS One *9*, e101925.

Chen, Y.G., Zhang, Y., Deng, L.Q., Chen, H., Zhang, Y.J., Zhou, N.J., Yuan, K., Yu, L.Z., Xiong, Z.H., Gui, X.M.*, et al.* (2016). Control of Methicillin-Resistant Staphylococcus aureus Pneumonia Utilizing TLR2 Agonist Pam3CSK4. PloS One *11*, e0149233.

Errea, A., Gonzalez Maciel, D., Hiriart, Y., Hozbor, D., and Rumbo, M. (2015). Intranasal administration of TLR agonists induces a discriminated local innate response along murine respiratory tract. Immunol. Lett. *164*, 33-39.

Gueders, M.M., Paulissen, G., Crahay, C., Quesada-Calvo, F., Hacha, J., Van Hove, C., Tournoy, K., Louis, R., Foidart, J.M., Noel, A., and Cataldo, D.D. (2009). Mouse models of asthma: a comparison between C57BL/6 and BALB/c strains regarding bronchial responsiveness, inflammation, and cytokine production. Inflamm. Res. *58*, 845-854.

Hemmi, H., Takeuchi, O., Kawai, T., Kaisho, T., Sato, S., Sanjo, H., Matsumoto, M., Hoshino, K., Wagner, H., Takeda, K., and Akira, S. (2000). A Toll-like receptor recognizes bacterial DNA. Nature *408*, 740-745.

Hickey, A.J., Lin, J.S., Kummer, L.W., Szaba, F.M., Duso, D.K., Tighe, M., Parent, M.A., and Smiley, S.T. (2013). Intranasal prophylaxis with CpG oligodeoxynucleotide can protect against Yersinia pestis infection. Infect. Immun. *81*, 2123-2132.

Hiroshima, Y., Hsu, K., Tedla, N., Chung, Y.M., Chow, S., Herbert, C., and Geczy, C.L. (2014). S100A8 induces IL-10 and protects against acute lung injury. J. Immunol. *192*, 2800-2811.

Huber, W., Carey, V.J., Gentleman, R., Anders, S., Carlson, M., Carvalho, B.S., Bravo, H.C., Davis, S., Gatto, L., Girke, T.*, et al.* (2015). Orchestrating high-throughput genomic analysis with Bioconductor. Nat. Methods *12*, 115-121.

LeMessurier, K.S., Hacker, H., Chi, L., Tuomanen, E., and Redecke, V. (2013). Type I interferon protects against pneumococcal invasive disease by inhibiting bacterial transmigration across the lung. PLoS Pathog. *9*, e1003727.

Marichal, T., Bedoret, D., Mesnil, C., Pichavant, M., Goriely, S., Trottein, F., Cataldo, D., Goldman, M., Lekeux, P., Bureau, F., and Desmet, C.J. (2010). Interferon response factor 3 is essential for house dust mite-induced airway allergy. J. Allergy Clin. Immunol. *126*, 836-844.

Marichal, T., Ohata, K., Bedoret, D., Mesnil, C., Sabatel, C., Kobiyama, K., Lekeux, P., Coban, C., Akira, S., Ishii, K.J., *et al.* (2011). DNA released from dying host cells mediates aluminum adjuvant activity. Nat. Med. *17*, 996-1002.

Marino, R., Thuraisingam, T., Camateros, P., Kanagaratham, C., Xu, Y.Z., Henri, J., Yang, J., He, G., Ding, A., and Radzioch, D. (2011). Secretory leukocyte protease inhibitor plays an important role in the regulation of allergic asthma in mice. J. Immunol. *186*, 4433-4442.

Munoz, N., Van Maele, L., Marques, J.M., Rial, A., Sirard, J.C., and Chabalgoity, J.A. (2010). Mucosal administration of flagellin protects mice from Streptococcus pneumoniae lung infection. Infect. Immun. *78*, 4226-4233.

Reppe, K., Radunzel, P., Dietert, K., Tschernig, T., Wolff, T., Hammerschmidt, S., Gruber, A.D., Suttorp, N., and Witzenrath, M. (2015). Pulmonary immunostimulation with MALP-2 in influenza virus-infected mice increases survival after pneumococcal superinfection. Infect. Immun. *83*, 4617-4629.

Subramanian, A., Tamayo, P., Mootha, V.K., Mukherjee, S., Ebert, B.L., Gillette, M.A., Paulovich, A., Pomeroy, S.L., Golub, T.R., Lander, E.S., and Mesirov, J.P. (2005). Gene set enrichment analysis: a knowledge-based approach for interpreting genome-wide expression profiles. P. Natl. Acad. Sci. U.S.A *102*, 15545-15550.

Swirski, F.K., Nahrendorf, M., Etzrodt, M., Wildgruber, M., Cortez-Retamozo, V., Panizzi, P., Figueiredo, J.L., Kohler, R.H., Chudnovskiy, A., Waterman, P., *et al.* (2009). Identification of splenic reservoir monocytes and their deployment to inflammatory sites. Science *325*, 612-616.

Van, L.P., Bardel, E., Gregoire, S., Vanoirbeek, J., Schneider, E., Dy, M., and Thieblemont, N. (2011). Treatment with the TLR7 agonist R848 induces regulatory T-cell-mediated suppression of established asthma symptoms. Eur. J Immunol. *41*, 1992-1999.

Vogel, A.J., and Brown, D.M. (2015). Single-Dose CpG Immunization Protects Against a Heterosubtypic Challenge and Generates Antigen-Specific Memory T Cells. Front. Immunol. *6*, 327.